

ON THE EFFICIENCY OF THE TIDAL STIRRING MECHANISM FOR THE ORIGIN OF DWARF SPHEROIDALS: DEPENDENCE ON THE ORBITAL AND STRUCTURAL PARAMETERS OF THE PROGENITOR DISKY DWARFS

STELIOS KAZANTZIDIS¹, EWA L. ŁOKAS², SIMONE CALLEGARI³,
LUCIO MAYER^{3,4}, AND LEONIDAS A. MOUSTAKAS⁵

The Astrophysical Journal, submitted

ABSTRACT

The tidal stirring model posits the formation of dwarf spheroidal galaxies (dSphs) via the tidal interactions between late-type, rotationally-supported dwarfs and Milky Way-sized host galaxies. Using a comprehensive set of collisionless N -body simulations, we investigate the efficiency of the tidal stirring mechanism for the origin of dSphs. In particular, we examine the degree to which the tidal field of the primary galaxy affects the sizes, masses, shapes, and kinematics of the disk dwarfs for a range of dwarf orbital and structural parameters. Our study is the first to employ self-consistent, equilibrium models for the progenitor dwarf galaxies constructed from a composite distribution function and consisting of exponential stellar disks embedded in massive, cosmologically-motivated dark matter halos. Exploring a wide variety of dwarf orbital configurations and initial structures, we demonstrate that in the majority of cases the disk dwarfs experience significant mass loss and their stellar distributions undergo a dramatic morphological, as well as dynamical, transformation. Specifically, the stellar components evolve from disks to bars and finally to pressure-supported, spheroidal systems with kinematic and structural properties akin to those of the classic dSphs in the Local Group (LG) and similar environments. The self-consistency of the adopted dwarf models is crucial for confirming this complex transformation process via tidally-induced dynamical instabilities and impulsive tidal heating of the stellar distribution. Our results suggest that such tidal transformations should be common occurrences within the currently favored cosmological paradigm and highlight the key factor responsible for an effective metamorphosis to be the strength of the tidal shocks at the pericenters of the orbit. We also demonstrate that the combination of short orbital times and small pericentric distances, characteristic of dwarfs being accreted by their hosts at high redshift, induces the strongest and most complete transformations. Our models also indicate that the efficiency of the transformation via tidal stirring is affected significantly by the structure of the progenitor disk dwarfs. While the mass-to-light ratios, M/L , of the dwarf galaxies typically decrease monotonically with time as the extended dark matter halos are efficiently tidally stripped, we identify a few cases where this trend is reversed later in the evolution when stellar mass loss becomes more effective. We also find that the dwarf remnants satisfy the relation $V_{\max} = \sqrt{3} \sigma_*$, where σ_* is the one-dimensional, central stellar velocity dispersion and V_{\max} is the maximum halo circular velocity, which has intriguing implications for the missing satellites problem. Assuming that the distant dSphs in the LG, such as Leo I, Tucana, and Cetus are the products of tidal stirring, our findings suggest that these galaxies should have only been partially stirred by the tidal field of their hosts. We thus predict that these remote dwarfs should exhibit higher values of V_{rot}/σ_* , where V_{rot} is the stellar rotational velocity, compared to those of dSphs located closer to the primary galaxies. Overall, we conclude that the action of tidal forces from the hosts constitutes a crucial evolutionary mechanism for shaping the nature of dwarf galaxies in environments such as that of the LG. Environmental processes of this type should thus be included as ingredients in models of dwarf galaxy formation and evolution.

Subject headings: galaxies: dwarfs – galaxies: fundamental parameters – galaxies: kinematics and dynamics – galaxies: Local Group – galaxies: structure – cosmology: dark matter

1. INTRODUCTION

The currently favored cold dark matter (CDM) paradigm of hierarchical structure formation (e.g., White & Rees 1978; Blumenthal et al. 1984) generically predicts that dwarf galaxies comprise the primary building blocks of more massive systems. Observational evidence has recently confirmed this expectation with the discovery of streams

and complex stellar structures associated with accreted and tidally disrupted dwarfs in the Milky Way (MW) (e.g., Ibata et al. 1994; Yanny et al. 2000; Ibata et al. 2001b; Newberg et al. 2002; Majewski et al. 2003; Martin et al. 2004; Martínez-Delgado et al. 2005; Grillmair & Dionatos 2006; Belokurov et al. 2006), the Andromeda galaxy (M31) (Ibata et al. 2001a; Ferguson et al. 2002, 2005; Kalirai et al. 2006; Ibata et al. 2007), and beyond the Local Group (LG) (e.g., Malin & Hadley 1997; Shang et al. 1998; Peng et al. 2002; Forbes et al. 2003; Pohlen et al. 2004). Understanding the formation and evolution of dwarf galaxies is crucial for testing the predictions of the CDM theory and gaining insight into the physical processes of structure formation.

In this context, the dwarf spheroidal galaxies (dSphs) of the LG (see Mateo 1998 and Tolstoy et al. 2009 for comprehensive reviews) constitute excellent candidates for constraining the CDM model, as they are believed to be highly dark matter

¹ Center for Cosmology and Astro-Particle Physics; and Department of Physics; and Department of Astronomy, The Ohio State University, Columbus, OH 43210, USA; stelios@mps.ohio-state.edu

² Nicolaus Copernicus Astronomical Center, 00-716 Warsaw, Poland; lokas@camk.edu.pl

³ Institute for Theoretical Physics, University of Zürich, CH-8057 Zürich, Switzerland; callegar@physik.uzh.ch

⁴ Institute of Astronomy, Department of Physics, ETH Zürich, CH-8093 Zürich, Switzerland; lucio@phys.ethz.ch

⁵ Jet Propulsion Laboratory, California Institute of Technology, Pasadena, CA 91109, USA; leonidas@jpl.nasa.gov

(DM) dominated, with mass-to-light ratios of $M/L_V \sim 10^{1-3}$ (e.g., Mateo 1998; Gilmore et al. 2007; Simon & Geha 2007; Walker et al. 2009) (for alternative explanations of their extreme DM content see, e.g., Kuhn & Miller 1989; Milgrom 1995; Kroupa 1997; Łokas 2001). dSphs are the faintest galaxies known and their stellar components are supported by random motions, with a ratio of rotational velocity to line-of-sight, central velocity dispersion of $V_{\text{rot}}/\sigma_* \lesssim 1$ (Mateo 1998). Among the dwarf galaxies in the LG, dSphs are also the most numerous and they tend to be clustered around the massive spirals MW and M31 (though some outliers exist including the distant dwarf Leo I and the isolated dSphs Cetus and Tucana that lie on the outskirts of the LG). This tendency is referred to as the morphology-density relation where rotationally-supported dwarf irregular galaxies (dIrrs) are found in the periphery of the LG (e.g., Mateo 1998; Grebel 1999). Moreover, dSphs are gas poor or completely devoid of gas (e.g., Mateo 1998; Grcevich & Putman 2009) and they exhibit a wide diversity in their star formation histories (e.g., Grebel 2000; Orban et al. 2008). Owing to their proximity, dSphs have been most thoroughly studied in the LG. However, dwarfs with the properties of dSphs have been recently identified in nearby groups and clusters of galaxies (Chiboucas et al. 2009; Penny et al. 2009) suggesting that these intriguing galaxies are not unique to the LG.

While our understanding of dSphs has grown impressively in the past decade, a definitive model for their origin still remains elusive (see Mayer 2010 and Kravtsov 2010 for recent reviews). Two main classes of models have been proposed so far to explain their formation and present-day properties. In the first, dSphs are the result of the interplay between cosmic reionization and stellar feedback suppressing gas accretion and star formation in low-mass galaxies (e.g., Dekel & Silk 1986; Bullock et al. 2000; Susa & Umemura 2004; Ricotti & Gnedin 2005; Tassis et al. 2008; Sawala et al. 2010; Macciò et al. 2010). In the second, the origin of dSphs is intimately linked to various environmental mechanisms, including tidal and ram pressure stripping (e.g., Einasto et al. 1974; Faber & Lin 1983; Mayer et al. 2001a,b; Kravtsov et al. 2004; Mayer et al. 2006, 2007; Klimontowski et al. 2007; Peñarrubia et al. 2008; Klimontowski et al. 2009a) and resonant stripping (D’Onghia et al. 2009).

Using controlled simulations of individual disk dwarf galaxies orbiting inside a MW-sized host, Mayer et al. (2001a,b) demonstrated for the first time that the repeated action of tidal forces from the primary galaxy can transform the dwarfs into pressure-supported stellar systems with the structural and kinematic properties of dSphs (see also Klimontowski et al. 2007, 2009a). This transformation mechanism, termed “tidal stirring”, involves a combination of tidally-induced dynamical instabilities in stellar disks (e.g., the bar and buckling instabilities) and impulsive tidal heating of the stellar distribution. In the context of CDM, tidal stirring should be particularly effective since satellites of massive galaxies are affected by strong tidal forces due to their highly eccentric orbits (e.g., Ghigna et al. 1998; Diemand et al. 2007).

Although the tidal stirring model naturally explains the tendency of dSphs to be concentrated near the dominant spiral galaxies, it is only applicable to classic dSphs, namely those that were known before the discovery of the ultra-faint dwarfs by the Sloan Digital Sky Survey (SDSS) (e.g., Simon & Geha 2007). When combined with ram pressure stripping and the

effect of radiation fields at high redshift, such as the cosmic ionizing ultraviolet background, the tidal stirring mechanism can also account for both the low gas fraction and the extremely high DM content in some of the classic dSphs such as Draco and Ursa Minor (Mayer et al. 2006, 2007). Recently, the structure and kinematics of the stellar core of the nearby Sagittarius dwarf galaxy have also been successfully modeled within the framework of tidal stirring (Łokas et al. 2010b).

In addition to controlled numerical experiments, significant theoretical effort has been devoted to performing fully cosmological, hydrodynamical simulations of dwarf galaxy formation (e.g., Ricotti & Gnedin 2005; Read et al. 2006a; Tassis et al. 2008; Governato et al. 2010; Sawala et al. 2010). While pressure-supported objects with the properties of LG dSphs have been produced in some cases, (e.g., Ricotti & Gnedin 2005; Sawala et al. 2010), other studies have demonstrated the formation of systems with properties similar to those of the likely progenitors of dSphs according to the tidal stirring model (Governato et al. 2010). Successes notwithstanding and despite the continuing increase in dynamic range, limited resolution prohibits current cosmological simulations with hydrodynamics to address in detail the dynamical and structural evolution of dwarf *satellite* galaxies. In addition, due to numerical loss of angular momentum and overcooling, satellites in cosmological simulations of galaxy formation are too bright and too dense (e.g., Governato et al. 2007).

Given these facts, we are motivated to explore the tidal evolution of individual, rotationally-supported dwarf galaxies inside MW-sized hosts using a large ensemble of controlled N -body simulations. While our work is informed by many past numerical investigations aimed to elucidate the tidal stirring scenario for the origin of dSphs (Mayer et al. 2001a,b, 2002; Klimontowski et al. 2007, 2009a), our numerical experiments extend those of earlier studies in several important respects. For example, unlike previous work, we employ self-consistent, equilibrium numerical models of disk dwarfs for our experiments. These models are derived from three-integral composite distribution functions (DFs) and are thus superior to those constructed from simpler approximate prescriptions that produce models that are initially out of equilibrium (e.g., Hernquist 1993). The transformation via tidal stirring is an intricate process with several distinct stages that depends sensitively on the development of tidally-induced dynamical instabilities (e.g., bars) and the detailed response of the stellar distribution to tidal shocks. For this reason, the self-consistency of the adopted models is crucial.

Moreover, we explore a wide variety of orbital configurations and structural parameters for the progenitor dwarf galaxies, conducting a simulation campaign that allows the investigation of a much larger parameter space than before. Our ultimate goal is to determine the degree to which the evolution of rotationally-supported dwarfs is affected by the strong tidal field of their host galaxies under a broad range of initial conditions, and through this to establish the generic efficiency of the tidal stirring mechanism for the origin of dSphs. Lastly, our numerical experiments are characterized by much higher numerical resolution than that of previous related studies. This fact, in conjunction with the increasing accuracy of current observational data (e.g., Walker et al. 2009), offers unique opportunities for a systematic and quantitative comparison with observations, and we undertake such a task in a companion paper (Łokas et al. 2010, in preparation).

In this study, we focus on the evolution of the intrinsic,

global parameters of accreted disk dwarfs orbiting inside a MW-sized primary galaxy. Our results firmly establish that tidal interactions between late-type dwarf galaxies and their hosts can produce objects with kinematic and structural properties akin to those of the *classic* dSphs in the LG and similar environments under a wide variety of initial conditions. We conclude that such tidal transformations should be common occurrences within the currently favored cosmological paradigm. Environmental mechanisms of the type highlighted in the present work should thus constitute important ingredients in models of dwarf galaxy formation and evolution.

The outline of this paper is as follows. In § 2, we introduce the dwarf and host galaxy models. In this section, we also describe the methods adopted and the setup of the numerical experiments performed in the present study. In § 3 and § 4, we investigate the degree to which the orbital parameters and initial structure of the progenitor disk dwarfs can influence their morphological and dynamical transformation into dSphs. Implications and extensions of our findings are presented in § 5, which also includes a discussion of the caveats of the current study and a number of promising directions for future work. Lastly, in § 6 we summarize our main results and conclusions.

2. SIMULATIONS AND METHODS

2.1. Models of Dwarf Galaxies

The present investigation utilizes fully self-consistent, equilibrium models of dwarf galaxies for tidal stirring experiments. This aspect of the modeling constitutes one of the major improvements we introduce in this study. As we discussed in the previous section, the nature of the transformation mechanism is such that the self-consistency of the adopted dwarf models is essential. Specifically, we employ the method of Widrow & Dubinski (2005) to construct numerical realizations of dwarf galaxies consisting of exponential stellar disks embedded in cuspy, cosmologically-motivated Navarro et al. (1996, hereafter NFW) DM halos. The Widrow & Dubinski (2005) models are specified by a large number of parameters. They are derived from three-integral, composite DFs and thus represent self-consistent, equilibrium solutions to the coupled Poisson and collisionless Boltzmann equations. The Widrow & Dubinski (2005) method has been recently used in a variety of numerical studies associated with instabilities in disk galaxies, including the dynamics of warps and bars (Dubinski & Chakrabarty 2009; Dubinski et al. 2009) and the heating of galactic disks by halo substructure (Gauthier et al. 2006; Kazantzidis et al. 2008; Purcell et al. 2009; Kazantzidis et al. 2009). We refer the reader to Widrow & Dubinski (2005) for an overview of all relevant parameters and a detailed description of this technique.

The density distributions of the dwarf DM halos are given by

$$\rho_{\text{NFW}}(r) = \frac{\rho_s}{\left(\frac{r}{r_s}\right) \left(1 + \frac{r}{r_s}\right)^2}, \quad (1)$$

where ρ_s is a characteristic inner density, and r_s denotes the scale radius of the density profile defined as the distance from the center where the logarithmic slope, $d \ln \rho(r) / d \ln r$, is equal to -2 . The NFW density profile is formally infinite in extent with a cumulative mass that diverges as $r \rightarrow \infty$. In order to keep the total mass finite, Widrow & Dubinski (2005) impose a tidal radius in the DM halo, R_h , which represents the outer edge of the system. In our modeling, R_h is chosen in such

a way that it becomes roughly equal to the cosmologically-motivated virial radius, $R_h \approx r_{\text{vir}}$. As a result of this choice, the total mass of the halo within R_h , which we denote M_h , would be equivalent to the virial mass. We control the shape of the halo density profile via the concentration parameter $c \equiv r_{\text{vir}}/r_s \approx R_h/r_s$. Higher values of concentration correspond to a larger fraction of the mass contained in the inner regions of the halo. Lastly, all DM halos were constructed with no net angular momentum.

The surface density profiles of the dwarf disks follow an exponential distribution in cylindrical radius R , while the vertical structure is modeled by constant-thickness, self-gravitating isothermal sheets (Spitzer 1942)

$$\rho_d(R, z) \propto \exp\left(-\frac{R}{R_d}\right) \text{sech}^2\left(\frac{z}{z_d}\right), \quad (2)$$

where R_d and z_d denote the radial scale length and the (sech^2) vertical scale height of the disk, respectively. The phase-space DF of the disk is fully determined once the disk velocity ellipsoid is specified. The radial velocity dispersion, $\sigma_R(R)$, is assumed to be exponential with $\sigma_R^2(R) = \sigma_{R0}^2 \exp(-R/R_d)$, where σ_{R0} denotes the central radial velocity dispersion. The disk azimuthal dispersion, $\sigma_\phi(R)$, is related to $\sigma_R(R)$ via the epicycle approximation (Binney & Tremaine 2008), while the vertical velocity dispersion, $\sigma_z(R)$, is set by the requirement that the adopted value of the scale height z_d is maintained in the total potential of the galaxy model. Here we parametrize the disk thickness as z_d/R_d and the disk mass as a given fraction, m_d , of the halo mass, M_h . For simplicity, we also assume a constant value of $\sigma_{R0} = 10 \text{ km s}^{-1}$ for all our dwarf models. This choice results in a decreasing ratio of V_{rot}/σ_* with decreasing mass, where V_{rot} and σ_* denote the stellar rotational velocity and line-of-sight central velocity dispersion, a trend that is indeed observed in dIrrs of the LG (Mateo 1998).

Our goal is to assess the degree to which the structure of late-type disk dwarfs can influence their tidal evolution inside their host galaxies. For this reason, we generated a number of dwarf galaxy models that differed in a number of important structural parameters, including the disk thickness, mass, and scale length, and the halo mass and concentration parameter. To investigate the impact of all these quantities on the tidal evolution of the dwarfs, we first constructed a “reference” or “default” dwarf galaxy model and subsequently initialized additional models by varying (increasing and decreasing) all relevant parameters in a systematic way, modifying only one at a time. Throughout the paper, we compare the effect of changing a single parameter in three distinct dwarf models, namely the reference one and those with the largest and smallest values of a given parameter. We also stress that we do not attempt any explicit rescaling of our dwarf galaxy models with redshift to account for the cosmic epoch at which the dwarfs were accreted by their hosts, as was done in previous studies (Mayer et al. 2001a,b). On the one hand, this allows us to avoid any uncertainties regarding the applicability of such scalings to dwarf galaxies. On the other hand, our systematic parameter survey aims to address different choices for the basic structural parameters of the progenitors of present-day dSphs. As such, it should account to at least a certain extent for the wide diversity of dwarf galaxy structures expected at various cosmological epochs.

In total, we constructed 11 high-resolution numerical models of rotationally-supported dwarfs, which we denote D1-D11. The initial structural parameters of these models are listed in Table 1 (see § 2.4 for details on how the parameters

TABLE 1
INITIAL STRUCTURAL PARAMETERS OF THE DWARF GALAXY MODELS

Model	z_d/R_d	m_d (M_h)	λ	c	M_h ($10^9 M_\odot$)	r_s (kpc)	R_d (kpc)	Q	V_{\max} (km s^{-1})	r_{\max} (kpc)	M/L (M_\odot/L_\odot)	V_{rot}/σ_*	β	A_2	b/a	c/a
(1)	(2)	(3)	(4)	(5)	(6)	(7)	(8)	(9)	(10)	(11)	(12)	(13)	(14)	(15)	(16)	(17)
D1	0.2	0.02	0.040	20	1	1.29	0.41	3.93	19.8	2.07	29.5	2.93	0.15	0	1.00	0.12
D2	0.1	0.02	0.040	20	1	1.29	0.41	3.90	19.9	2.12	30.4	3.04	0.29	0	1.00	0.06
D3	0.3	0.02	0.040	20	1	1.29	0.41	3.91	19.8	2.19	31.1	2.85	0.02	0	1.00	0.18
D4	0.2	0.01	0.040	20	1	1.29	0.41	7.60	19.4	2.44	64.3	2.85	0.21	0	1.00	0.12
D5	0.2	0.04	0.040	20	1	1.29	0.41	2.05	21.0	1.69	14.2	3.06	0.03	0	1.00	0.13
D6	0.2	0.02	0.024	20	1	1.29	0.25	2.25	19.8	1.99	27.2	2.71	0.05	0	1.00	0.11
D7	0.2	0.02	0.066	20	1	1.29	0.66	6.32	19.8	2.32	35.8	3.06	0.27	0	1.00	0.12
D8	0.2	0.02	0.040	10	1	2.58	0.41	2.97	16.5	4.54	42.4	2.07	0.27	0	1.00	0.10
D9	0.2	0.02	0.040	40	1	0.65	0.41	5.00	24.8	1.19	32.6	3.78	0.13	0	1.00	0.13
D10	0.2	0.02	0.040	20	0.2	0.76	0.24	7.95	11.6	1.29	31.2	1.38	0.58	0	1.00	0.12
D11	0.2	0.02	0.040	20	5	2.21	0.70	2.14	32.0	3.52	25.9	4.38	-0.51	0	1.00	0.12

NOTES.—The quantities in each column are as follows. Column 1: Dwarf galaxy model. Column 2: Scale height of the disk of the dwarf in units of the disk radial scale length, R_d . Column 3: Mass of the disk of the dwarf in units of the mass of the dwarf halo, M_h . Column 4: Spin parameter of the DM halo of the dwarf used to determine the scale length of the dwarf disk (see text for details). The corresponding disk scale lengths are listed in column 8. Column 5: Concentration parameter of the DM halo of the dwarf. Column 6: Mass of the DM halo of the dwarf in units of $10^9 M_\odot$. This parameter is equivalent to the cosmologically-motivated virial mass. Column 7: Scale radius of the DM halo of the dwarf in kpc. Column 8: Radial scale length of the disk of the dwarf in kpc. Column 9: Toomre stability parameter of the dwarf disk at $R = 2.5R_d$. Column 10: Maximum circular velocity of the dwarf in kms^{-1} . Column 11: Radius at which the maximum circular velocity occurs in kpc. Column 12: Mass-to-light ratio of the dwarf in units of M_\odot/L_\odot . Column 13: Ratio of stellar rotational velocity to one-dimensional stellar velocity dispersion of the dwarf. Column 14: Anisotropy parameter of the stellar distribution of the dwarf. Column 15: Amplitude of the $m = 2$ Fourier component of the surface density distribution of the dwarf stars. Column 16: Axis ratio b/a of the stellar component of the dwarf. Column 17: Axis ratio c/a of the stellar component of the dwarf. See § 2.4 for details on how the parameters listed in columns 12-17 are calculated. Note that the entries in these columns are computed within r_{\max} .

corresponding to columns (12)-(17) of this table are calculated). Particular emphasis should be placed on column 4 of this table which lists the dimensionless spin parameters of the dwarf DM halos, λ . This parameter is a measure of the total energy content of a DM halo stored in rotation and it is defined as $\lambda \equiv J|E|^{1/2}/GM^{5/2}$ (Peebles 1969), where J is the total angular momentum, E is the binding energy, and M is the mass of the halo. Although our halos are non-rotating, we still employ the parameter λ to assign scale lengths to the dwarf disks. This is because the disk scale length is not a free parameter in our modeling, but rather is derived via the semi-analytic model of Mo et al. (1998) for the structure of disk galaxies in the Λ CDM paradigm⁶. According to this model, the baryons settle into a rotationally supported structure whose scale length is determined by the mass, spin parameter and concentration of the DM halo, and the fraction of mass and angular momentum in baryons relative to that of the halo. Assuming that the specific angular momentum of baryons is conserved during their infall and that the halo and baryons start with the same specific angular momentum, R_d is uniquely determined in our models by M_h , λ , c , and m_d . We note that the Widrow & Dubinski (2005) method for building disk galaxies does not explicitly take into account the adiabatic contraction of the halo in response to the slow accumulation of the baryons (e.g., Blumenthal et al. 1986). Therefore, in order to be consistent, we derive the values for the disk scale lengths without considering this effect. In summary, the

values of λ that we discuss throughout this study do not reflect the angular momentum content of the DM halos, but rather serve the practical purpose of enabling us to derive the values of R_d in the dwarf disks according to Mo et al. (1998).

Our reference dwarf model D1 is characterized by the following values for the adopted set of parameters: $z_d/R_d = 0.2$, $m_d = 0.02$, $\lambda = 0.04$, $c = 20$, and $M_h = 10^9 M_\odot$. The details of how we varied these values in our simulation campaign are described in each relevant subsection of § 4. In what follows, we motivate the choices for the default values of the various parameters in dwarf model D1. Our choices are mainly guided by studies of the properties of cosmological halos.

Using a constrained simulation of the LG, Klimentowski et al. (2010) studied the distribution of subhalo masses at the time of infall onto the primary as a function of redshift. These authors found that a significant fraction of satellites that were accreted by their hosts since $z \lesssim 2$ and survived until the present time had masses of $\approx 10^9 M_\odot$ (see Figure 8 of Klimentowski et al. 2010). Assuming a concordance Λ CDM model, the median concentration value for a $z = 0$ cosmological halo at this mass scale is $c \approx 20$ (e.g., Bullock et al. 2001b; Macciò et al. 2007). In addition, both observational and theoretical evidence suggests that dwarf galaxies are not formed as thin disks, but rather are born as thick, puffy systems (e.g., Dalcanton et al. 2004; Kaufmann et al. 2007). This is a consequence of the greater importance of feedback processes and turbulent motions in dwarf galaxies. We take this expectation into account by conservatively adopting $z_d/R_d = 0.2$, instead of the typical value $z_d/R_d = 0.1$ employed throughout the literature which would be more appropriate for massive disk galaxies (e.g., Kregel et al. 2002).

As has been established by a large number of studies, the distribution of halo spin parameters in N -body simulations is well described by a log-normal distribu-

⁶ In reality, the Mo et al. (1998) formalism and its assumptions for the formation of galactic disks may be inappropriate at the scales of dwarf galaxies. This is due to the greater importance of thermal over rotational support in such low-mass systems which modify the simple analytic scalings of Mo et al. (1998). Nonetheless, given that our purpose is not to derive exact scale lengths for our dwarf galaxies but simply to determine the degree to which the tidal evolution of disk galaxies is affected by the sizes of their disks, following Mo et al. (1998) is reasonable and does not bias our results in any way.

tion, with median values of $\lambda_{\text{med}} \approx 0.04$ and dispersions of $\sigma_\lambda \sim 0.5$ (e.g., Bullock et al. 2001a; Shaw et al. 2006; Macciò et al. 2007; Bett et al. 2007; Macciò et al. 2008). According to Macciò et al. (2007) (see also Bett et al. 2007 and Macciò et al. 2008), the distribution of halo spins shows no dependence on halo mass. We stress that this conclusion does hold for halos with masses of the order of $\sim 10^9 M_\odot$ that we consider here (A. Macciò 2010, private communication). Lastly, we choose the default value for the disk mass fraction of our dwarfs equal to $m_d = 0.02$. This value is much lower than the universal baryon fraction but quite typical for present-day low surface brightness (LSB) or dIrr galaxies (e.g., Jimenez et al. 2003; Geha et al. 2006; Oh et al. 2008), and is also in agreement with results of hydrodynamical simulations of dwarf galaxy formation (e.g., Tassis et al. 2003; Governato et al. 2010).

For each dwarf galaxy model, we generated an N -body realization containing a total of 2.2 million particles ($N_h = 10^6$ DM particles and $N_d = 1.2 \times 10^6$ disk particles). The gravitational softening was set to $\epsilon_h = 60$ pc and $\epsilon_d = 15$ pc for the particles in the two components, respectively. The process of transforming a disk dwarf into a dSph via tidal stirring is fairly complex and depends on a number of subtle dynamical effects (e.g., Mayer et al. 2001a). It is thus important to establish both the quality and the sufficient resolution of our dwarf galaxy models. For this reason, we evolved all dwarf galaxies in isolation for a period of 10 Gyr. These test simulations revealed that the dwarfs retained their equilibrium configuration within the adopted force resolution over the timescales of the experiments. Therefore, our models should be largely unaffected by both two-body relaxation and artificial numerical heating of the dwarf disk through interactions with the massive particles of the dwarf halo. The same simulations also confirmed the stability of all dwarf galaxy models against bar formation. Thus, any significant bar growth identified in the dwarfs during the course of the numerical experiments should be the result of the tidal field of the host galaxy, rather than a consequence of noise present in the initial conditions. All of these precautions imply that our dwarf galaxy models should indeed be adequate to resolve the generic tidal evolution of late-type disk dwarfs and to elucidate their transformation via tidally-induced dynamical instabilities and impulsive tidal heating.

2.2. Primary Galaxy Model

Another improvement we introduce in the present study is the fact that we employ self-gravitating primary galaxies as opposed to static host potentials adopted in the majority of earlier related investigations. The motivation behind this choice is twofold. First and most importantly, live primary galaxies can trigger instabilities in the disks of the dwarfs, that otherwise may not develop, and which could influence the dynamical and morphological evolution of the dwarf galaxies themselves (Weinberg & Blitz 2006). Second, by representing the host galaxies as a distribution of interacting particles, we enable the dwarf galaxies to suffer dynamical friction. As a result of a progressively decaying orbit, the mass loss and tidal stripping experienced by the dwarfs will be enhanced with obvious consequences for their dynamical evolution inside the host.

For simplicity, we assume a single primary galaxy with the present-day structural properties of the MW. In particular, we employ model MWb of Widrow & Dubinski (2005), which satisfies a broad range of observational constraints for the

MW galaxy. Specifically, the exponential stellar disk has a mass of $M_D = 3.53 \times 10^{10} M_\odot$, a radial scale length of $R_D = 2.82$ kpc, and a sech² scale height of $z_D = 400$ pc. The bulge which follows the Hernquist (1990) density profile has a mass and a scale radius of $M_B = 1.18 \times 10^{10} M_\odot$ and $a_B = 0.88$ kpc, respectively. The DM halo has an NFW profile with a tidal radius of $R_H = 244.5$ kpc, a mass of $M_H = 7.35 \times 10^{11} M_\odot$, and a scale radius of $r_H = 8.82$ kpc.

The simulations reported here use $N_D = 10^6$ particles in the disk, $N_B = 5 \times 10^5$ in the bulge, and $N_H = 2 \times 10^6$ in the DM halo of the host galaxy, and employ a gravitational softening of $\epsilon_D = 50$ pc, $\epsilon_B = 50$ pc, and $\epsilon_H = 2$ kpc, respectively. The choice for the fairly large softening in the DM particles of the primary galaxy was motivated by our desire to minimize discreteness noise in the host potential. Such noise may lead to spurious two-body heating between the excessively massive halo particles of the primary galaxy and those of the dwarf disk, potentially interfering with the interpretation of our results. In order to confirm the adequacy of our choice for ϵ_H , we placed the reference dwarf model D1 at rest at various distances inside the host galaxy and monitored the changes of its basic properties (e.g., surface density, velocity dispersions, thickness) as a function of time. The evolution of the structural parameters within radii of interest (see § 2.4 below) was found to be fairly small, specifically $\lesssim 20\%$, during a period of several Gyr. This indicates that the chosen numerical parameters are indeed appropriate to suppress the effect of two-body heating between the halo particles of the primary galaxy and those of the dwarf disk.

2.3. Description of Tidal Stirring Simulations

Our simulation campaign comprised 17 numerical experiments, which we denote R1-R17, of the tidal interactions between rotationally-supported dwarf galaxies and their hosts. Table 2 provides a summary of all simulations we performed in this study. The various dwarf galaxy models are placed on bound orbits inside the primary galaxy. Except for varying the initial structure of the disk dwarf galaxies, we also investigated the degree to which their tidal evolution is affected by the orbital parameters and, in particular, on the sizes and the eccentricities of the dwarf orbits.

The size of the orbit is expected to be crucial for the efficiency of tidal stirring, since the tidal force exerted by the primary galaxy depends strongly on the distance from its center. To explore this effect, we conducted a set of simulations where the default dwarf galaxy model D1 is placed on three orbits with different sizes. Although the orbits of LG dwarfs are currently poorly constrained observationally, their current distances, which give an indication of the apocenters of their orbits, coupled with studies of the orbital properties of cosmological halos, can be used to inform our choices. Indeed, using a cosmological simulation of the LG, Klimentowski et al. (2010) studied the orbital distribution of present-day satellites that were identified inside the virial radius of their hosts and had completed at least one orbit around them. These authors found that a significant fraction of this satellite population had apocentric distances between $r_{\text{apo}} \approx 250$ and ≈ 85 kpc, with typical values of $r_{\text{apo}} \approx 125$ kpc (see Figure 6 of Klimentowski et al. 2010). Adopting $R_{\text{vir}} \approx 250$ kpc as the virial radius of the MW halo at $z = 0$ (e.g., Klypin et al. 2002), the previous numbers would roughly correspond to R_{vir} , $R_{\text{vir}}/3$, and $R_{\text{vir}}/2$. The value $r_{\text{apo}} = 125$ kpc also approximately matches the virial radius of the MW halo at $z \sim 1$ (e.g., Wechsler et al. 2002). A critical reader may note that

TABLE 2
SUMMARY OF SIMULATIONS

Simulation (1)	Dwarf Model (2)	r_{apo} (kpc) (3)	r_{peri} (kpc) (4)	$r_{\text{apo}}/r_{\text{peri}}$ (5)	i (deg) (6)	z_d/R_d (7)	m_d (M_h) (8)	λ (9)	c (10)	M_h ($10^9 M_\odot$) (11)
R1	D1	125	25	5	45	0.2	0.02	0.040	20	1
R2	D1	85	17	5	45	0.2	0.02	0.040	20	1
R3	D1	250	50	5	45	0.2	0.02	0.040	20	1
R4	D1	125	12.5	10	45	0.2	0.02	0.040	20	1
R5	D1	125	50	2.5	45	0.2	0.02	0.040	20	1
R6	D1	125	25	5	0	0.2	0.02	0.040	20	1
R7	D1	125	25	5	90	0.2	0.02	0.040	20	1
R8	D2	125	25	5	45	0.1	0.02	0.040	20	1
R9	D3	125	25	5	45	0.3	0.02	0.040	20	1
R10	D4	125	25	5	45	0.2	0.01	0.040	20	1
R11	D5	125	25	5	45	0.2	0.04	0.040	20	1
R12	D6	125	25	5	45	0.2	0.02	0.024	20	1
R13	D7	125	25	5	45	0.2	0.02	0.066	20	1
R14	D8	125	25	5	45	0.2	0.02	0.040	10	1
R15	D9	125	25	5	45	0.2	0.02	0.040	40	1
R16	D10	125	25	5	45	0.2	0.02	0.040	20	0.2
R17	D11	125	25	5	45	0.2	0.02	0.040	20	5

NOTES.—Columns 3-5 refer to the initial orbital parameters of the disk dwarfs. Columns 7-11 list the initial structural parameters of the dwarf galaxy models. The quantities in each column are as follows. Column 1: Abbreviation for the tidal stirring simulations. Column 2: Dwarf galaxy model. Column 3: Apocentric distance of the orbit of the dwarf in kpc. Column 4: Pericentric distance of the orbit of the dwarf in kpc. Column 5: Eccentricity of the orbit of the dwarf. Column 6: Inclination of the disk of the dwarf with respect to the orbital plane in degrees. Column 7: Scale height of the disk of the dwarf in units of the disk radial scale length, R_d . Column 8: Mass of the disk of the dwarf in units of the mass of the dwarf halo, M_h . Column 9: Spin parameter of the DM halo of the dwarf used to determine the scale length of the dwarf disk (see text for details). The corresponding disk scale lengths are listed in column 8 of Table 1. Column 10: Concentration parameter of the DM halo of the dwarf. Column 11: Mass of the DM halo of the dwarf in units of $10^9 M_\odot$. This parameter is equivalent to the cosmologically-motivated virial mass.

the characteristic orbits of the $z = 0$ subhalo population that we have considered may not be representative of those at the time of satellite infall onto the primary. This is especially true for systems that are accreted at high redshift ($z \gtrsim 1$). Given the complexity of halo formation in a cosmological context, this is a valid concern. While addressing this issue is certainly beyond the scope of the present paper, we note that at least dynamical friction should not have a major effect, if any, in altering the orbits of satellites with masses of the order of $\sim 10^9 M_\odot$ that we have adopted here (Colpi et al. 1999).

Motivated by the previous discussion, we adopt $r_{\text{apo}} = 125$, 85, and 250 kpc as the apocentric distances of the dwarfs in the experiments with different sizes of orbits. We refer to these simulations as “R1”, “R2”, and “R3”, respectively, and discuss them in § 3.1. Fixing the eccentricity of the orbits will determine the corresponding pericentric distances. Specifically, we adopt an eccentricity of $r_{\text{apo}}/r_{\text{peri}} = 5$, close to the median ratio of apocentric to pericentric radii found in cosmological N -body simulations (e.g., Ghigna et al. 1998; Diemand et al. 2007). Interestingly, the pericentric distance of the tightest orbit with $r_{\text{peri}} = 17$ kpc roughly corresponds to that inferred for the Sagittarius dwarf galaxy (e.g., Law et al. 2005). In addition, the pericentric distance of the most extended orbit with $r_{\text{peri}} = 50$ kpc is similar to that of the Large Magellanic Cloud (LMC), provided that the LMC has just crossed the pericenter of its orbit around the MW (Besla et al. 2007). Given the typical parameters associated with experiment R1, throughout this work we refer to it as the “reference” or “default” simulation that we use as the basis for the comparison with other experiments.

Apart from the size of the orbit, we also investigate the impact of the orbital eccentricity on the tidal transformation

of the dwarfs. Cosmological simulations (e.g., Ghigna et al. 1998; Diemand et al. 2007; Klimentowski et al. 2010). indicate that satellite orbits range from nearly circular ($r_{\text{apo}}/r_{\text{peri}} \approx 1$) to highly eccentric ($r_{\text{apo}}/r_{\text{peri}} \gtrsim 10$). On high-eccentricity orbits, the effective duration of the tidal shock becomes so short that the response of the system is prone to be impulsive rather than adiabatic and, as a result, tidal heating is particularly efficient (e.g., Gnedin et al. 1999). To this end, we considered two additional simulations in which we placed the dwarf galaxy model D1 on a highly and a mildly eccentric orbit, respectively. In particular, we considered orbits with eccentricities that were by a factor of 2 larger ($r_{\text{apo}}/r_{\text{peri}} = 10$) and smaller ($r_{\text{apo}}/r_{\text{peri}} = 2.5$) compared to that of R1. We refer to these experiments as “R4” and “R5” (see Table 2) and discuss them in § 3.2. In order to meaningfully compare the results of this set of simulations, we kept the apocentric distance of the reference experiment R1 constant ($r_{\text{apo}} = 125$ kpc). The desired value of eccentricity is then achieved by simply varying the pericentric distance, r_{peri} . This modeling results in a pericentric distance of $r_{\text{peri}} = 12.5$ kpc in simulation R4, which is the smallest in all experiments we performed in the present study.

Initial conditions for the tidal stirring experiments were generated by building models of dwarf galaxies and placing them at the apocenters of their orbits. In the coordinate system chosen to describe the simulations, the orbital plane is the xy plane, and the center of mass of the combined system of dwarf and primary coincides with the coordinate origin. We stress that we did not impose any truncation in the density distribution of the dwarfs (i.e., at the corresponding Jacobi tidal radius) to reflect their placement in the host tidal field. In addition, the dwarf galaxies are not grown adiabatically in their

orbits, but rather are introduced in the simulations directly. We have explicitly checked that this set of assumptions does not bias our results. Indeed, the initial starting positions of the dwarfs correspond to a rather low density in the host galaxy. This results in a fairly weak tidal perturbation that does not affect the very inner regions of the dwarf, which constitute the primary target of the present study.

According to the LG cosmological simulation of Klimentowski et al. (2010), most satellites that survived until the present time and whose masses at the epoch of infall onto the primary were in the range that we consider here (around $10^9 M_\odot$), entered their hosts at $z \lesssim 2$. Motivated by this finding, we follow the tidal evolution of the dwarfs inside their host galaxies for 10 Gyr. In the great majority of our experiments, the alignments of the internal angular momentum of the dwarf, that of the primary disk and the orbital angular momentum were all mildly prograde and equal to 45° . We discuss the implications of this choice in § 5.6 but emphasize at the outset that our results should not be affected by any strong coupling of angular momenta.

Lastly, all numerical experiments discussed in this work were performed with PKDGRAV, a multisteping, parallel, tree N -body code (Stadel 2001). In all experiments, we set the base time step to be equal to 1% of the dynamical time at the half-mass radius of the dwarf model and allowed the individual particle time steps to be at most a factor of 2^{20} smaller. The time integration was performed with high enough accuracy such that the total energy was conserved to better than 0.5% in all cases, which is adequate for the type of study that we undertake in this paper. As we have already stated, our main goal is to investigate the dynamical evolution of the dwarfs which is driven by the response of their inner regions to the tidal shocks. The total energy contained in the inner parts of our dwarf models is a few percent of that of the entire system, so the accuracy of the energy conservation must be at least comparable to that in order to resolve meaningfully the dynamics of the region of interest.

2.4. Parameters of Relevance

In order to illustrate the evolution of the intrinsic, global properties of the dwarf galaxies as they orbit inside their hosts, we calculated a set of parameters as a function of time. Specifically, we examined the degree to which the mass, size, shape, and kinematics of the dwarfs is affected subject to the strong tidal field of the primary galaxy.

For each simulation output, we first constructed the circular velocity profile of the dwarf galaxy, $V_c(r) = [GM(< r)/r]^{1/2}$, where $M(< r)$ is the spherically-averaged total mass profile about its center. As a measure of how the mass of the dwarf is affected at any stage, we employed the maximum circular velocity, V_{\max} , which reflects the mass distribution in the inner regions and is a commonly adopted quantity throughout the literature. The attractive feature of V_{\max} is that it is well defined and allows us to overcome difficulties regarding the determination of the tidal radius (e.g., Read et al. 2006b).

In order to demonstrate how the size of the dwarf galaxy is affected by tides, we investigated the evolution of the radius at which V_{\max} occurs, r_{\max} . Following Klimentowski et al. (2009a), we chose r_{\max} as the characteristic scale where we computed the remaining properties of the dwarfs. This radius is large enough to include a significant fraction of the mass of the dwarf at all times, while at the same time is small enough not to be affected by the tidal tails (see Klimentowski et al. 2007, 2009b). Due to the fact that tidal stripping truncates

the dwarf galaxies at increasingly smaller physical radii, this characteristic radius decreases with time, from a few kpc initially down to a fraction of a kpc at the end of the evolution.

Because of the copious amounts of DM in dSphs, another quantity of particular interest is the mass-to-light ratio, M/L . Since the bulk of the stellar populations in these galaxies is old ($t \gtrsim 8-10$ Gyr; see, e.g., Grebel 2000), we chose to calculate the M/L ratio by conservatively adopting a fixed stellar mass-to-light ratio of $(M/L)_* = 3M_\odot/L_\odot$ (e.g., Schulz et al. 2002). We note that while such values for $(M/L)_*$ should be appropriate for the present time, they may not be necessarily representative for the whole evolution, as the dwarfs might undergo periodic bursts of star formation triggered by tidal compression at pericentric passages (Mayer et al. 2001a). However, for dwarf galaxies accreted by their hosts as early as 10 Gyr ago, as assumed here, most of the gas should be quickly stripped by ram pressure aided by the cosmic ionizing background radiation (Mayer et al. 2007). As a result, star formation should cease soon after the dwarfs are accreted by the host galaxy. In addition, using the stellar population synthesis models of Bruzual & Charlot (1993), Mayer et al. (2001a) showed that even when a burst of star formation occurs at first pericentric approach, the final $(M/L)_*$ ratio would correspond to that of an old stellar population after 7–8 Gyr of evolution inside the primary potential. This is because the effect of the newly-formed population on the $(M/L)_*$ ratio and on the color of the dwarf galaxy diminishes quite rapidly. The above discussion suggests that the assumption of $(M/L)_* = 3M_\odot/L_\odot$ in the present study is fairly reasonable.

Obviously, one of the most representative properties of dSphs is their spheroidal shape. We quantified the shape of the stellar component by calculating the moments of the inertia tensor for all stars within r_{\max} and deriving principal axis ratios b/a and c/a , where a , b , and c denote the major, intermediate, and minor axis of the stellar distribution, respectively. Another interesting quantity which can illuminate the dynamical and morphological evolution of the dwarf galaxies inside their hosts, is the amplitude of the $m = 2$ Fourier component of the stellar surface density distribution, A_2 , given by

$$A_2 = \frac{1}{N} \left| \sum_{j=1}^N e^{2i\phi_j} \right|. \quad (3)$$

Here ϕ_j denotes the two-dimensional cylindrical polar angle coordinate of particle j projected onto the xy plane (along the shortest axis) and the summation is performed over all stars within r_{\max} . The motivation behind studying the evolution of A_2 is twofold. First, it can be used as an auxiliary measure of the shape of the stellar component since the triaxiality parameter, $T = (a^2 - b^2)/(a^2 - c^2)$ (Franx et al. 1991), can be very noisy for systems close to spherical symmetry. We note, however, that A_2 can still be ambiguous as its value is close to zero for both nearly spherical and disk shapes. Second, as we discuss below, in the majority of cases we studied, the strong tidal shocks at pericentric passages trigger the formation of bars in the disks of the dwarfs. The parameter A_2 will allow us to determine when a bar forms and to quantify the strength of the bar instability.

For the purposes of the present study, we designate the formation of a bar when the amplitude of the $m = 2$ Fourier component satisfies $A_2 \gtrsim 0.2$ between two consecutive pericentric passages, namely for one full orbital period of the dwarf around its host. These conditions ensure that any tidally-induced bars that we detect in our simulations will be rela-

tively strong (see, e.g., Debattista et al. 2006 for even weaker bars in isolated disk galaxies). They also guarantee that any temporary increase of A_2 , when the dwarfs are strongly elongated by tidal forces at the pericenters of the orbit, will not be ascribed to a true bar instability.

dSphs are low-angular momentum systems, as highlighted by their low ratio of rotational velocity to line-of-sight central velocity dispersion, $V_{\text{rot}}/\sigma_* \lesssim 1$ (e.g., Mateo 1998). It is thus important to investigate the evolution of the kinematics in the tidally-stirred disk dwarfs. To this end, after determining the directions of the principal axes of the stellar component in each output, we introduced a spherical coordinate system (r, θ, ϕ) so that the z -axis is along the shortest axis of the stellar distribution and the angle ϕ is computed on the xy plane. We measured the kinematics of the dwarfs within r_{max} by calculating the rotational velocity around the shortest axis $V_{\text{rot}} = V_\phi$ and the dispersions σ_r, σ_θ and σ_ϕ around the mean values. We combined these dispersions into the one-dimensional stellar velocity dispersion parameter, $\sigma_* \equiv [(\sigma_r^2 + \sigma_\theta^2 + \sigma_\phi^2)/3]^{1/2}$, which we adopted as a measure of the amount of random motions in the stars. We note that throughout this paper we compare the derived values of σ_* with those of observed dSphs. Defining σ_* as an average over three directions makes such comparisons more meaningful, since the observed one-dimensional stellar velocity dispersions depend on the random line-of-sight.

Another illuminating quantity related to stellar kinematics is the anisotropy parameter, $\beta \equiv 1 - \sigma_r^2/2\sigma_t^2$, where σ_r and $\sigma_t = (\sigma_\theta^2 + \sigma_\phi^2)^{1/2}$ denote the radial and tangential velocity dispersion, respectively. This quantity describes the degree of anisotropy of the velocity distribution by indicating the amount of radial ($\beta = 1$) versus circular ($\beta \rightarrow -\infty$) orbits in the stellar population. We stress that this parameter cannot be measured directly from observations, but only determined by dynamical modeling (e.g., Łokas 2002). Given that a well established range for the velocity anisotropy of observed dSphs does not yet exist, our simulations can provide useful predictions for the possible values of β in such systems.

2.5. Classification Criteria

The goal of the present study is to determine the conditions under which systems with the properties of dSphs can be produced via the tidal interactions between disk dwarfs and their host galaxies. Observed dSphs possess a unique set of kinematic and structural properties that we can utilize in order to perform comparisons with simulated dwarfs. In particular, we imposed two criteria for establishing the formation of a dSph in our simulations.

The first criterion is related to the shape of the stellar component. Specifically, only simulated dwarf galaxies whose final states are characterized by $c/a \gtrsim 0.5$ may be regarded as dSphs. The motivation behind this choice stems from the fact that most classic dSphs (e.g., Fornax, Draco, Leo I, Tucana, Sextans, Carina) have projected ellipticities, $\epsilon \equiv 1 - b/a$, in the range $0.1 \lesssim \epsilon \lesssim 0.5$ (e.g., Mateo 1998; McGaugh & Wolf 2010), or equivalently projected axis ratios $b/a \gtrsim 0.5$, where b and a denote the minor and major axis of the stellar distribution, respectively. Given that an elongated shape cannot appear more elongated in projection, the condition that *intrinsic* $c/a \gtrsim 0.5$ in the simulated dwarfs (n.b. by definition $b/a \geq c/a$) ensures that the *projected* b/a will also satisfy $b/a \gtrsim 0.5$ in any possible projection, in accord with the values inferred for observed dSphs. We note that the intrinsic

axis ratios of the dwarf remnants do not vary significantly with radius. Thus, they are appropriate for comparisons with observed ellipticities that are not computed within r_{max} , but rather estimated either at the outer parts of the stellar distribution (Mateo 1998) or within some observationally-defined radius (e.g., half-light radius).

The second classification criterion is related to the kinematics of the stellar component. In particular, we classify as dSphs only those systems which, after 10 Gyr of evolution inside the primary galaxy, exhibit $V_{\text{rot}}/\sigma_* \lesssim 1$ in accordance with the results of observational studies of classic dSphs (e.g., Mateo 1998). We stress that the values we compute for V_{rot} and σ_* are fairly close to what an observer would measure using line-of-sight velocities, making the comparison with observations reasonable. Indeed, at r_{max} the rotation is close to the maximum value and can be readily measured if the line-of-sight is perpendicular to the rotation axis. Moreover, the velocity dispersion profiles of our remnants do not strongly vary with radius (as well as with line-of-sight) suggesting that our derived values for σ_* should not differ significantly from those of the central velocity dispersion commonly used by observers. As a result of all these facts, the condition $V_{\text{rot}}/\sigma_* \lesssim 1$ that we impose here guarantees that $V_{\text{rot}}/\sigma_* \lesssim 1$ will also be satisfied for a significant fraction, if not all, of random lines-of-sight.

Overall, for the purposes of the present study, the above classification scheme is adequate to establish the formation of a dSph in our simulations. A more direct comparison between theoretical and observational measurements for the properties of dSphs will be performed in a companion paper (Łokas et al. 2010, in preparation).

3. EFFICIENCY OF TIDAL STIRRING AND ORBITAL PARAMETERS OF THE PROGENITOR DISKY DWARFS

In this section, we gauge the dependence of the efficiency of tidal stirring on the orbital parameters of the progenitor rotationally-supported dwarfs, and in particular, on the size and eccentricity of their orbits.

3.1. Size of the Orbit

We first investigate the degree to which the tidal evolution of a disk dwarf is affected by the size of its orbit. The size of the orbit should be crucial for the outcome of tidal stirring since the tidal force depends strongly on the distance of the dwarf from the center of the host galaxy. In order to ascertain this, we considered two additional simulations (R2, R3) in which we placed the dwarf galaxy model D1 on orbits with sizes that were different from that of the reference experiment R1. Specifically, in this set of simulations, we kept the eccentricity constant, but varied the default apocentric and pericentric distance by the same factor, leaving all other simulation parameters unchanged (see Table 2). Figure 1 shows the orbital trajectories of the dwarf galaxies from the respective center of their host as a function of time for experiments R1, R2, and R3. In Figure 2, we present the time evolution of the relevant parameters discussed in § 2.4 ($V_{\text{max}}, r_{\text{max}}, b/a, c/a, V_{\text{rot}}/\sigma_*, \beta, M/L$, and A_2) for the same simulations.

In order to highlight some general trends in the evolution of these quantities with time, we first focus on the reference experiment R1. As a result of the continuous action of the host galaxy tidal field, the overall structure of the orbiting dwarf is altered as it experiences a gradual decrease of its mass and physical size. This is reflected in the evolution of r_{max} and V_{max} , respectively, which are both reduced systemat-

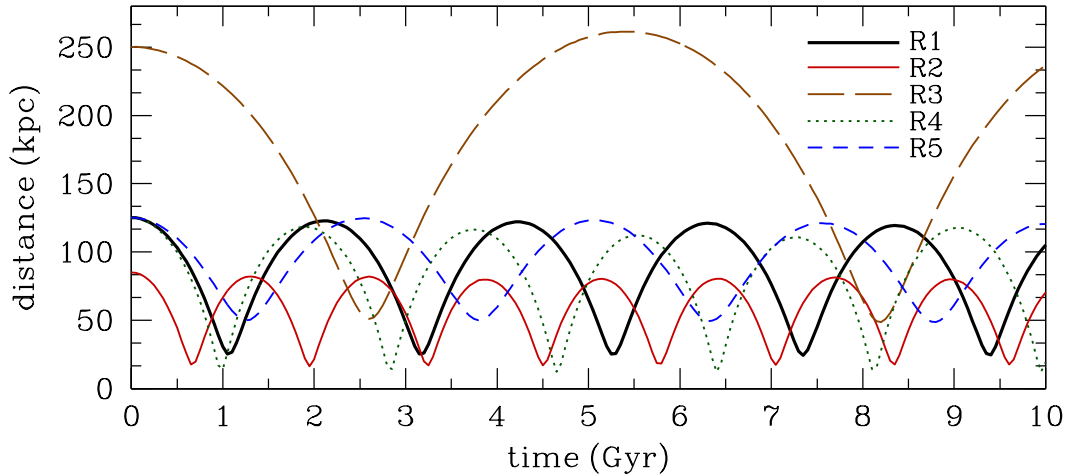


FIG. 1.— Distances of the orbiting dwarf galaxies from the centers of their hosts as a function of time. Results are presented for simulations R1-R5, where the dwarfs are characterized by different orbital parameters.

ically as a function of time. The preferential stripping of the mass from the outer, low-density regions of the dwarf galaxy leads to the adjustment of the circular velocity profile in such a way that both r_{\max} and V_{\max} decrease. The temporary but substantial increase of r_{\max} at the first pericentric approach can be attributed to the fact that the dwarf is being deformed by strong tidal forces for the first time and, as a result, its density distribution becomes very extended. This increase in r_{\max} is not observed at subsequent pericentric passages as the dwarf galaxy becomes progressively more compact during its evolution and thus the ability of the tidal field to distort it is reduced. As we show below, in cases where the dwarfs are initially more concentrated (as a result of either being embedded in halos of higher concentration or hosting more compact or massive disks) or are on wider orbits and experience weaker tidal forces, this increase in r_{\max} does not occur.

The evolution of V_{\max} shows two interesting features. First, V_{\max} decreases significantly near the pericenters of the orbit, where the intensity and variation of the time-dependent tidal force is the strongest, and the tidal shocks occur. This drop in V_{\max} is associated with mass loss from all regions of the dwarf galaxy. Because tidal shocks act on a very short timescale, even the inner regions of the dwarf, which are characterized by the highest densities and thus the shortest dynamical times, respond impulsively to the external tidal perturbation and mass is tidally stripped directly from regions within r_{\max} . However, V_{\max} also decreases because a fraction of the particles that are removed from larger radii are, in fact, on eccentric orbits with large apocentric distances. Although these particles spend most of their time outside of r_{\max} , they still contribute to the total mass in the inner regions. These are preferentially DM particles, since stars are confined to the central region of the dwarf by construction. After experiencing the tidal shock, it takes a few hundred million years, i.e., a multiple of the dynamical time of the system, for the dwarf to readjust to a new equilibrium state with a new value of V_{\max} .

Second, V_{\max} remains remarkably constant between pericentric approaches as the dwarf responds adiabatically to the weak intensity and variation of the tidal force. Overall, tides act nearly impulsively at pericentric passages and have little influence on the dwarf galaxy between pericentric passages. This general behavior of V_{\max} and r_{\max} is observed in all our simulations, and is in agreement with results reported in earlier studies (e.g., Hayashi et al. 2003; Kazantzidis et al. 2004b; Kravtsov et al. 2004; Peñarrubia et al. 2008). We note

that, in the reference experiment R1, the dwarf loses $\sim 90\%$ of its initial mass within r_{\max} during its orbital evolution but still survives as a bound entity. For such substantial mass loss, V_{\max} and r_{\max} decreased by a factor of ~ 1.7 and ~ 4 , respectively. This finding has interesting implications as it suggests that tidal stripping affects the evolution of the $r_{\max} - V_{\max}$ relation expected in the Λ CDM cosmological model (see also Kravtsov 2010).

Focusing on the evolution of the M/L ratio, which we also estimate within r_{\max} , Figure 2 shows that it decreases monotonically as a function of time. This is a consequence of two facts. First, the stellar distributions of the dwarfs are naturally less extended than their DM halos. This implies that, within r_{\max} , the particles with the smallest binding energies and longest dynamical timescales, namely the particles that are most susceptible to be unbound by the tidal shocks, belong predominantly to the extended DM halos. Second, as discussed above, particles that are stripped from the outer parts of the dwarf but still contribute to the total mass in the inner regions belong preferentially to the DM component. For these reasons, DM is stripped more readily than the stars within r_{\max} and this decreases the M/L ratio. In addition to these two processes, during the orbital evolution of the dwarfs, r_{\max} decreases monotonically and moves towards the inner, stellar-dominated regions, resulting in a natural increase of the fraction of mass in stars within r_{\max} .

The evolution of the Fourier component A_2 shows a sudden increase after the first pericentric approach which signifies the formation of a tidally-induced bar. The onset of the bar instability coincides with a drop of V_{rot}/σ_* , whose value continuously decreases thereafter. Loss of angular momentum caused by the bar and simultaneous increase of the stellar velocity dispersion due to tidal heating lead to a final value of $V_{\text{rot}}/\sigma_* \approx 0.55$. As a result of the tidal shocks, the strength of the bar diminishes as a function of time and the dwarf becomes progressively more spherical. After 10 Gyr of evolution inside the host, the initially-disky stellar distribution is transformed into a spheroid with axis ratios of $c/a \approx 0.7$ and $b/a \approx 0.9$.

In what follows, we shall concentrate on comparing the tidal response of the dwarf in the reference simulation R1 with that in experiments R2 and R3. Figure 2 demonstrates that the dependence of the evolution of r_{\max} , V_{\max} , and M/L ratio on the size of the orbit is dramatic. As expected, the tighter the orbit is, the stronger and more rapid the decrease in all param-

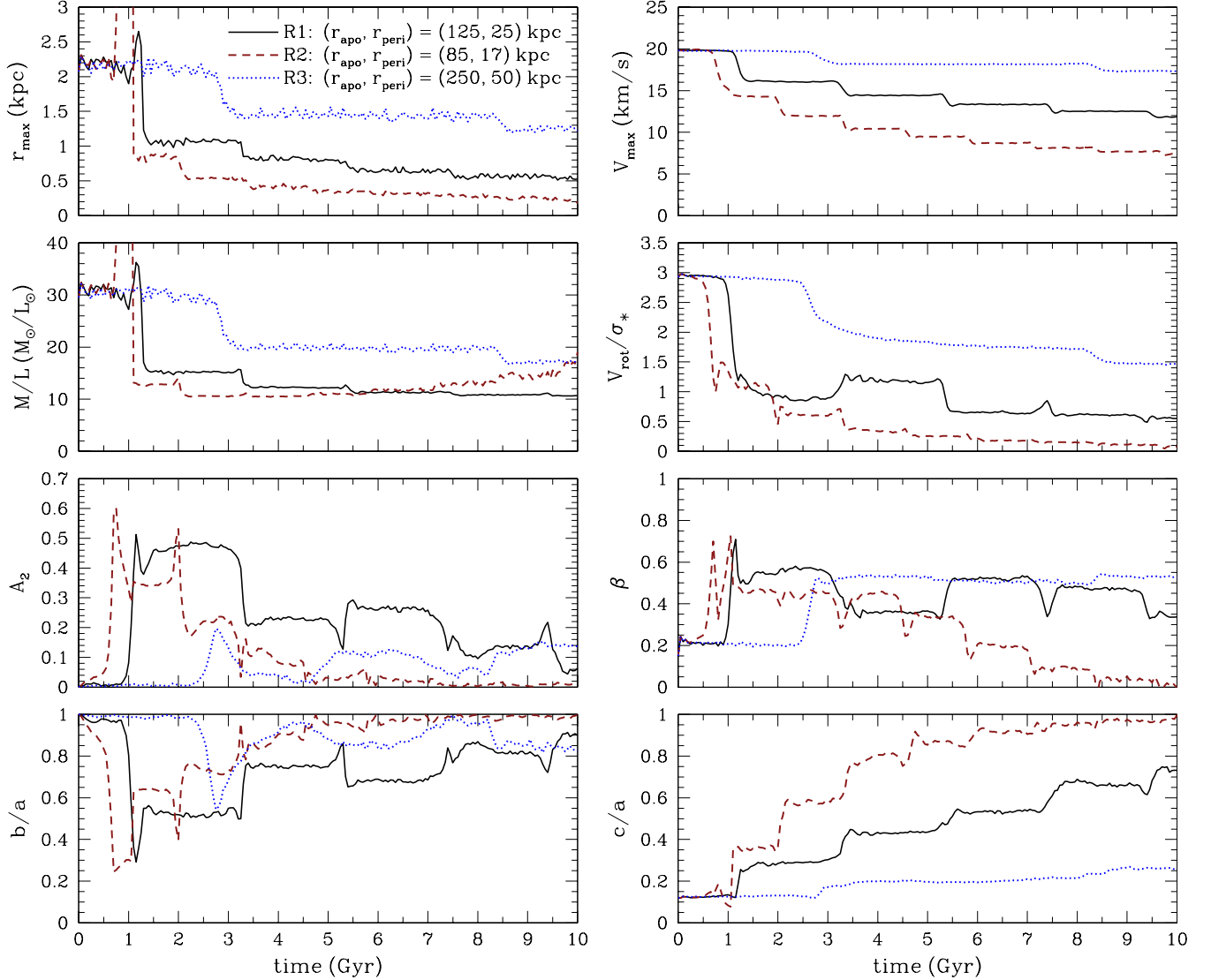


FIG. 2.— Comparison of the evolution of various parameters as a function of time illustrating the dependence of the tidal transformation of disk dwarf galaxies on the sizes of their orbits. Results are presented for the default simulation R1 and for experiments R2 and R3. The description of the simulations is presented in Table 2. For a fixed eccentricity, $r_{\text{apo}}/r_{\text{peri}}$, rotationally-supported dwarfs on tighter orbits with smaller pericentric distances, r_{peri} , exhibit stronger tidal evolution inside their host galaxies and the efficiency of their transformation into dSphs is enhanced considerably.

eters. Specifically, the dwarf galaxy in simulation R2 with the smallest pericentric distance loses $\sim 99\%$ of its initial mass within r_{max} during its orbital evolution. In this case, V_{max} and r_{max} decreased by a factor of ~ 2.7 and ~ 11.5 , respectively.

In addition, Figure 2 illustrates two interesting features in the behavior of the dwarfs in experiments R1 and R2. First, the monotonic decrease of the M/L ratio is reversed for the tightest orbit in simulation R2 during the late stages of the evolution, indicating that the stars begin to be stripped more effectively compared to the DM. Second, the systematic decrease of V_{rot}/σ_* is reversed temporarily for simulation R1 between the second and third pericentric passage. We postpone the investigation of both issues for § 5.

In the case of experiments R1 and R2, the evolution of the anisotropy parameter β reflects the transition to more radial orbits after the first pericentric approach, as the dwarfs change shapes to prolate spheroids. The stellar orbits tend to become more isotropic with time, especially for simulation R2 where the velocity distribution of the dwarf at the end is completely isotropic ($\beta \approx 0$). The velocity anisotropy of the remnant in

experiment R1 is mildly radial with $\beta \approx 0.3$.

Interestingly, the most strongly perturbed dwarf in simulation R2 is almost entirely pressure-supported ($V_{\text{rot}}/\sigma_* \lesssim 0.1$) and its final shape is also spherically-symmetric ($b/a \approx c/a \approx 1$). Furthermore, while the dwarf in experiment R2 develops a strong bar, its counterpart in simulation R3 does not. The least evolved dwarf in experiment R3 remains oblate for the whole time except for a short period after the first pericentric approach. According to the criteria described in § 2.5, the final dwarfs in simulations R1 and R2 would be classified as dSphs but the remnant in experiment R3 would not as it has a disk shape and it is still dominated by rotation ($V_{\text{rot}}/\sigma_* > 1$). It is also important to highlight the strong association between bar formation and the formation of dSphs reported in this set of simulations. Such a connection is observed in all but one of our experiments.

The final structural parameters of the simulated dwarfs after 10 Gyr of evolution inside the primary galaxy are listed in Table 3. Special emphasis should be placed on columns 10 and 11 of this table. Column 10 refers to whether a tidally-

TABLE 3
SUMMARY OF RESULTS

Simulation (1)	V_{\max} (km s^{-1}) (2)	r_{\max} (kpc) (3)	M/L (M_{\odot}/L_{\odot}) (4)	V_{rot}/σ_* (5)	β (6)	A_2 (7)	b/a (8)	c/a (9)	Bar Formation (10)	Classification (11)	T_{orb} (Gyr) (12)
R1	11.9	0.53	10.7	0.55	0.34	0.06	0.90	0.73	yes	dSph	2.09
R2	7.3	0.18	19.2	0.08	0.00	0.00	1.00	1.00	yes	dSph	1.28
R3	17.3	1.22	16.9	1.46	0.52	0.14	0.82	0.26	no	non-dSph	5.40
R4	7.2	0.24	15.3	0.03	0.03	0.03	0.95	0.94	yes	dSph	1.81
R5	16.0	0.98	14.0	1.25	0.54	0.06	0.88	0.36	no	non-dSph	2.50
R6	12.2	0.51	10.3	0.24	0.51	0.04	0.95	0.73	yes	dSph	2.09
R7	12.4	0.55	10.7	0.23	0.48	0.16	0.80	0.74	yes	dSph	2.09
R8	12.7	0.50	10.3	0.74	0.42	0.10	0.86	0.66	yes	dSph	2.09
R9	12.0	0.55	11.8	0.61	0.23	0.04	0.94	0.77	yes	dSph	2.09
R10	10.4	0.55	18.8	0.56	0.19	0.04	0.93	0.80	yes	dSph	2.09
R11	16.0	0.49	6.7	0.40	0.48	0.28	0.67	0.58	yes	dSph	2.09
R12	14.6	0.41	6.7	0.56	0.45	0.29	0.67	0.53	yes	dSph	2.09
R13	10.4	0.56	22.3	0.26	0.13	0.03	0.95	0.91	yes	dSph	2.09
R14	7.3	0.40	6.5	0.31	0.15	0.01	0.98	0.89	yes	dSph	2.10
R15	20.3	0.67	23.3	1.18	0.49	0.07	0.88	0.52	no	non-dSph	2.08
R16	7.1	0.36	11.6	0.62	0.33	0.04	0.94	0.73	no	dSph	2.14
R17	19.0	0.77	9.2	0.70	0.23	0.09	0.87	0.68	yes	dSph	1.88

NOTES.—Columns 2-9 refer to the final structural parameters of the simulated dwarfs. The quantities in each column are as follows. Column 1: Abbreviation for the tidal stirring simulations. Column 2: Maximum circular velocity of the dwarf in km s^{-1} . Column 3: Radius at which the maximum circular velocity occurs in kpc. Column 4: Mass-to-light ratio of the dwarf in units of M_{\odot}/L_{\odot} . Column 5: Ratio of stellar rotational velocity to one-dimensional stellar velocity dispersion of the dwarf. Column 6: Anisotropy parameter of the stellar distribution of the dwarf. Column 7: Amplitude of the $m = 2$ Fourier component of the surface density distribution of the dwarf stars. Column 8: Axis ratio b/a of the stellar component of the dwarf. Column 9: Axis ratio c/a of the stellar component of the dwarf. Column 10: Formation of a tidally-induced bar during the orbital evolution of the dwarf galaxies according to the criteria discussed in § 2.4. Column 11: Classification of the final systems according to the criteria imposed in § 2.5. Column 12: Orbital time in Gyr defined as the average time elapsed between consecutive apocentric passages. Note that the entries in columns 4-9 are estimated within r_{\max} .

induced bar was formed in the stellar distribution of the dwarf galaxy during the course of its evolution inside the host. Column 11 indicates whether a dSph was produced as a result of the tidal interaction between the progenitor disk dwarf and the primary galaxy. The entries in column 6 demonstrate that the values of β in the dSph remnants range from isotropic to mildly radial ($0 \lesssim \beta \lesssim 0.5$). Given that a well established range for the velocity anisotropy of observed dSphs does not yet exist, a direct comparison with observations is not possible. However, we note that the magnitude of the radial velocity anisotropy in our dSphs is rather similar to that observed in the outer parts of CDM halos formed in cosmological simulations (e.g., Cole & Lacey 1996). Lastly, the orbital times listed in the last column of Table 3 are defined as the average time elapsed between consecutive apocentric passages.

Figure 3 shows the surface density maps of the final stellar distributions of the dwarfs in simulations R1, R2, and R3. Results are presented for projections onto the xz , yz , and xy planes and particles are color-coded on a logarithmic scale, with hues ranging from orange to white indicating increasing stellar density. This figure visually confirms the conclusions advanced above regarding the degree of morphological transformation experienced by the dwarfs in this set of experiments.

3.2. Eccentricity of the Orbit

In this section, we explore the extent to which the tidal evolution of a rotationally-supported dwarf is influenced by the eccentricity of its orbit. As we discussed earlier, this effect is worth investigating as the effective duration of the tidal shock, and thus the response of the system to the tidal perturbation, depends on the orbital eccentricity (e.g., Gnedin et al. 1999).

To this end, we conducted two additional simulations (R4, R5) in which we placed the dwarf galaxy model D1 on orbits with eccentricities that are larger ($r_{\text{apo}}/r_{\text{peri}} = 10$) and smaller ($r_{\text{apo}}/r_{\text{peri}} = 2.5$) by a factor of 2 from that of the reference experiment R1 (see Table 2). Simulations R4 and R5 should be viewed as corresponding to a highly and a mildly eccentric orbit, respectively. Figure 1 shows the orbital trajectories of the dwarf galaxies from the centers of their hosts in these experiments.

Figure 4 shows the main results related to this set of simulations. As expected, this figure demonstrates that for a fixed apocentric distance, higher eccentricity orbits induce a much stronger transformation in the orbiting dwarfs. The evolution of the various parameters in this set of experiments proves to be analogous to the one presented in Figure 2. The dwarf galaxies in simulations R4 and R5 evolve similarly to those in R2 and R3, respectively, and the same strong link between bar formation and the formation of dSphs is reported. Indeed, the disk dwarf in experiment R4 develops a bar and the final product is a nearly spherical ($b/a \approx c/a \gtrsim 0.9$), isotropic ($\beta \approx 0.03$), and non-rotating ($V_{\text{rot}}/\sigma_* \approx 0.03$) dSph, with final properties akin to those of the remnant in simulation R2. The evolution of V_{\max} , r_{\max} , and mass within r_{\max} is also similar in the two cases. This is due to the fact that although the orbital time of the dwarf in experiment R4 is significantly larger, it has a smaller pericentric distance compared to that of R2. On the other hand, the dwarf in experiment R5 does not form a bar and remains oblate, radially anisotropic and rotating, analogous to the one in simulation R3, despite the shorter orbital time and larger number of pericentric passages (see Figure 1).

A last interesting thing to note is that the bar instability that develops in the most strongly perturbed dwarf (R4) is weaker

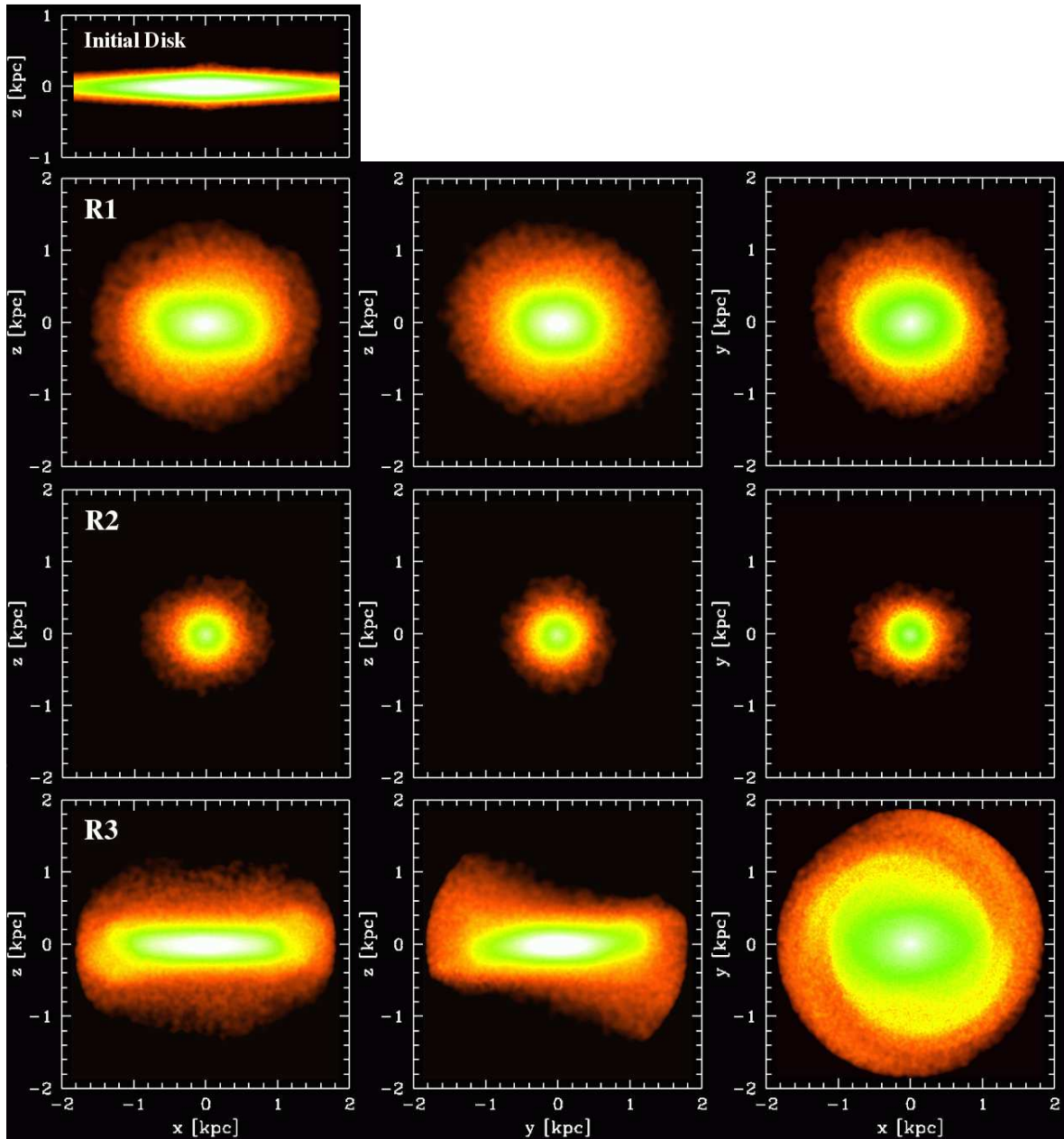


FIG. 3.— Surface density maps of the final stellar distributions of the dwarfs in simulations R1 (upper panels), R2 (middle panels), and R3 (lower panels). In order to aid comparison, the first panel also includes the edge-on view of the initial disk. Particles are color-coded on a logarithmic scale, with hues ranging from orange to white indicating increasing stellar density. Local density is calculated using an SPH smoothing kernel of 32 neighbors. Results are presented for projections onto the xz (left columns), yz (middle columns), and xy planes (right columns), where the x , y , and z axes lie along the major, intermediate, and minor axes of the stellar distribution, respectively. R1 is our reference simulation. Experiment R2 with the shortest orbital time and the second smallest pericentric distance all our experiments ($T_{\text{orb}} = 1.28$ Gyr and $r_{\text{peri}} = 17$ kpc) yields a spherically-symmetric ($b/a \approx c/a \approx 1$) and isotropic ($\beta \approx 0$) stellar system with negligible amounts of rotation ($V_{\text{rot}}/\sigma_* \lesssim 0.1$) that would be classified as a dSph. The dwarf in simulation R3, whose orbit is characterized by the longest orbital time and largest pericentric distance ($T_{\text{orb}} = 5.40$ Gyr and $r_{\text{peri}} = 50$ kpc), is not transformed into a dSph and remains disk-like even after 10 Gyr of tidal evolution inside the host galaxy.

compared to that of the reference simulation, despite the fact that the pericentric distance is much smaller in the former case. The same behavior, although to a lesser degree, is observed in Figure 2. We speculate that this is a consequence of the very strong tidal forces in simulations R2 and R4. The tidal shocks may heat the newly formed bar so substantially that they actually cause the instability to rapidly dissipate.

To summarize, the results of this and the previous section highlight that the effectiveness of the transformation into a dSph via tidal stirring depends crucially on the orbital parameters of the progenitor disk dwarfs. The relative importance

of the orbital time and the pericentric distance in this process will be addressed in § 5.

4. EFFICIENCY OF TIDAL STIRRING AND STRUCTURAL PARAMETERS OF THE PROGENITOR DISKY DWARFS

In this section, we explore how the initial structure of the progenitor disk dwarfs could influence the outcome of their tidal evolution inside the gravitational field of their host galaxies. We begin by focusing on the parameters of the dwarf disk and discuss in turn the effect of the disk inclination, thickness, mass, and scale length. In § 4.2, we turn our attention to the properties of the DM halo of the dwarf and investigate the ex-

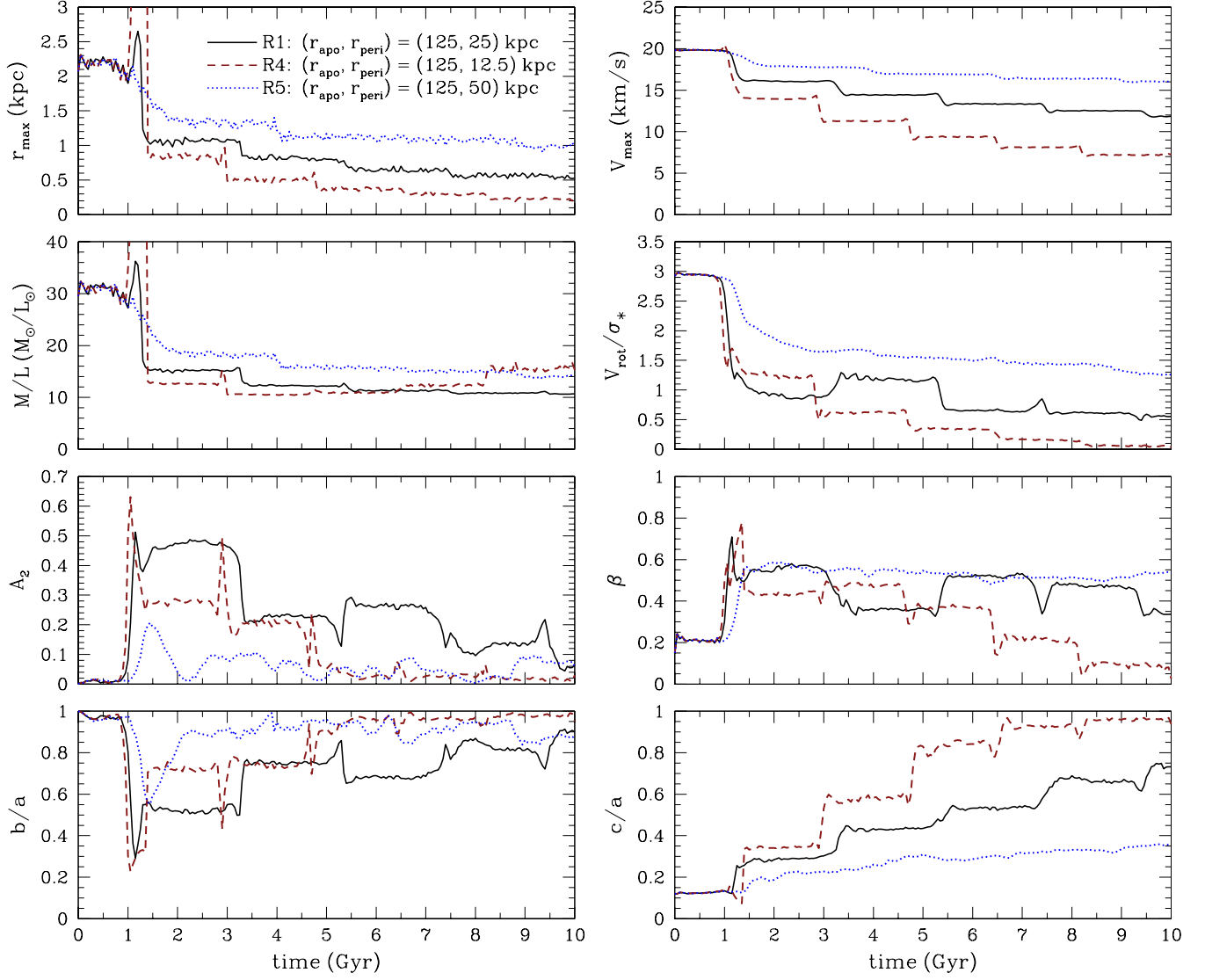


FIG. 4.— Comparison of the evolution of various parameters as a function of time illustrating the dependence of the tidal transformation of disk dwarf galaxies on the eccentricities of their orbits. Results are presented for the default simulation R1 and for experiments R4 and R5. The description of the simulations is presented in Table 2. For a fixed apocentric distance, r_{apo} , rotationally-supported dwarfs on orbits with higher eccentricities, $r_{\text{apo}}/r_{\text{peri}}$, and thus smaller pericentric distances, r_{peri} , display stronger tidal evolution inside their host galaxies and the efficiency of their transformation into dSphs is increased substantially.

tent to which the effectiveness of tidal stirring is affected by the halo concentration parameter and mass.

4.1. Varying the Parameters of the Disk

4.1.1. Disk Inclination

We first investigate the extent to which the tidal evolution of a late-type disk dwarf is affected by the initial inclination of its disk with respect to the orbital plane. This is worth exploring as stronger alignments between the orbital angular momentum of the dwarf and the internal angular momentum of its disk can result in more effective stripping (e.g., Read et al. 2006b). For this purpose, we performed two additional simulations in which we placed the dwarf galaxy model D1 on the same orbit as in simulation R1 after changing the default inclination from $i = 45^\circ$ to $i = 0^\circ$ and to $i = 90^\circ$ (see Table 2). Figure 5 contains the results pertaining to this set of simulations.

Although the initial inclination of the dwarf disk is very different, the size (in terms of r_{max}), the mass (in terms of V_{max}),

and the M/L ratio evolve fairly similarly. This is a consequence of two facts. First, DM halos were constructed with no net angular momentum. Thus, their stripping should be independent of such considerations and proceed in exactly the same way. Second, the dwarfs are not stripped down to such small scales that the alignment between the stellar angular momentum and the orbital angular momenta would have an important effect on the stripping of the stars (e.g., Read et al. 2006b). Indeed, we find the decrease in mass within r_{max} for both stars and DM to be independent of the initial disk inclination.

It is important to note that Klimentowski et al. (2009a) reported that disk inclination has a significant effect on the evolution of V_{max} in similar tidal stirring experiments. Specifically, they found that V_{max} decreased much more strongly in the $i = 0^\circ$ case compared to the $i = 45^\circ$ and $i = 90^\circ$ cases (see Figure 10 of Klimentowski et al. 2009a). This was because the DM halos in the Klimentowski et al. (2009a) experiments were constructed with net angular momentum which was aligned with the angular momentum of the dwarf disk.

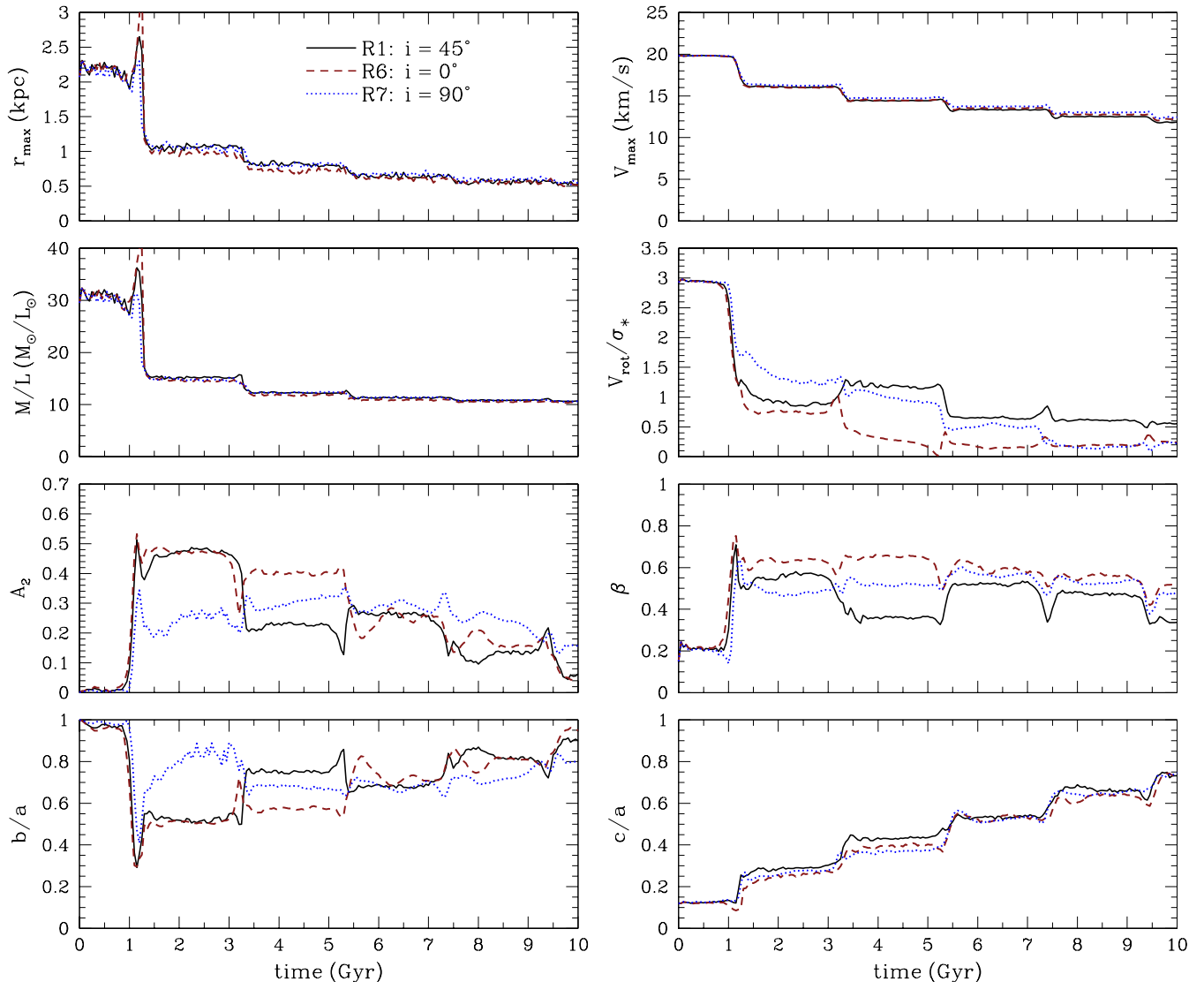


FIG. 5.— Comparison of the evolution of various parameters as a function of time illustrating the dependence of the tidal transformation of disk dwarf galaxies on the inclinations of their disks with respect to the orbital plane, i . Results are presented for simulations R1, R6, and R7. For the specific choices of i in this set of experiments, the tidal evolution of the rotationally-supported dwarfs inside their host galaxies and the efficiency of their transformation into dSphs depend very weakly on the disk inclination.

Moreover, the stellar disks were much more extended compared to those of the present study and, as a result, the stripping of the dwarfs down to the smallest scales of stars did occur at some point during the evolution. In fact, the mass within r_{max} of both stars and DM in the Klimontowski et al. (2009a) experiments decreased more in the $i = 0^\circ$ case lending support to the previous arguments.

The behavior of the bar strength amplitude A_2 in Figure 5, demonstrates that all dwarfs possess a tidally-induced bar after the first pericentric passage. However, the bar appears to be much weaker in simulation R7, indicating that the tidal forces acting on the dwarf disk were smaller in this case. During subsequent pericentric passages the situation becomes progressively more complex as strong variations in the values of A_2 are observed among the three simulations. At the end of the evolution, the tidally-induced bars are diminished in all cases. Investigating the reasons for the very different evolution of the bars in this set of experiments is clearly beyond the scope of the present paper. However, it is interesting to note that recent targeted numerical experiments have highlighted

the importance of stochasticity in the evolution of *isolated* disk galaxies leading to macroscopic differences in the evolution of bars (Sellwood & Debattista 2009). Among the causes for this stochastic evolution, Sellwood & Debattista (2009) identified interference between multiple disk modes, amplification of noise, bending modes, dynamical friction between the bar and the halo, and intrinsic chaos. Obviously, further analysis would be required to determine whether the observed behavior of the bars in this set of simulations can also be attributed to stochasticity and/or possibly to other considerations such as the different initial disk inclinations and resonances.

The final systems in simulations R6 and R7 are characterized by $c/a \approx 0.7$ and $V_{\text{rot}}/\sigma_* \approx 0.2$ (see Table 3) and, therefore, would be classified as dSphs according to the criteria described in § 2.5. While the evolution of kinematics and shape is, in broad terms, fairly similar among the three experiments, there are some interesting differences that are worth mentioning. For example, the rotation is lost more quickly in simulation R6 ($i = 0^\circ$), where V_{rot}/σ_* drops almost to zero at

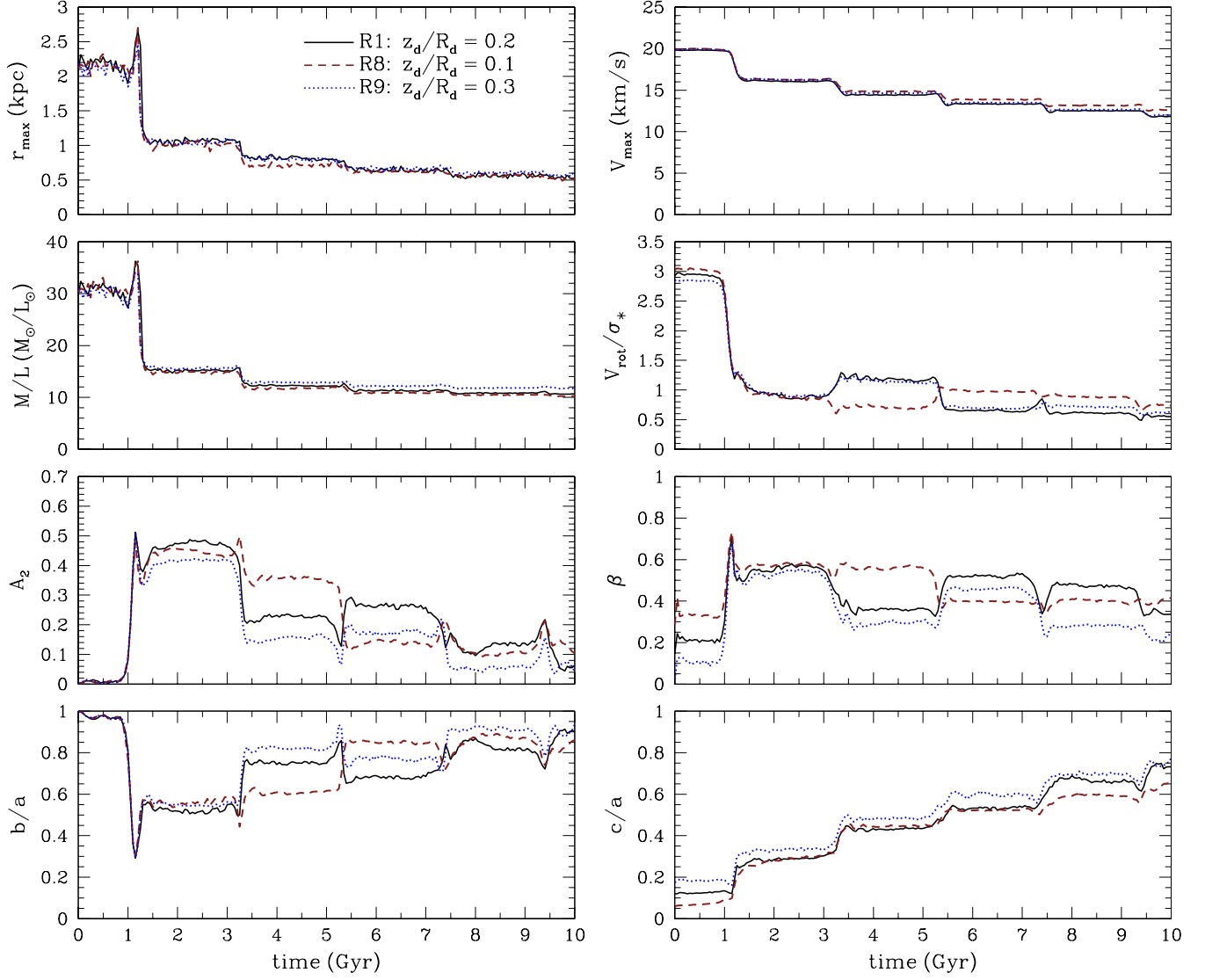


FIG. 6.— Comparison of the evolution of various parameters as a function of time illustrating the dependence of the tidal transformation of disk dwarf galaxies on the thicknesses of their disks. Disk thicknesses are parametrized as z_d/R_d and results are presented for simulations R1, R8, and R9. For the specific choices of z_d/R_d in this set of experiments, the tidal evolution of the rotationally-supported dwarfs inside their host galaxies and the efficiency of their transformation into dSphs are essentially independent of the disk thickness.

~ 5 Gyr and remains constant thereafter. The substantial and rapid decrease of V_{rot}/σ_* in this experiment is explained by the presence of a very strong bar instability between ~ 1 and ~ 5 Gyr. We also note that in experiment R7 the axis ratio b/a remains almost constant with time and significantly different from unity, so that the stellar component is triaxial rather than prolate at early times.

4.1.2. Disk Thickness

In this section, we investigate the dependence of the tidal evolution of a disk dwarf on the thickness of its disk. Such an investigation is important for two reasons. First, feedback mechanisms and turbulent motions in dwarf galaxies should be effective in producing thicker systems. Second, the efficiency of tidal heating and the strength of bar instabilities that are both vital for tidal stirring should be different in thicker stellar distributions (e.g., Kazantzidis et al. 2009). To this end, we generated two additional dwarf galaxy models that were identical to D1 except for their scale height, which was chosen equal to $z_d/R_d = 0.1$ and $z_d/R_d = 0.3$. We re-

fer to these models as “D2” and “D3”, respectively (see Table 1). The choice for the larger thickness in model D2 reflects the greater importance of pressure support in low-mass galaxies and was motivated by both observations as well as results of recent numerical simulations of the formation of isolated galaxies (Kaufmann et al. 2007), including systems with $V_{\text{max}} \approx 20 \text{ km s}^{-1}$ as our default dwarf model. On the other hand, model D3 with the thinner disk was constructed mainly for completeness. After building these two new dwarf models, we placed them on the same orbit as in simulation R1 and followed their tidal evolution inside the host galaxy. We refer to these experiments as “R8” and “R9” (see Table 2) and present the relevant results in Figure 6.

Overall, for the specific choices of initial thickness in this set of experiments, no significant difference in the evolution of the dwarfs can be discerned. Had we adopted thicker and/or thinner disks, such differences may have been more pronounced. The final properties of the systems in simulations R8 and R9 indicate that the remnants can be classified as dSphs (see Table 3).

Figure 6 demonstrates that r_{\max} , V_{\max} , and the M/L ratio evolve almost identically in the three experiments. A similarly strong bar is induced in all dwarfs after the first pericentric approach. While the thicker disk is initially more isotropic by construction, all three dwarfs exhibit nearly identical values of β between the first and second pericentric approach. At later times, the evolution is somewhat different, but generally the stellar component of the thicker disk (R9) has a more spherical shape and is characterized by more isotropic orbits. All dwarfs end up mildly triaxial and very similar to the remnant in simulation R1, but their paths to this state are slightly different. Occasionally, departures from the typical trend of decreasing rotational velocity occur (see Figure 11) but they happen at different pericentric passages for different experiments. We come back to this issue in § 5.

4.1.3. Disk Mass

In this section, we investigate the degree to which the tidal evolution of a rotationally-supported dwarf is affected by the mass of its disk. In order to ascertain this, we generated two additional dwarf galaxy models that were identical to D1 except for their disk mass, which differed by a factor of 2: $m_d = 0.01$ and $m_d = 0.04$ ⁷. We refer to these models as “D4” and “D5”, respectively (see Table 1). This range of m_d values is consistent with that inferred from exquisite measurements of the mass distribution of nearby dwarfs combining high resolution gas kinematics in the THINGS survey and deep Spitzer photometry (Oh et al. 2010, in preparation). It is also in agreement with results of hydrodynamical simulations of dwarf galaxy formation (e.g., Tassis et al. 2003; Governato et al. 2010). After building these two new dwarf models, we placed them inside the host galaxy on the same orbit as in simulation R1 and followed their tidal evolution. We refer to these experiments as “R10” and “R11” (see Table 2) and present their results in Figure 7.

This figure demonstrates that the mass of their disk has a substantial effect on the tidal evolution of the disk dwarfs. Interestingly, although the initial values of r_{\max} are different and smaller for the more massive disks due to the more concentrated mass distribution, at the end of the evolution they converge to nearly the same values. The opposite is true for the mass, as quantified by V_{\max} . Indeed, the least massive disk increases the susceptibility of the dwarf to tidal effects and the mass loss within r_{\max} is larger in this case. Overall, the results presented in Figure 7 indicate that the masses of the dwarfs are differentiated as a result of the tidal evolution.

The M/L ratios, which differed significantly in the beginning, evolve in a fairly different way. The most massive disk, which had the smallest value of M/L initially, is affected most weakly and its M/L ratio decreases only slightly. The weak evolution of the M/L ratio in this case can be attributed to the fact that the initial r_{\max} is very small (and remains so until the end of the evolution). As a result, r_{\max} probes the central regions of the dwarf, where the reasons that we have indicated in § 3.1 for the preferential stripping of DM over stars do not apply. Indeed, DM particles within this inner region

are very unlikely to be on orbits of high enough eccentricity to have apocenters larger than the tidal radius and be stripped. Moreover, the slopes of the density profiles of stars and DM are similar below ~ 1 kpc, implying that the average binding energies of DM and stars do not differ significantly in this region. Interestingly, despite the different evolution, the hierarchy of M/L is preserved; the dwarf which has the highest M/L ratio initially also exhibits the highest M/L ratio in the end.

The mass of the disk affects the evolution of the stellar shape substantially, and to some degree also influences that of the stellar kinematics. Owing to its higher self-gravity, the most massive disk (R11) develops the strongest tidally-induced bar after the first pericentric approach, leading to a pronounced decrease in V_{rot}/σ_* . We note that the values of A_2 remain the largest in this case until the end of the evolution ($t = 10$ Gyr). As a result, the dwarf galaxy in simulation R11 retains a strongly prolate shape with final values of $c/a \approx 0.6$ and $b/a \approx 0.7$. On the other hand, the dwarf with the least massive disk (R10) remains triaxial rather than prolate for most of the time. Due to the significantly lower disk self-gravity in this case, the tidal shocks heat the disk much more effectively, producing a quite spherical stellar component in the end ($c/a \approx 0.8$, $b/a \approx 0.9$).

However, the interpretation of the evolution of kinematics is less obvious. While the least massive disk loses its rotation monotonically (see Figure 11), the evolution of its most massive counterpart is more chaotic with occasional strong increases of the rotational velocity, even after two consecutive pericentric passages (third and fourth). We note that this behavior is observed in only one more simulation (R12; see next section) but is not as strong as reported here. Overall, the values of c/a , in conjunction with the fact that $V_{\text{rot}}/\sigma_* \lesssim 0.6$, indicate that the final systems in simulations R10 and R11 would be classified as dSphs (see Table 3).

4.1.4. Disk Scale Length

This section addresses the extent to which the tidal evolution of a disk dwarf is influenced by the radial scale length of its disk, R_d . For this purpose, we generated two additional dwarf galaxy models that were identical to D1 except for the scale lengths of their disks. We reiterate that the disk scale length is not a free parameter in our simulations, but rather is derived via the semi-analytic galaxy formation model of Mo et al. (1998). Because of this choice our method requires us to assign values to the halo spin parameter λ in order to derive the scale length of the dwarf disk, despite the fact that the halos of our dwarfs are constructed with no net angular momentum.

Recall that we chose $\lambda = 0.04$ for our reference dwarf model D1, close to the median value of halo spins found in cosmological N -body simulations (e.g., Bullock et al. 2001a; Shaw et al. 2006; Macciò et al. 2007; Bett et al. 2007). To investigate the effect of the disk scale length, we initialized two additional dwarf models with $\lambda = 0.024$ and $\lambda = 0.066$. These values correspond to the 1σ deviations from the median λ , assuming a log-normal distribution with $\lambda_{\text{med}} = 0.04$ and $\sigma_\lambda = 0.5$, in agreement with the previous cosmological studies. We refer to these dwarf models as “D6” and “D7”, respectively, and list their disk scale lengths in Table 1. In the corresponding experiments “R12” and “R13”, we placed these dwarfs on the same orbit as in simulation R1 and followed their tidal evolution inside the host galaxy. Note that for consistency we have kept the thickness z_d/R_d in this set

⁷ We note that formally, according to the model of Mo et al. (1998), varying the disk mass and keeping the other relevant parameters (M_h , λ , and c) constant would result in different scale lengths for the dwarf disk. However, for consistency and in order to isolate the effect of a single parameter on the tidal evolution of the dwarfs, we adopt identical disk scale lengths in this set of experiments. The same convention applies to the simulations described in § 4.2.1 in which we construct dwarf models with different halo concentration parameters.

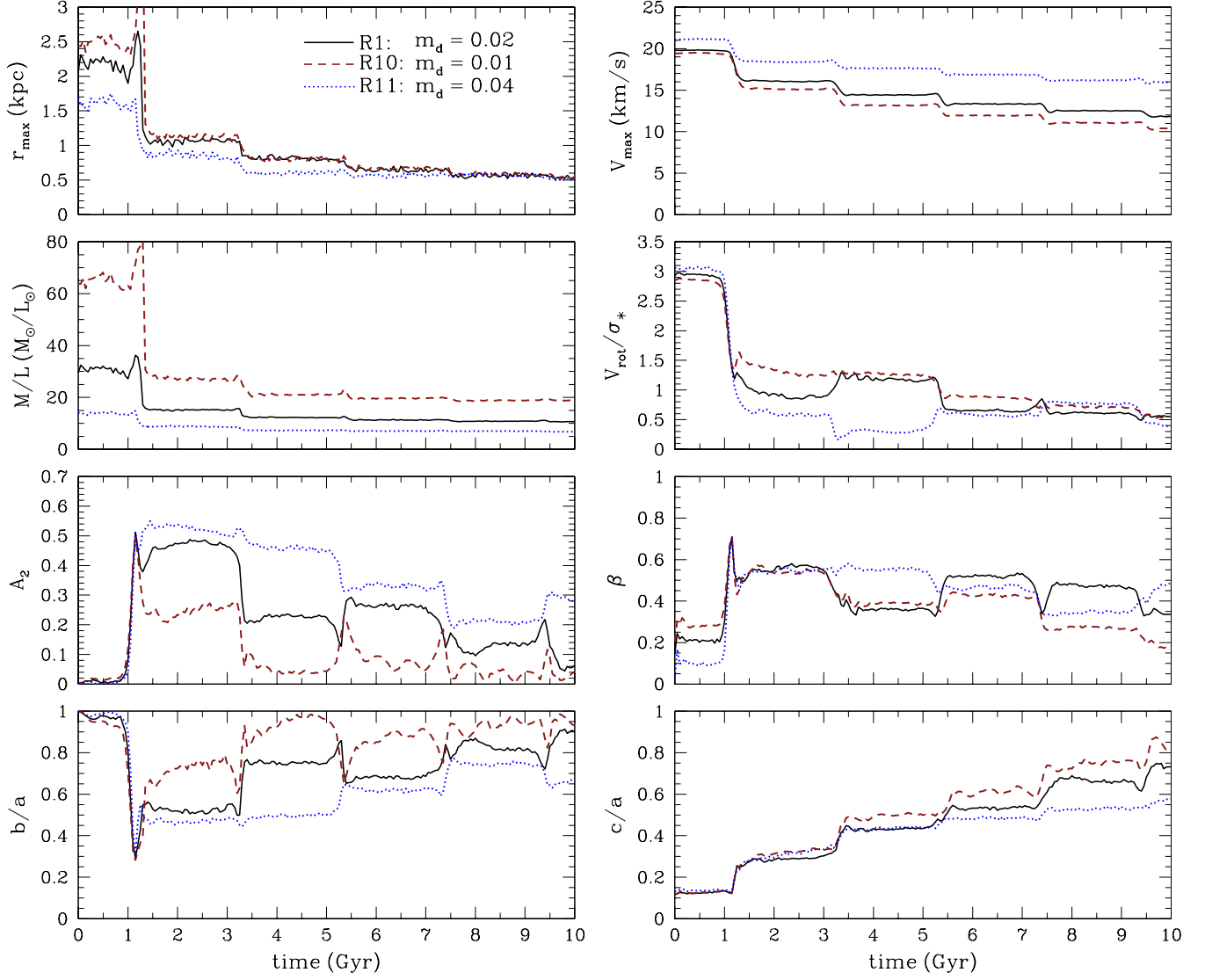


FIG. 7.— Comparison of the evolution of various parameters as a function of time illustrating the dependence of the tidal transformation of disk dwarf galaxies on the masses of their disks. Disk masses are parametrized as a given fraction, m_d , of the halo mass, M_h , and results are presented for simulations R1, R10, and R11. Rotationally-supported dwarfs with less massive disks exhibit stronger tidal evolution inside their host galaxies and the efficiency of their transformation into dSphs is augmented significantly.

of experiments constant. As a result, the disk becomes larger (smaller) in both the radial and vertical direction when λ is increased (decreased). The relevant results are presented in Figure 8 which demonstrates that the remnant dwarfs in this set of simulations would be classified as dSphs (see Table 3).

This figure shows that the scale length of the dwarf disk is a parameter that affects significantly the tidal evolution of the disk dwarf galaxies. The initial value of r_{\max} is smaller for the more compact disk in simulation R12 and it remains so until the end of the evolution. This experiment does not show the characteristic temporary increase of r_{\max} at the first pericentric approach observed in the reference simulation R1. This is because the more compact disk diminishes the ability of the host tidal field to distort the inner regions of the dwarf galaxy. As expected, the mass loss within r_{\max} measured by the decreasing value of V_{\max} is more pronounced for the more extended disks with a larger value of λ . This is simply a consequence of the fact that larger disk scale lengths make the potential well of the dwarf shallower and decrease the total binding energy in the inner parts.

As expected, the dwarf with the most extended disk (R13) has a larger initial value of the M/L ratio within r_{\max} . Due to the dissimilar values of R_d , the stripping of the stars proceeds differently in this set of experiments and, as expected, is much more effective in the case of the most extended disk. This differential stripping of the stars manifests itself in the evolution of the M/L ratio. Although the initial values of the M/L ratios are not very different, the final value of M/L is much larger in simulation R13. Interestingly, the M/L ratio in this experiment starts to increase during the intermediate stages of the evolution ($t \sim 5$ Gyr). Such a behavior is similar to that reported in § 3 for experiments R2 and R4, even though this transition occurred earlier there and the final M/L values obtained were slightly lower. We discuss this issue in § 5. Overall, Figure 8 indicates that the M/L ratios are differentiated as a result of the tidal evolution.

Evidently, the size of the disk affects substantially the evolution of the stellar shape, and to some degree also influences that of the stellar kinematics. The behavior of the Fourier component A_2 after the first pericentric passage is slightly

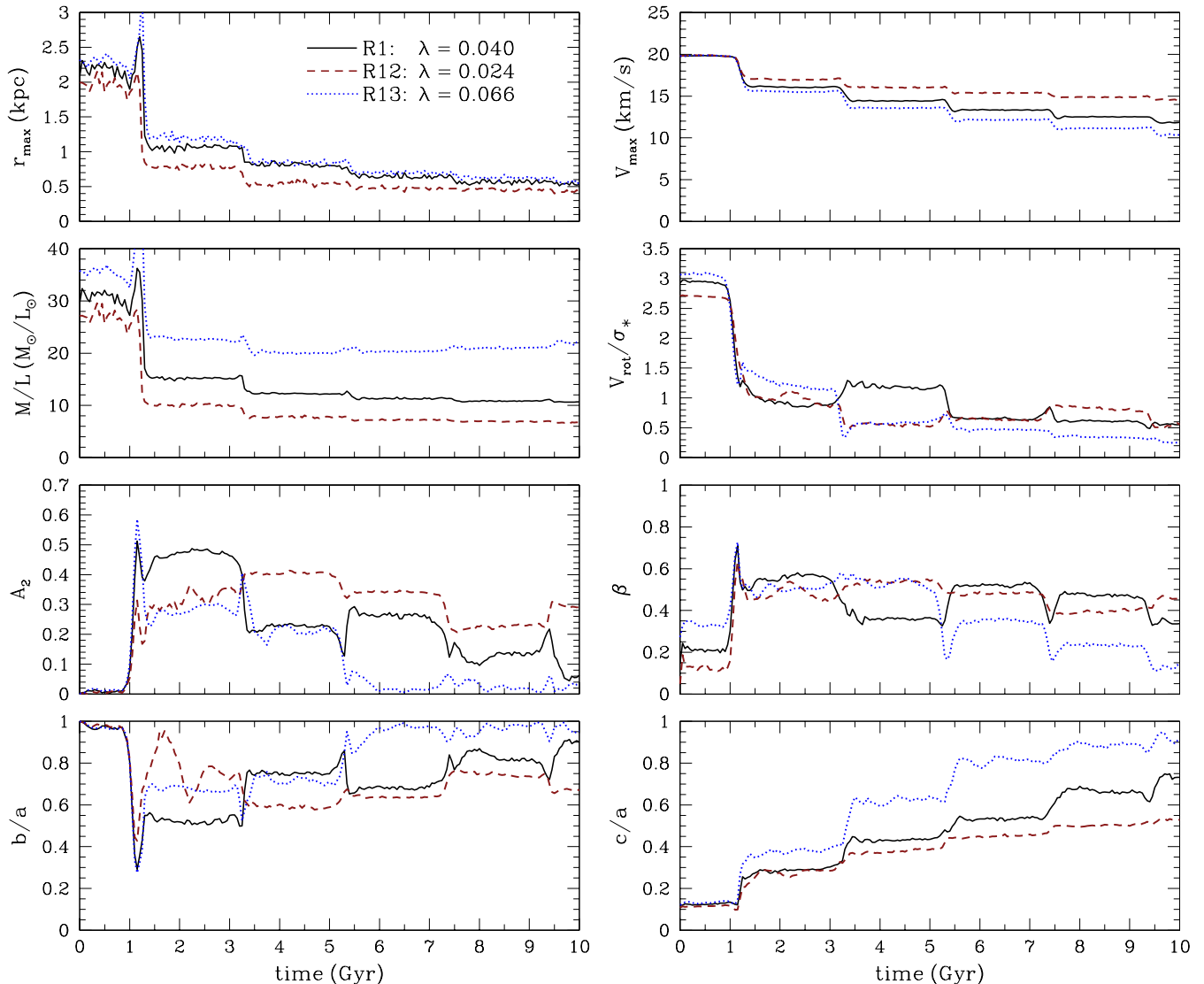


FIG. 8.— Comparison of the evolution of various parameters as a function of time illustrating the dependence of the tidal transformation of disk dwarf galaxies on the radial scale lengths of their disks, R_d . Results are presented for simulations R1, R12, and R13. The spin parameters of the dwarf DM halos, λ , used to determine the disk scale lengths in this set of experiments are indicated in the labels (see text for details). The corresponding values of R_d for the three different choices of λ are equal to $R_d = (0.41, 0.25, 0.66)$ kpc, respectively (see Table 1). Rotationally-supported dwarfs with more extended disks experience stronger tidal evolution inside their host galaxies and the efficiency of their transformation into dSphs is enhanced substantially.

misleading. Indeed, both lower and larger λ cases show similar values of this parameter, but for different reasons. While the most compact disk (R12) retains an oblate shape, the most extended one (R13) is triaxial, but neither shows such a strong bar mode as our reference experiment R1. The situation changes radically after the second pericentric passage. On the one hand, owing to its higher self-gravity, the low- λ dwarf forms a fairly strong bar and remains prolate until the end of the evolution with final values of $c/a \approx 0.5$ and $b/a \approx 0.7$. In fact, the remnant in this experiment exhibits the least spheroidal shape of all our classified dSphs, highlighting the resilience of the most compact disk to tidal heating. This system could be the analogue of the most elongated dSphs in the LG such as Ursa Minor (Irwin & Hatzidimitriou 1995). On the other hand, tidal effects are quite efficient in the case of the high- λ disk with the lowest self-gravity and cause its rapid transformation into a nearly isotropic ($\beta \approx 0.1$) and spherical stellar component ($b/a \approx c/a \gtrsim 0.9$) that retains little rotation ($V_{\text{rot}}/\sigma_* \lesssim 0.3$).

4.2. Varying the Parameters of the Halo

4.2.1. Halo Concentration

In this section, we investigate the degree to which the tidal evolution of a disk dwarf is affected by the concentration parameter of its DM halo, c . To this end, we constructed two additional dwarf galaxy models that were identical to D1 except for the halo concentration parameters. Recall that we chose $c = 20$ for our reference model D1, close to the median concentration value for $z = 0$ cosmological halos of mass $\sim 10^9 M_{\odot}$ (e.g., Bullock et al. 2001b; Macciò et al. 2007). To investigate the effect of the halo concentration on our results, we constructed two additional dwarf models with $c = 10$ and $c = 40$. These values roughly correspond to the 2σ deviations from the median $c = 20$, in accordance with the previous cosmological studies⁸. We refer to these dwarf models as “D8”

⁸ We note that $c = 40$ is markedly incompatible with results of the distribution of DM in present-day LSB and dIrr galaxies through the modeling of rotation curves (see the recent review of de Blok 2010 for a discussion on this

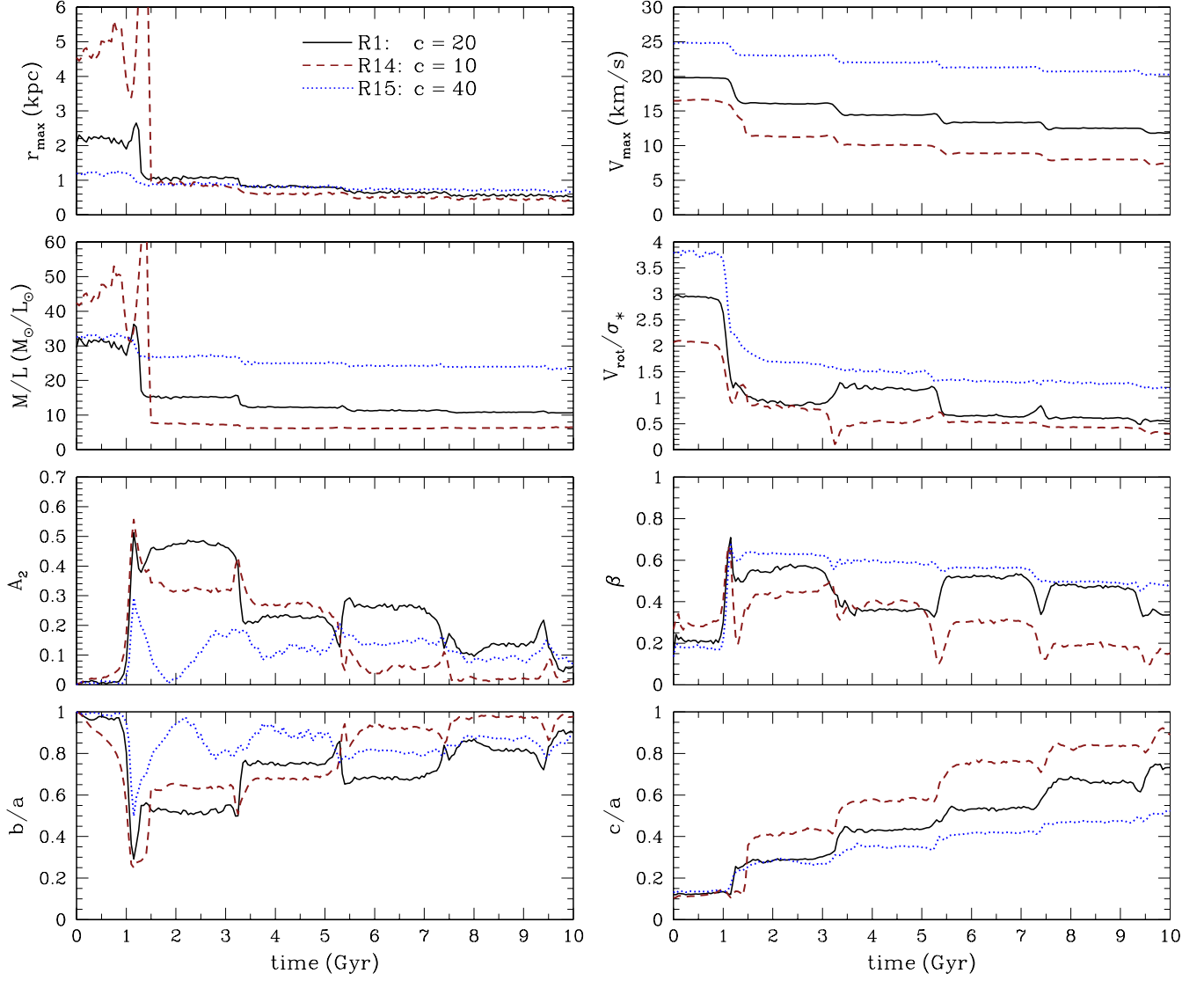


FIG. 9.— Comparison of the evolution of various parameters as a function of time illustrating the dependence of the tidal transformation of disk dwarf galaxies on the concentration parameters of their DM halos, c . Results are presented for simulations R1, R14, and R15. Rotationally-supported dwarfs embedded in less concentrated DM halos exhibit stronger tidal evolution inside their host galaxies and the efficiency of their transformation into dSphs is increased considerably.

and “D9”, respectively, and list their structural parameters in Table 1. In the corresponding experiments “R14” and “R15”, we placed these dwarfs on the same orbit as in simulation R1 and followed their tidal evolution inside the host galaxy. Figure 9 contains the results of these simulations.

As expected, the less concentrated dwarf is characterized by a larger initial r_{\max} . As in the case of the experiments with different disk masses (R10, R11), after the first pericentric approach the values of r_{\max} converge. Interestingly, at late times the hierarchy is even reversed (the dwarf with the most concentrated halo exhibits the largest r_{\max}) but the differences are not significant. As demonstrated by the weakest decrease in the value of V_{\max} , the most concentrated halo increases the resilience of the dwarf galaxy to tides and mass loss. Since the higher concentration makes the potential well of the dwarf deeper, this effect is similar to that of the larger disk mass discussed in § 4.1.3. The effect on the M/L ratio is, however, the opposite; although the M/L ratio within r_{\max} was initially

larger for the $c = 10$ case it soon becomes the smallest. This is because the DM particles are much more weakly bound in this case and, as a result, are stripped fairly efficiently. After a period of $t = 10$ Gyr inside the host galaxy, the M/L ratios of the dwarfs with the most and the least concentrated halo differ by a factor of ~ 4 . The weak evolution of the M/L ratio in simulation R15 is of similar origin to that of the experiment with the most massive disk (R11).

The susceptibility to tides of the low-concentration dwarf in experiment R14 also manifests itself in the evolution of the shape and kinematics. The stellar component in this experiment evolves rapidly and becomes nearly spherical rather quickly with a final $c/a \approx 0.9$. The stronger effect of the tidal shocks in this case reflects the fact that the dwarf responds more impulsively to the tidal perturbation owing to its lower characteristic densities and, correspondingly, longer internal dynamical times. After the first pericentric passage, a strong bar develops in the dwarf disk ($A_2 \gtrsim 0.3$) and the V_{rot}/σ_* ratio starts to decrease, reaching a final value of $V_{\text{rot}}/\sigma_* \approx 0.3$. The structure of the remnant in this case would resemble that of

issue). Nevertheless, even though it is clearly inconsistent with observations, we decided to consider this limiting case simply for completeness.

observed dSphs.

On the other hand, the stellar component of the high-concentration dwarf retains its disk shape, since it is less affected by tides. This is similar to the cases of simulations R3 and R5 where the dwarf galaxies experienced weaker tidal forces due to the larger pericentric distances. In experiment R15, the final axis ratio is higher ($c/a \approx 0.5$) but still the stellar component remains oblate. Most importantly, as demonstrated by the very low values of A_2 throughout the evolution, a bar does not form in this case. As a result, the angular momentum content of the dwarf does not decrease efficiently and the V_{rot}/σ_* ratio remains larger than unity until the end of the simulation. The absence of the bar in this case is consistent with results of numerical experiments showing that high values of halo concentration suppress the formation of bars in isolated disk galaxies embedded in CDM halos (Mayer & Wadsley 2004). To summarize, experiment R15 constitutes the only case where a rotationally-supported dwarf is placed on the reference orbit of simulation R1 and neither develops a bar nor yields a dSph. This lends further support to the fact that bar formation and the formation of dSphs are intimately linked in the context of the tidal stirring model.

4.2.2. Halo Mass

In this section, we explore the degree to which the tidal evolution of a disk dwarf depends on the mass of its DM halo, M_h . Such a dependence may be expected as various effects, including the strength of tidal shocks as well as dynamical friction, will be affected by the halo mass. For this purpose, we generated two additional dwarf galaxy models that were identical to D1 except for the masses of their halos, which differed by a factor of 5: $M_h = 0.2 \times 10^9 M_\odot$ and $M_h = 5 \times 10^9 M_\odot$. This mass range roughly corresponds to the range of initial subhalo masses that were accreted since $z \lesssim 2$ and survived until the present time in the LG simulation of Klimontowski et al. (2010). We refer to these models as “D10” and “D11”, respectively (see Table 1). The motivation behind using the same values for m_d , z_d/R_d , c , and λ in these models as in the reference one (D1) was imposed mainly by simplicity. However, we do note that our choices are reasonable given the scatter in m_d (e.g., Jimenez et al. 2003; Tassis et al. 2003), z_d/R_d (e.g., Dalcanton et al. 2004; Kaufmann et al. 2007), and c (e.g., Bullock et al. 2001b; Macciò et al. 2007) for galaxies in this mass range, and the fact that the distribution of halo spins shows no dependence on halo mass (e.g., Macciò et al. 2007). In the corresponding experiments “R16” and “R17”, we placed dwarf models D10 and D11 on the same orbit as in simulation R1 and followed their tidal evolution inside the host galaxy. Figure 10 presents the results of these simulations.

As a result of our choices for the initial structural parameters of the dwarf galaxies in this set of experiments, r_{max} is larger for the dwarf with the most massive halo (R17). This is simply because $r_{\text{max}} \approx 2.16 R_h/c$ for the NFW profile, where R_h in our modeling corresponds to the cosmologically motivated virial radius of the system ($R_h \approx r_{\text{vir}}$). Figure 10 shows that r_{max} remains larger for the most massive dwarf until the end of the evolution. We emphasize that the pericentric passages which are marked by sudden drops in V_{max} do not occur at the same time for all three dwarfs, despite the fact that the orbital parameters were initially identical. Specifically, the orbit of the most massive dwarf becomes progressively much tighter with continuously reduced apocentric distances, leading to a shorter orbital time (see Table 3). This is due to the

effect of dynamical friction, whose strength depends strongly on the mass of the moving body.

Interestingly, after 10 Gyr of evolution inside the host, all three dwarf galaxies lose approximately the same fraction of their initial mass within r_{max} ($\sim 90\%$) and their V_{max} decreases by approximately the same factor of ~ 1.7 . This is intriguing given that mass loss is generically affected, among other things, by the depth of the potential well of the dwarf and the details of the dwarf orbit (e.g., the pericentric distance) around the primary galaxy. We note that by construction the three dwarfs have approximately equal average densities within r_{max} , and therefore comparable dynamical times at r_{max} . Using this fact coupled with some order-of-magnitude calculations it is possible to gain qualitative insight as to the relative evolution of V_{max} and mass within r_{max} is similar in simulations R1, R16, and R17.

According to the tidal approximation of the impulse (which should be valid in our simulations for the purposes of dimensional analysis), the energy injected at each pericentric passage is given by $\Delta E \propto M_{\text{host}}^2 M R^2 V_{\text{rel}}^{-2}$, where M_{host} is the mass of the host, M denotes the mass of the dwarf, R is a characteristic radius of the dwarf (related to r_{max}), and V_{rel} is the relative velocity between the two galaxies at the pericenter of the orbit (Spitzer 1958; Binney & Tremaine 2008). Since, as noted above, the average density within r_{max} is roughly constant among the dwarfs, we have $R \propto M^{1/3}$ in the three different models. Given that M_{host} is the same and V_{rel} is fairly similar in the three experiments considered here, it follows that $\Delta E \propto M^{5/3}$. By virtue of the virial theorem, the energy content of the dwarf should scale as $E \propto GM^2/R \propto M^{5/3}$, and also $E \propto MV^2$, where V is a characteristic velocity of particles within the dwarf (related to V_{max}). Hence, the fractional increase in energy caused by the tidal shocks, $\Delta E/E$, is roughly constant, explaining why the V_{max} and M_{max} of the dwarfs in simulations R1, R16, and R17 evolve in a fairly similar way. We stress that similar conclusions would be reached had we used extensions of the standard impulse approximation appropriate for perturbers with extended mass distributions as well as for satellites that move on either straight-path or eccentric orbits (Gnedin et al. 1999). This is because such extensions are characterized by analogous scalings of the relevant variables in our calculations above.

The M/L ratios are similar in all cases and decrease monotonically with time reaching a value of $\sim 10 M_\odot/L_\odot$ in the end of the evolution. The behavior of kinematics shows an interesting feature. While the values of V_{rot}/σ_* and β were quite different for the three models initially, they become very similar after the first pericentric passage and remain so until the end of the evolution. The evolution of the shape shows a more clear trend with mass. After the first pericentric approach, the bar is stronger in the most massive dwarf compared to that of the default case and it remains so until the end of the evolution. This simply reflects the higher self-gravity of the disk in simulation R17. On the other hand, while the least massive dwarf remains disk during the entire evolution, its axis ratio c/a increases significantly with a final value of $c/a \approx 0.75$. The dwarf remnants in simulations R16 and R17 are characterized by $c/a \approx 0.7$ and $V_{\text{rot}}/\sigma_* \lesssim 0.7$ (see Table 3) and hence would be classified as dSphs.

A last point of interest is that simulation R16 constitutes the only case where the formation of a dSph is not associated with the presence of a tidally-induced bar. Indeed, the increase of the bar amplitude, A_2 , in this case is only tem-

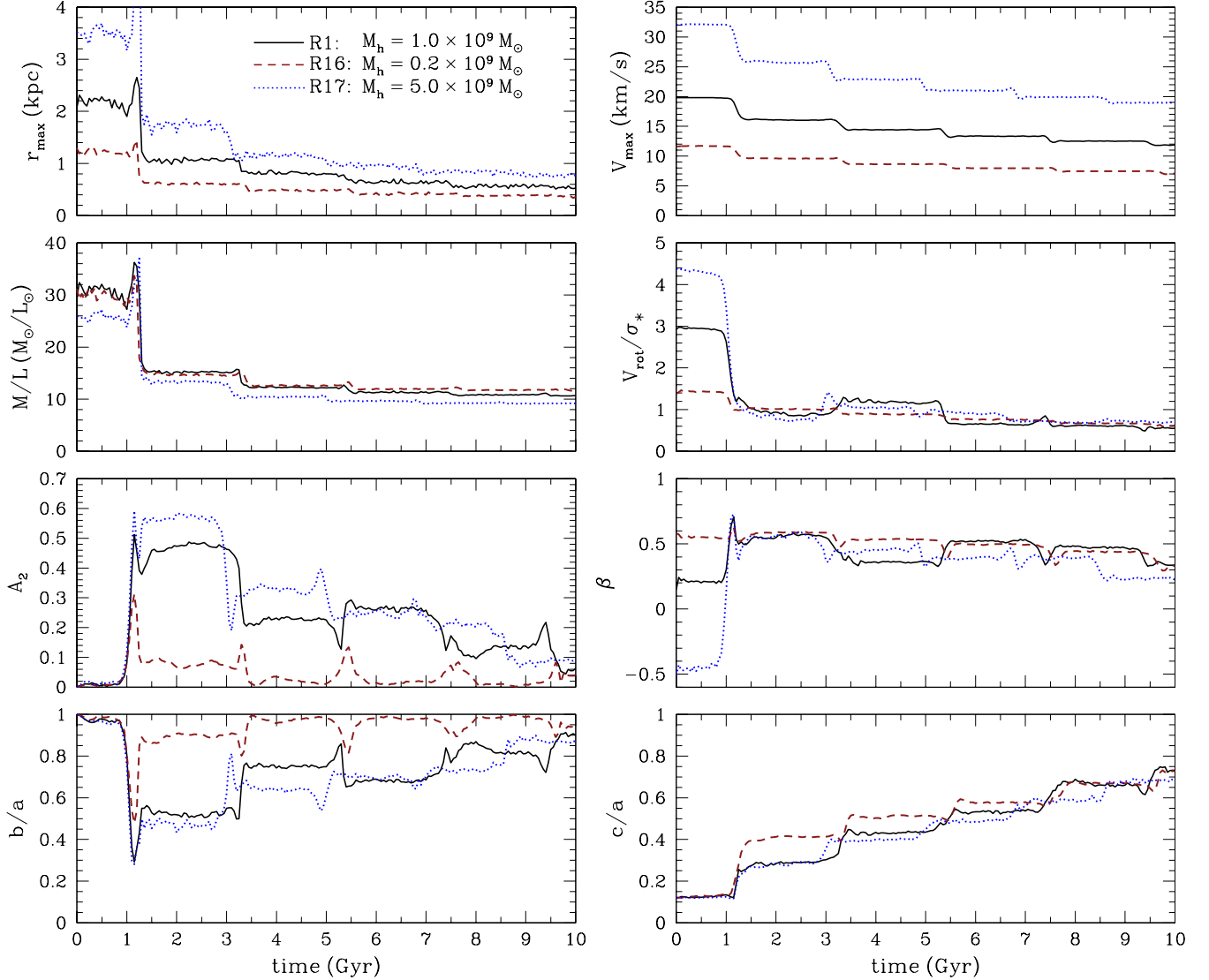


FIG. 10.— Comparison of the evolution of various parameters as a function of time illustrating the dependence of the tidal transformation of disk dwarf galaxies on the masses of their DM halos, M_h . Results are presented for simulations R1, R16, and R17. Owing to the interplay between the effects of dynamical friction and the depth of the potential well, rotationally-supported dwarfs embedded in DM halos of substantially different mass display similar tidal evolution inside their host galaxies and the efficiency of their transformation into dSphs is of comparable magnitude.

porary and occurs at the first pericentric passage when the dwarf is strongly elongated by tidal forces. The absence of a bar is consistent with the fact that the disk of this dwarf exhibits the highest value of the Toomre stability parameter (see Table 1). Bar formation causes rotational motion to be transformed into radial motion and thus, in conjunction with tidal heating which also increases the velocity dispersion, is intimately linked to the decrease of V_{rot}/σ_* required for the transformation to a pressure-supported dSph (Mayer et al. 2001a; Debattista et al. 2006). In the case of the least massive dwarf, the initial V_{rot}/σ_* within r_{max} is rather low ($V_{\text{rot}}/\sigma_* \lesssim 1.5$) and therefore the bar stage is not necessary to decrease it considerably to levels that are appropriate for dSphs ($V_{\text{rot}}/\sigma_* \lesssim 1$). The decrease of V_{rot}/σ_* in the dwarf of experiment R16 occurs almost exclusively at pericentric approaches and is driven by the decrease in V_{rot} (see Figure 11). The decrease in rotational velocity within r_{max} is simply caused by tidal heating which perturbs the circular orbits of the disk stars converting part of the rotation (ordered motions) in the disk to random motions. It is worth noting that in the reference simulation R1,

for example, the combination of tidal heating and the tidally-induced bar lead to a decrease in the V_{rot}/σ_* of the dwarf by approximately a factor of 5, illustrating the importance of bar formation in reducing the initial high values of V_{rot}/σ_* appropriate for disk dwarfs to those characteristic of dSphs.

5. DISCUSSION

We begin this section by investigating the $V_{\text{max}} - \sigma_*$ relation in our simulations, which is of particular interest for the missing satellites problem. In § 5.2 and § 5.3, we explore the reasons for the increasing rotational velocity and the increasing M/L ratio, respectively, observed in some of our experiments. In § 5.4, we elucidate the fundamental orbital parameter that influences the transformation of disk dwarfs into dSphs and thus the efficiency of the tidal stirring mechanism. In § 5.5, we discuss some additional implications related to the findings of this work. Lastly, in § 5.6 we conclude with a few words of caution and a discussion of promising directions for future work that may lead to more conclusive statements about the role of environmental processes in shaping the nature of dwarf

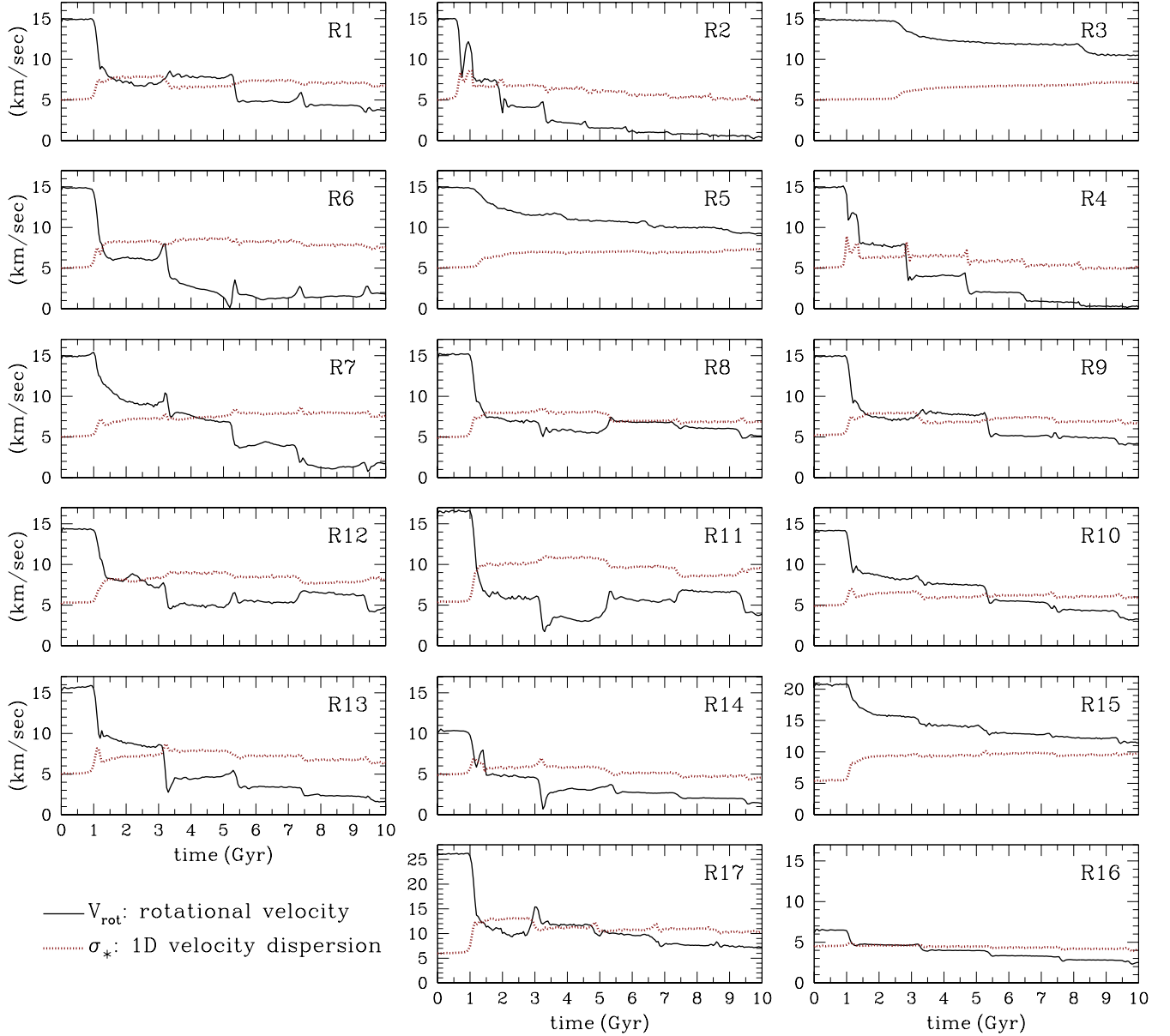


FIG. 11.— Evolution of the stellar rotational velocity, V_{rot} , (solid lines) and the one-dimensional stellar velocity dispersion, σ_* , (dotted lines) of the dwarfs in simulations R1-R17. Parameters V_{rot} and σ_* are computed within r_{max} . The repeated action of tidal forces exerted by the host galaxy decreases the ratio of V_{rot}/σ_* , gradually transforming the initially rotationally-supported disk dwarfs to pressure-supported stellar systems dominated by random motions.

galaxies in environments such as that of the LG.

5.1. $V_{\text{max}} - \sigma_*$ Relation

Here we investigate the relation between the one-dimensional, central stellar velocity dispersion, σ_* , and the maximum circular velocity, V_{max} , in our simulated dwarf galaxies. The knowledge of this relation is crucial, particularly in the context of the missing satellite problem (Moore et al. 1999; Klypin et al. 1999), as it reflects the link between observable properties and dark halo properties in dwarf galaxies. One of the main difficulties intrinsic to this problem lies in the fact that the mapping between V_{max} and σ_* , the latter being a directly observable quantity, depends sensitively on the assumed density structure of the DM halo of the dwarf. For example, adopting an isothermal halo model with a flat circular velocity profile to estimate V_{max} would yield $V_{\text{max}} \sim \sqrt{2}\sigma_*$ (e.g., Moore et al. 1999), while assum-

ing an isotropic stellar velocity dispersion tensor would result in $V_{\text{max}} \sim \sqrt{3}\sigma_*$ (e.g., Klypin et al. 1999). Given the uncertainties regarding the conversion of σ_* to V_{max} (see Kravtsov 2010 for a thorough discussion on this issue), it is interesting to check the general validity of these assumptions directly in our simulations. The relevant analysis is presented in Figure 12.

The left panel of this figure shows the relation between the one-dimensional stellar velocity dispersion and the maximum circular velocity V_{max} in the final stages of all simulated dwarfs ($t = 10$ Gyr). We remind the reader that the velocity dispersion profiles of our remnants do not strongly vary with radius and thus our dispersion measurements are close to the central values commonly used by observers. For the purposes of this presentation, we have also replaced σ_* used throughout the paper by $\sigma'_* \equiv [(\sigma_r^2 + \sigma_\theta^2 + \sigma_\phi^2)/3]^{1/2}$, where

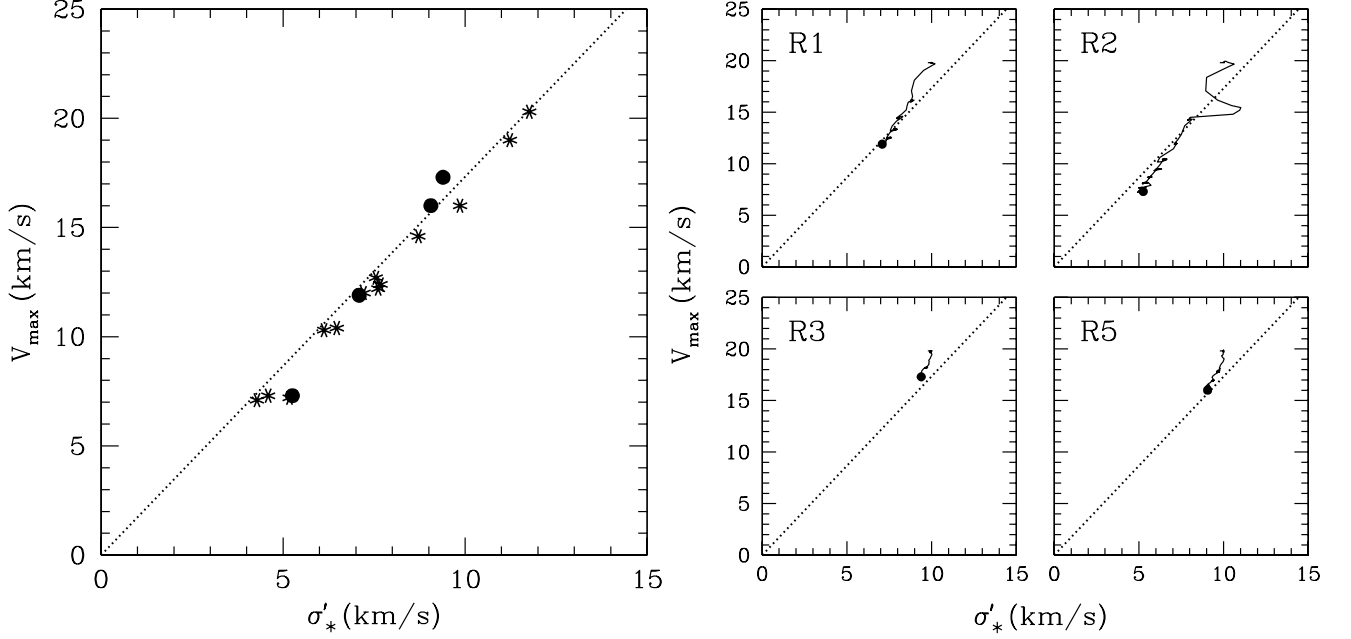


FIG. 12.— Relation between the maximum circular velocity, V_{\max} , and the one-dimensional, central stellar velocity dispersion, σ'_* , of the dwarfs in our simulations. The latter quantity corresponds to the line-of-sight central velocity dispersion measured in the observations and includes the contribution of rotation (see text for details). Left: The data points indicate the values calculated in the final stages of the dwarfs ($t = 10$ Gyr) in experiments R1-R17, and the dotted line is intended to identify a slope of $\sqrt{3}$ and is not a fit to the data. The formal best-fit slope differs by less than $\sim 4\%$ from $\sqrt{3}$. Circles show results for specific experiments R1, R2, R3, and R5 discussed in the right panel. The relation $V_{\max} = \sqrt{3}\sigma_*$, adopted by Klypin et al. (1999) to map the observed central stellar velocity dispersion of dSphs to the maximum circular velocities of their halos, is well justified within the context of the tidal stirring model. Right: Four examples of the evolution of individual dwarf galaxies on the $V_{\max} - \sigma'_*$ plane (solid lines). Results are shown for representative simulations R1, R2, R3, and R5, where the same dwarf model (D1) was placed on different orbits. R1 is our reference experiment. R2 produces one of the most strongly evolved dwarfs in our simulations, while R3 and R5 correspond to the least tidally-transformed systems in our experiments. In all panels, the filled circles mark the end of the evolution inside the host ($t = 10$ Gyr). As in the left panel, dotted lines correspond to slopes of $\sqrt{3}$. The dwarf galaxies exhibit fairly different types of trajectories depending on their orbital parameters and can move substantially on the $V_{\max} - \sigma'_*$ plane over the course of their evolution inside their hosts.

$\sigma'^2_\phi = \sigma_\phi^2 + V_{\text{rot}}^2$. This is because rotation was found to be important in some of the remnants, specifically those of simulations R3, R5, and R15 which do not produce dSphs, and thus it had to be included in the calculation of their velocity dispersion. We stress that this modification is not necessary in the majority of cases where dSphs with minimal intrinsic rotation are formed.

The panel demonstrates a strong correlation between σ'_* and V_{\max} in all dwarf remnants regardless of their morphology and kinematics. This is not entirely unexpected as both of these quantities are measures of the depth of the potential of the dwarfs. Interestingly, the relation $V_{\max} = \sqrt{3}\sigma_*$, formally valid for a tracer stellar population with an isotropic velocity dispersion tensor, reproduces the results of the simulations remarkably well (see also Klimontowski et al. 2009a). Indeed, the formal best-fit slope of the $V_{\max} - \sigma'_*$ relation in our simulations differs by less than $\sim 4\%$ from $\sqrt{3}$. Given the wide range of orbital and structural parameters that we adopted for the progenitor disk dwarfs in our experiments, this finding is particularly noteworthy. We stress that the relation between σ_* and V_{\max} is derived by directly probing the stellar kinematics of the simulated dwarfs. It may thus be reliably used to map the observed central stellar velocity dispersions to halo maximum circular velocities in dwarf galaxies when addressing the missing satellites problem.

Overall, we conclude that moderate conversion factors between σ_* and V_{\max} such as those originally adopted by Moore et al. (1999) and Klypin et al. (1999) to formulate the missing satellites problem were reasonable. Recently, using controlled simulations of subhalo evolution, Peñarrubia et al.

(2008) have argued in favor of much larger conversion factors in observed MW satellites ($\approx 2-3$; see, however, Kravtsov 2010 for a discussion of possible caveats in the approach of Peñarrubia et al. 2008). We stress that our results should at least hold for dwarf galaxies that have moderate M/L ratios as our final systems (e.g., Leo I or Fornax). Dwarfs that are much more DM dominated (e.g., Draco or Ursa Minor) may, in principle, exhibit a different relation between σ_* and V_{\max} owing to their (possibly) different formation and evolutionary histories (e.g., Mayer et al. 2007).

Furthermore, the relation between V_{\max} and σ_* reported here is valid for dwarfs that were originally embedded in cuspy NFW-like DM halos, like the ones employed in the present study, and would likely be different with other halo density structures. Indeed, if the halo density profiles in the progenitor disk dwarfs were shallower than NFW in the inner regions that are probed by the stars (e.g., Governato et al. 2010), the resulting circular velocity profiles will still be slowly rising within the luminous radius, and the conversion factor between σ_* and V_{\max} can be substantially larger ($\gtrsim 2-4$; see, e.g., Stoehr et al. 2002).

Our findings are corroborated by a number of studies. For example, applying Jeans modeling and varying the anisotropy in the velocity distribution of stars, Kazantzidis et al. (2004b) found that the stellar kinematics of Fornax ($\sigma_* \sim 11-13 \text{ km s}^{-1}$) and Draco ($\sigma_* \sim 8-10 \text{ km s}^{-1}$), can be reproduced in halos with $V_{\max} \sim 20-30 \text{ km s}^{-1}$, which would imply $\sigma_*/V_{\max} \sim 0.3-0.65$. Similar results were obtained by Zentner & Bullock (2003) and this range of V_{\max} was also confirmed by Madau et al. (2008) using the cosmological Via Lactea simulation of the formation of a MW-sized halo. An-

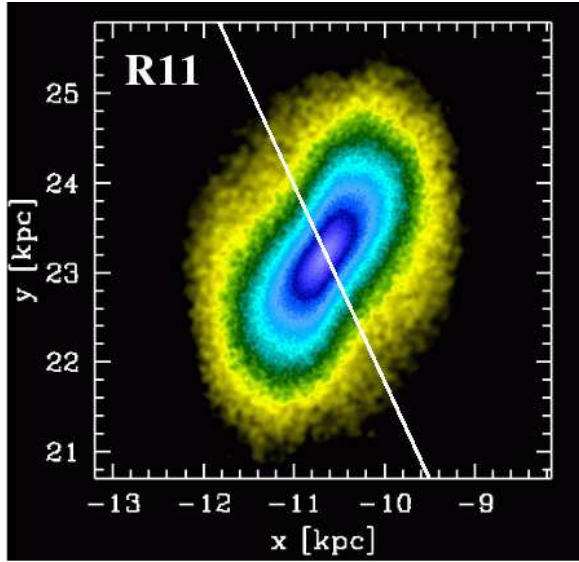


FIG. 13.— Surface density map of the stellar distribution of the dwarf in simulation R11. Particles are color-coded on a logarithmic scale, with hues ranging from yellow to blue indicating increasing stellar density. Local density is calculated using an SPH smoothing kernel of 32 neighbors. The distribution of stars is projected onto the orbital plane and is visualized at the third pericentric approach ($t = 5.25$ Gyr from the start of the simulation). The solid line indicates the direction towards the center of the host galaxy, located at $(x, y) = (0, 0)$. A bar is evident in the stellar component and the rotational velocity of the stars, V_{rot} , is anticlockwise in this image. The tidal forces point in the same direction as the rotational velocity vectors of the stars in the dwarf, resulting in an increase of V_{rot} .

other investigation of Draco by Łokas et al. (2005), which considered the contamination of the stars by tidal tails and included the fourth velocity moment in the analysis, found $\sigma_* \sim 8 \text{ km s}^{-1}$ and $V_{\text{max}} \sim 16 \text{ km s}^{-1}$, again in agreement with our results. Lastly, Walker et al. (2009) have recently analyzed the observed velocity dispersion profiles of a number of classic dSphs. Treating the anisotropy of the stellar velocity distribution as a free parameter, these authors estimated the V_{max} of the host halos in the range $\sim 10\text{--}25 \text{ km s}^{-1}$, similar to those that would be obtained assuming the relation between V_{max} and σ_* reported here.

The right panel of Figure 12 illustrates four examples of the evolution of individual dwarfs on the $V_{\text{max}} - \sigma'_*$ plane. Results are presented for representative experiments R1, R2, R3, and R5, where the same dwarf galaxy (D1) was placed on different orbits, but the general trends are confirmed in all simulations. The combination of tidal stripping and loss of angular momentum dominating over tidal heating dictates the characteristic evolution toward lower values of V_{max} and σ'_* seen in all cases. The panel also shows that the dwarf galaxies exhibit different trajectories depending on their orbital parameters and can move substantially on the $V_{\text{max}} - \sigma'_*$ plane during the course of their evolution inside their hosts. Both facts imply that the final $V_{\text{max}} - \sigma'_*$ relation in our simulations is not a consequence of the initial conditions.

5.2. Increasing Rotational Velocity

In the majority of cases we studied, the rotational velocity of the stars within r_{max} , V_{rot} , decreased systematically with time leading from the initial rotationally-supported dwarfs to pressure-supported stellar systems dominated by random motions. There are instances in the evolution, however, where V_{rot} increases at pericentric passages. As seen in Figure 11, this occurs in simulations R1, R9, and R17 (after the sec-

ond pericentric approach), R8 (after the third pericentric approach), and R11 and R12 (after the third and fourth pericentric passage).

Investigating for the reason behind the temporary increases of the rotational velocity we checked the orientation of the elongated stellar component at the pericentric approaches at which such increases occur. We found that the typical orientation of the bar is similar to that illustrated in Figure 13 where we see the stellar component of simulation R11 at the third pericentric approach projected onto the orbital plane. The rotational velocity of the stars is anticlockwise in this plot. Therefore, the tidal forces which act along the direction towards the host galaxy (solid line) point in the same direction as the rotational velocity vectors of the stars in the dwarf, effectively speeding up the rotation. Note that the case shown in Figure 13 is the only instance in the entire evolution of the whole suite of 17 experiments where the total angular momentum of the stars within r_{max} increases significantly. In all other cases of increasing V_{rot} the angular momentum does not increase because it is controlled not only by the rotational velocities of the stars but also by r_{max} , which decreases at each pericentric passage.

Lastly, we note that the observed increases in V_{rot} are always associated with changes in the shape of the stellar component from a more prolate to a more triaxial configuration, or equivalently with an increase of the difference between the axis ratios b/a and c/a . This is most evident in experiment R11, where the prolate shape with $b/a \approx c/a \approx 0.4$ at the third pericentric passage transforms into a triaxial one (with $b/a > c/a$). A similar phenomenon occurs at the subsequent (fourth) pericentric approach. These changes are also accompanied by changes in other parameters. As verified in Figure 2 and Figures 3–10, when the rotational velocity (or V_{rot}/σ_*) increases, there is always a drop in the anisotropy parameter β and the bar strength amplitude A_2 . This means that at these instances the shape of the stellar component becomes less prolate and the orbital structure of the stellar distribution changes as the stellar orbits become less radial.

5.3. Increasing M/L Ratio

In most of our simulations, the M/L ratio computed within r_{max} decreases monotonically as a function of time for the reasons we discussed in § 3.1. In three of our 17 experiments, however, the M/L ratio starts to increase at some point during the evolution. This happens most prominently in simulations R2 and R4, which are characterized by the smallest pericentric distances and produce the most strongly tidally stirred dwarfs. Although much smaller, such an increase in the M/L ratio is also observed in experiment R13 where the stellar disk is more extended due to the larger initial value of the radial scale length, R_d , adopted in this case. We stress at the outset that these increases of the M/L ratio are rather moderate and thus cannot account for the exceptional DM content in some of the classic dSphs such as Draco and Ursa Minor. This implies that the very high values of M/L inferred for some dSph galaxies may not be a consequence of tidal evolution, but could be the result of either the formation process of their progenitors or other mechanisms that affected the baryonic mass fraction of dSphs. For example, the presence and subsequent removal of gas by the combination of tides and ram pressure has been shown to be vital in producing systems with extreme DM content (Mayer et al. 2006, 2007).

Figure 14 investigates the reason behind the increasing M/L ratio. This figure shows the relative mass loss, $|\Delta M|/M$, of

stars and DM separately in simulations R2, R4, and R13. For comparison, we also present the same quantities in our reference experiment R1. To avoid noise in the data, the values of $|\Delta M|/M$ were assigned at pericenters by taking the masses within r_{\max} at the following and preceding apocenter, namely $|\Delta M|/M = |M_{i+1} - M_i|/M_i$, where i is the apocenter number. Figure 14 demonstrates that in all four simulations the relative mass loss of the DM component is initially much larger than that of the stars, and that the former always dominates in experiment R1. In simulations R2, R4, and R13, however, the stars begin to be stripped more effectively at some point during the late stages of the evolution, leading to the increase of the M/L ratios reported in Figures 2, 4, and 8.

The reason for this behavior can be attributed to the fact that in these three cases the dwarf galaxies are stripped down to the scales where the alignment between the angular momenta of the stars and the orbital angular momenta of the dwarfs start to have an important effect on stellar stripping. In experiments R2 and R4, with the smallest pericentric distances, this is due to the very strong tidal forces. In simulation R13, the disk is much more extended and, consequently, the dwarf galaxy is stripped down to the stellar scales faster than, for example, in the reference experiment R1. Because in all experiments the stars retain a certain amount of angular momentum (while the DM halos were non-rotating by construction) and the orientation of the angular momentum vector does not strongly vary with time, the stars begin to get stripped more efficiently compared to the DM as their angular momenta are (on average) more strongly aligned with the orbital angular momentum of the dwarf (e.g., Read et al. 2006b). It is important to emphasize, however, that the details of how the M/L ratio would evolve depends, among other things, on the initial angular momentum content of the DM halos, the amount of angular momentum retained by the stars in the late stages of the evolution, and the degree of alignment between the angular momenta of stars and DM and the orbital angular momentum.

5.4. Orbital Time or Pericentric Distance?

In this section, we discuss the role of different orbital parameters in influencing the transformation of disk dwarfs into dSphs and thus the efficiency of the tidal stirring mechanism. Specifically, we focus on the relative importance of the orbital time, T_{orb} , and the pericentric distance, r_{peri} , which determine the number and the strength of the tidal shocks, respectively. The relevant analysis is presented in Figure 15. This figure shows, as a function of r_{peri} and T_{orb} , the final values for some of the parameters that we used throughout this study to describe the global evolution of the dwarf galaxies inside the tidal field of their hosts. In particular, we consider the parameters r_{\max} , V_{\max} , b/a , c/a , V_{rot}/σ_* , and β .

The filled symbols in Figure 15 present results for simulations R1-R5 which have been discussed in § 3 (see also Table 3). Open symbols correspond to two additional experiments, which were designed to complement the existing simulations R1-R5. In this new set of experiments, we placed the dwarf galaxy model D1 used in experiments R1-R5 on the following orbits: (i) a short orbital time-large pericentric distance orbit with $r_{\text{peri}} = 50$ kpc, $r_{\text{apo}} = 80$ kpc, and $T_{\text{orb}} \sim 1.7$ Gyr and (ii) a long orbital time-small pericentric distance orbit with $r_{\text{peri}} = 12.5$ kpc, $r_{\text{apo}} = 250$ kpc, and $T_{\text{orb}} \sim 4.6$ Gyr. This choice of parameters ensures that the pericentric distances and orbital times in these new simulations are not related in the same way as in experiments R1-R5, a fact that would be important for the interpretation of the results.

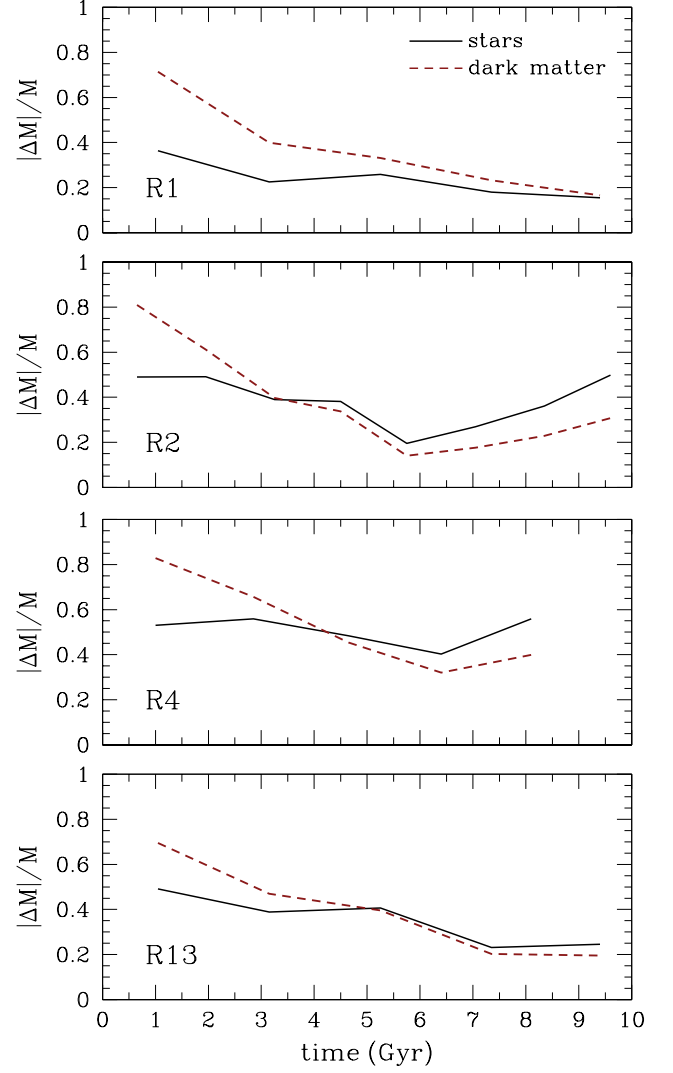


FIG. 14.— Relative mass loss, $|\Delta M|/M$, of the stellar (solid lines) and DM component (dashed lines) in simulations R1, R2, R4, and R13. The values of $\Delta M/M$ are assigned at pericenters and are computed as $|\Delta M|/M \equiv |M_{i+1} - M_i|/M_i$, where M_{i+1} and M_i are the masses within r_{\max} at the following and preceding apocenter, and i denotes the apocenter number. The relative mass loss of the DM initially exceeds that of the stars in all cases, reflecting the more efficient tidal stripping of the extended DM halos of the dwarfs. While the mass loss in DM dominates at all times in the reference experiment R1, in simulations R2, R4 and R13 the stars begin to be stripped more effectively at some point during the evolution. This preferential stripping of the stars leads to the increase of the M/L ratio reported at intermediate and late times in Figures 2, 4 and 8.

Figure 15 confirms that the final properties of the dwarfs vary dramatically depending on the parameters of the orbit. Although the behavior of the various quantities clearly shows that the final outcome of the transformation depends on both T_{orb} and r_{peri} , a closer inspection of the results in this figure illuminates the more crucial role of the pericentric distance compared to that of the orbital time in shaping dSphs via tidal stirring.

Let us first consider the filled symbols in Figure 15. Dwarf galaxies with the same pericentric distances but with orbital times that differ by approximately a factor of 2 (triangle and pentagon) end up with a similar set of final properties. On the other hand, dwarfs with comparable orbital times but with pericentric distances that differ by a factor of 2 (pentagon, circle, and star) display a wide range of final properties, a fact

which reflects the difference in pericentric distances.

Focusing now on the open symbols which correspond to the new experiments, Figure 15 shows that the dwarf galaxy on the long orbital time-small pericentric distance orbit (circle) is characterized by $c/a \gtrsim 0.5$ and $V_{\text{rot}}/\sigma_* \lesssim 1$ and hence would be classified as a dSph. We note that this dwarf has experienced only 2 pericentric passages. On the contrary, although it has suffered a much larger number of tidal shocks, the dwarf on the short orbital time-large pericentric distance orbit (square) has $c/a \approx 0.4$ and $V_{\text{rot}}/\sigma_* > 1$ and thus did not undergo a transformation into a dSph.

Overall, the results in Figure 15 lead to the following set of conclusions. First, the degree of the tidal transformation depends strongly on the combination of pericentric distance and orbital time. As expected, small pericentric distances and short orbital times, corresponding to orbits associated with a large number of strong tidal shocks and also characteristic of dwarfs being accreted by their hosts at high redshift, produce the most substantial tidal evolution. Furthermore, the larger the number of strong tidal shocks a disk dwarf suffers, the stronger and thus more complete is its transformation.

Second, in order to simply transform a disk dwarf into a dSph (according to the criteria of § 2.5) without necessarily inducing the strongest transformation, the pericentric distance is a more salient parameter than the orbital time. We stress that this conclusion depends on the condition that T_{orb} is short enough to allow the disk dwarfs to conclude at least two pericentric passages⁹. Such a requirement should be generally satisfied in the LG environment, as a significant fraction of LG dwarfs have likely had enough time to complete at least two orbits inside their hosts. Indeed, in the context of the CDM cosmogony, galaxy-sized halos form early and, in particular, the MW halo was probably already in place at $z \sim 2$ (e.g., Governato et al. 2007, 2009). In addition, structure formation in hierarchical models indicates that satellites which are found closer to the center of the primary system at $z = 0$ are typically those that fell into the host potential earlier (e.g., Diemand et al. 2007). According to this, the present distances of most dSphs would suggest that their progenitors should have been accreted by their hosts at relatively early epochs. Assuming a MW-type host potential and the range of orbital parameters of LG satellites that survived until the present time (Klimontowski et al. 2010), results in a typical orbital time of $T_{\text{orb}} \sim 2$ Gyr. Combining this value with a conservative redshift of accretion of $z \sim 1$ suggests that dwarf galaxies in the LG should have been able to complete 3 or even 4 passages inside their hosts. This line of reasoning establishes the pericentric distance, and not the orbital time, as the fundamental factor that controls the tidal transformation of disk dwarfs into dSphs in the LG and similar environments.

5.5. Implications

In the present study we have established that the strong tidal field of a MW-sized host galaxy can transform late-type, rotationally-supported dwarfs into stellar systems with the kinematic and structural properties of the classic dSphs in the LG and similar environments. Of course, tidal stirring does not constitute the only *environmentally-driven* mecha-

⁹ As discussed in Mayer et al. (2001a), disk dwarfs which due to their very long orbital times experience just one tidal shock during their orbital evolution would not be transformed, even if their pericentric distances are fairly small (except maybe in cases of very rare, nearly radial orbits). In such circumstances, the orbital time will play the key role in determining the dynamical evolution of infalling dwarfs.

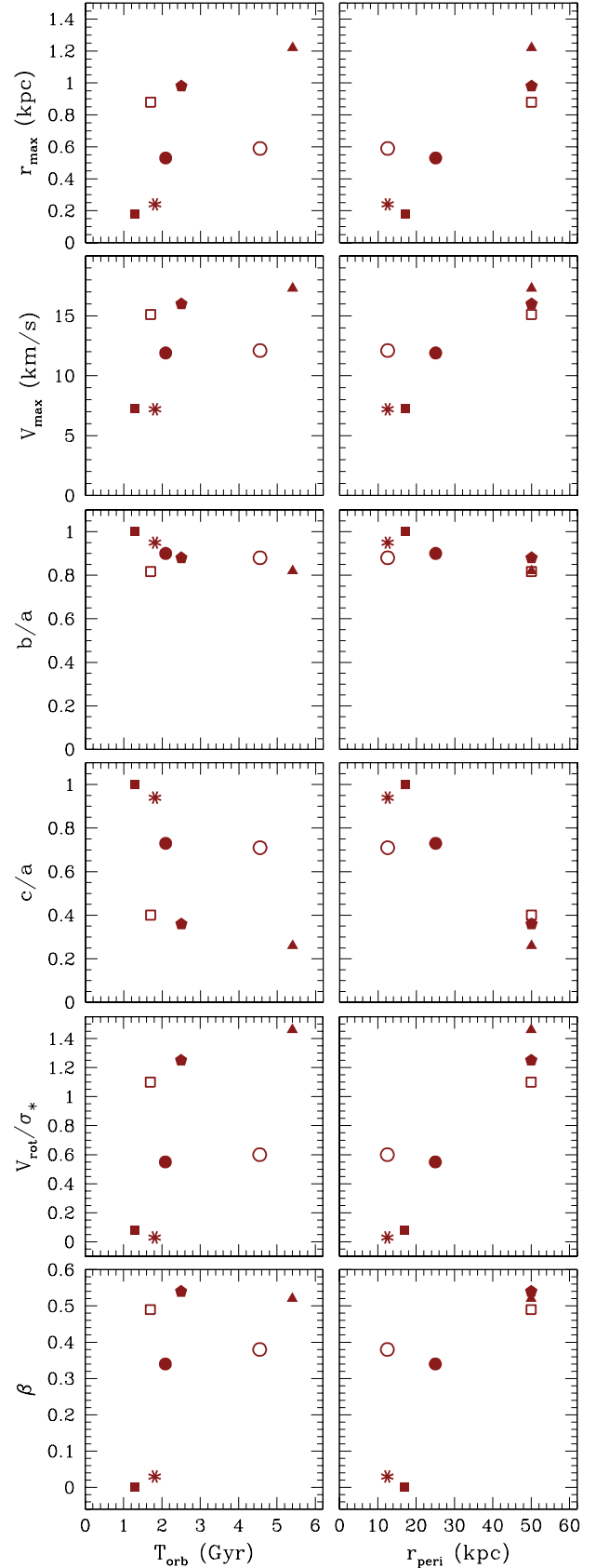


FIG. 15.— Final parameters of the simulated dwarfs as a function of orbital time (left column) and pericentric distance (right column). Filled symbols show results for simulations R1-R5 (see Table 2). Open symbols correspond to experiments where the dwarf galaxy model D1 used in simulations R1-R5 was placed on two additional orbits inside the host galaxy (see text for details). The pericentric distance which determines the strength of the tidal shocks constitutes the key factor responsible for the effective metamorphosis of a disk dwarf into a dSph. The combination of short orbital times and small pericentric distances, characteristic of dwarfs being accreted by their hosts at high redshift, induces the strongest and most complete transformations.

nism proposed for the origin of dSphs. An alternative promising model incorporates direct gravitational interactions between dwarf galaxies. Indeed, cosmological simulations of structure formation have indicated that some dwarfs may have entered their Galaxy-sized hosts as members of infalling groups (Kravtsov et al. 2004; D’Onghia & Lake 2008). It is thus plausible that these dwarfs could have experienced significant tidal perturbations before being accreted by the primary galaxies. Kravtsov et al. (2004) did demonstrate this possibility in their Λ CDM cosmological simulations of MW-sized halos.

Using controlled N -body experiments, D’Onghia et al. (2009) have recently shown how the interaction between a pair of disk galaxies with mass ratios ranging from 1:10 to 1:100 can result in the rapid formation of a dSph. As the less massive member of the pair plunges close to the disk of the more massive companion, its stellar component can experience substantial mass loss and can be tidally heated into a spheroidal configuration, even after only one close pericentric passage. This mechanism, termed “resonant stripping”, is effective when the spin angular frequency of the dwarf disk and the angular frequency of the orbit of the dwarf around the more massive system are comparable in magnitude, and the spin and orbital angular momenta are nearly aligned (that is, in a nearly prograde encounter). Such individual, close encounters between dwarf galaxies may have been more common during the assembly process of the host halos from accreting groups (Kravtsov et al. 2004; D’Onghia & Lake 2008). Given that the typical velocity dispersions in such groups should have been quite low (with a dominant group member of the size of the LMC), it is also possible that some of these interactions may have resulted in actual mergers between the dwarf galaxies.

While all these different tidal mechanisms which rely on *pre-processing* the dwarfs before they are accreted by the primary galaxy may play a role at some level, they must also be consistent with the morphology-density relation, a crucial constraint that the tidal stirring model can naturally satisfy. At present, there is no definitive observational or theoretical evidence to rule out any of the scenarios for the origin of dSphs. This also includes models that advocate the *ab initio* formation of dSphs from cosmological initial conditions (e.g., Ricotti & Gnedin 2005; Sawala et al. 2010). In all likelihood, all mechanisms do operate simultaneously to differing degrees in producing the population of dSphs in the LG and similar environments.

Our investigation of the role of different pericentric distances and orbital times on the efficiency of tidal stirring has interesting implications for the expected properties of dSphs. Our results show that in order to transform a disk dwarf with an orbital apocenter in excess of 200 kpc into a dSph, an orbit with an eccentricity that is substantially larger than the median expected eccentricity is required (see Figures 2 and 15). Given that the current distances of dwarf galaxies in the LG are suggestive of their orbital apocenters, the distant dSph Leo I (currently at a distance of ~ 250 kpc from the MW; e.g., Caputo et al. 1999) should be on a very wide, nearly radial orbit, assuming that it is the product of tidal stirring. Furthermore, even on such eccentric orbits the remnants possess some residual rotation at the level of $V_{\text{rot}}/\sigma_* \approx 0.5$ (see open circle in Figure 15). We thus predict that Leo I should have a higher V_{rot}/σ_* compared to the dSphs located closer to the primaries. Interestingly, albeit inconclusive, there are signatures of intrinsic rotation in Leo I (Sohn et al. 2007; Mateo et al.

2008). We note that such rotation has been shown to explain the observed kinematics of this dwarf (Łokas et al. 2008).

Our prediction that in the context of tidal stirring wider orbits should be associated with less evolved dSphs, and thus with higher values of V_{rot}/σ_* , should apply, even more so, to the oddly isolated galaxies Cetus and Tucana, which are located in the outskirts of the LG at more than 500 kpc from M31 and the MW, respectively. Although measurements of kinematics are extremely challenging due to the very large distances involved, recent spectroscopic studies have presented tentative evidence for rotation in Cetus (Lewis et al. 2007) and Tucana (Fraternali et al. 2009) with V_{rot}/σ_* values in the range of $0.5 \lesssim V_{\text{rot}}/\sigma_* \lesssim 1$. If confirmed by future observations, detection of rotation at such levels would be consistent with the predictions of the present study.

Furthermore, at distances in the range $\sim 300 - 600$ kpc from the MW and M31, we find the dwarf galaxies Phoenix and LGS3, which are classified as “transition-type” dwarfs (Mateo 1998). While these objects exhibit structural properties consistent with those of dSphs, they are associated with some residual gas (see, e.g., Grcevich & Putman 2009 and references therein). On the other hand, these transition-type dwarfs exhibit negligible or no ongoing star formation (no detection of H_{II} regions has been reported), a fact that differentiates them from standard gas-rich, star-forming dIrrs (e.g., Grebel 1999; Skillman 2005). Being at intermediate distances between dSphs and dIrrs and combining properties of both classes of objects, these transition-type dwarfs can provide valuable tests for the predictions of tidal stirring regarding the different stages of the transformation process.

One possibility for their origin is that their progenitors were disk satellites that were accreted only recently by their hosts on wide, fairly radial orbits, and are still in the process of being transformed into dSphs by tidal stirring. It is then plausible that these transition-type dwarfs have only concluded one pericentric passage (or they are on the way to their first pericentric approach), having lost most of their gas by ram pressure stripping. This is a reasonable assumption given that gas removal by the combination of tides and ram pressure proceeds faster than the morphological transformation of the stellar component (Mayer et al. 2006). If the scenario proposed here is correct and their transformation has only been partial, transition-type dwarfs should possess significant rotation in their stellar component (as in the case of the remote dSphs Leo I, Tucana, and Cetus discussed above). Verifying observationally this basic theoretical prediction would be important – unfortunately, the stellar kinematics of these systems is poorly known. Moreover, provided that they are at the intermediate stages of their transformation, our results suggest that they should also show signs of bar-like distortions. Definitive conclusions on all of these issues would require a synergy between detailed photometric and kinematic measurements as well as exhaustive comparisons with theoretical models. To this end, extending the search for evidence of tidal stirring in systems with more recent assembly histories than the LG may reveal a population of satellites in the process of being transformed, and thus offer unique opportunities to constrain the tidal stirring model. Interestingly, recent studies using the SDSS database have uncovered a population of dwarf galaxies in the Virgo cluster that exhibit disk-like features and bars, appearing to be in a transitional stage between a disk and a spheroid (Lisker et al. 2007). The existence of this class of objects is, in broad terms, consistent with the predictions of tidal stirring for the different stages of the transformation.

Several alternative scenarios to tidal stirring exist for explaining the nature of the spheroidal morphology of the distant LG dwarfs. For example, as a result of three-body interactions, satellites can acquire extremely energetic orbits with apocenters beyond the virial radius of the primary and be ejected to large distances (Sales et al. 2007). In this model, ejected subhalos are typically the less massive members of a pair of satellites that is tidally disrupted during the first approach onto the host. Such ejections can also occur during the tidal disruption of a bound system of *multiple* subhalos that is accreted as a single unit by the primary galaxy (Ludlow et al. 2009). In both of these scenarios, strong tidal interactions with the more massive companions can take place before the satellites are accreted by their hosts. Such encounters may eventually transform the dwarfs into dSphs, either via resonant stripping (D’Onghia et al. 2009) or other gravitational processes such as mergers. Interestingly, Kravtsov et al. (2004) reported in their cosmological simulations the existence of a few satellite systems at distances of ~ 1000 kpc from their MW-sized hosts. Based on their final V_{rot}/σ_* values, these objects would be classified as dSphs and could plausibly represent the counterparts of Cetus and Tucana in the context of the LG. The tidal heating of these systems did occur in small groups that were accreted by the primary halo at the present epoch. As the tidal forces unbind these accreting groups, energy redistribution can increase the orbital energy and apocentric distance for some of the satellites, providing an explanation for the presence of isolated dSphs in the periphery of the host galaxy. The extreme radial velocity of Leo I (e.g., Mateo et al. 2008) and the relatively high recession velocity of Tucana (Fraternali et al. 2009) may already suggest that these systems have been propelled into their highly energetic orbits through the type of interactions suggested by Sales et al. (2007) and Ludlow et al. (2009).

Binary mergers between individual satellite galaxies taking place outside of infalling groups may offer another alternative explanation for the puzzling presence of the isolated dSphs in the LG. Indeed, it has already been demonstrated that interactions and direct mergers of subhalos can lead to their very strong evolution (e.g., Knebe et al. 2004, 2006; Klimontowski et al. 2010). For example, Klimontowski et al. (2010) found in their constrained simulation of the LG that $\sim 10\%$ of all surviving subhalos in the MW and M31 have undergone a major encounter with another subhalo in the past. Most of these events occurred at very early times, between $z \sim 1$ and $z \sim 3$, while the interacting subhalos have not yet become satellites and are still outside their hosts. Whether binary mergers between dwarfs can explain the existence of dSphs orbiting far from the primary galaxies, such as Tucana and Cetus, is currently under investigation via a combination of cosmological simulations and controlled numerical experiments (Kazantzidis et al., 2010a, in preparation). Ongoing investigations aimed at studying in detail the stellar components of these isolated dSphs (e.g., Bernard et al. 2009; Monelli et al. 2010a), including their star formation histories (e.g., Monelli et al. 2010b), may soon provide useful constraints on the various competing models that have been proposed so far for their origin.

In this paper, we have investigated the tidal evolution of dwarf galaxies comprising exponential stellar disks. Recent cosmological simulations do support the idea that isolated dwarfs are rotating disks (Governato et al. 2010; see, however, Sawala et al. 2010). The morphological and dynamical transformation of such disk dwarf galaxies into dSphs under

the action of tidal forces is a rather rich process which involves several stages and is characterized by different events. Consequently, numerical simulations where a spheroidal stellar system is postulated from the beginning (e.g., Muñoz et al. 2008; Peñarrubia et al. 2008) may be inadequate to describe how dSphs have evolved to the present time subject to the tidal field of their hosts. Indeed, if the picture presented here is correct, dSph galaxies should have formed relatively late in most cases and only after concluding a number of pericentric passages inside the primary galaxies.

More specifically, Peñarrubia et al. (2008) performed a series of N -body simulations to study the dynamical evolution of dSphs in a host potential assuming a spherical King model for the stellar component embedded within an NFW halo. These authors reported that tidal effects lead to an increase in the M/L ratio in most cases, in contrast to the findings of the present study. This discrepancy is possibly due to the fact that the stellar distribution in the Peñarrubia et al. (2008) dwarfs followed the King profile which is characterized by a density core. As a result, the stars were loosely bound within the potential of the dwarf galaxy and the stellar component was much more heavily stripped compared to what is typically found here. In our experiments, the formation of tidally-induced bars, which is obviously missing from the Peñarrubia et al. (2008) models, is crucial. This is because bar formation enhances the resilience of the dwarf galaxies to mass loss and tidal stripping by increasing the stellar density and, correspondingly, the depth of the potential well.

Given the existence of a number of qualitatively different scenarios for the formation and evolution of dSphs, it is critical to be able to test these scenarios and discriminate among them. The growing kinematic data sets for dSph galaxies can already facilitate detailed comparisons with theoretical models (e.g., Walker et al. 2009). For example, the level of residual stellar rotation in the remnants can be used to constrain the competing models. Indeed, according to the results presented in Figure 11 and detailed analysis of similar simulations (see Łokas et al. 2010a), if the present-day dSph galaxies originated from disk dwarfs they should, at least in some cases, show signatures of intrinsic rotation. Interestingly, in addition to the cases of the isolated dSphs Leo I (Sohn et al. 2007; Mateo et al. 2008), Cetus (Lewis et al. 2007), and Tucana (Fraternali et al. 2009) mentioned already, detection of rotation at different levels of significance has also been claimed for Ursa Minor (Hargreaves et al. 1994; Armandroff et al. 1995) and Sculptor (Battaglia et al. 2008). It is important to stress, however, that intrinsic rotation may be difficult to distinguish from the velocity gradients induced either by the presence of tidal tails or, for nearby systems, caused by transverse motions (the so-called “perspective rotation”; see Walker et al. 2008). Due to such complications, Leo I seems to be the most promising candidate for detection of intrinsic rotation (see discussion in Łokas et al. 2008). In addition, as discussed above, our simulations predict a positive correlation between the magnitude of stellar rotation in dSphs and their distances from the center of the host galaxy (or equivalently the time of infall of the progenitor dwarf onto the primary). Such a correlation would be difficult to establish, for example, in models that propose the *ab initio* formation of isolated dSphs from cosmological initial conditions (e.g., Ricotti & Gnedin 2005; Sawala et al. 2010). Indeed, in this case the amount of rotation in the stellar components of dSphs should depend on the specifics of the formation process and the intrinsic properties of these systems (e.g., the initial

spin parameter of the DM halo of the dwarf) and thus be uncorrelated with the distance from the center of the host galaxy.

In the context of specific observational signatures of the tidal stirring model, bars play a prominent role. According to our results, bar-like structures should be relatively common in dSphs as the bar phase is one of the longest stages in the transformation process. In fact, some of the less evolved dSphs in the LG may still be in the bar stage and show signs of bar-like distortions. One irrefutable example of a LG dwarf that contains a bar is the LMC. Orbital evolution models using three-dimensional velocities constrained by recent proper motion measurements (Kallivayalil et al. 2006) suggest that the LMC may currently be on the first passage having just crossed the pericenter of its orbit around the MW (Besla et al. 2007). Confirming that the LMC is on a such extended orbit with a pericentric distance of $r_{\text{peri}} \sim 50$ kpc would be in line with our findings, as we expect its stellar component to be less evolved and thus in some early, transitory stage of the transformation between a disk and a spheroid.

Except for the LMC, however, the overall number of detections of bar-like structures among the dSphs in the LG is relatively low¹⁰. Indeed, markedly elongated isophotes that could be attributed to a residual bar-like component are observed in only a few cases, including Ursa Minor (Irwin & Hatzidimitriou 1995) and the newly discovered Hercules dSph (Coleman et al. 2007). Recently, the strongly non-spherical shape of the core of the disrupting nearby Sagittarius dSph has also been ascribed to a pre-existing bar (Łokas et al. 2010b). Interestingly, the recently discovered ultra-faint MW satellites also exhibit substantial degrees of flattening (e.g., Martin et al. 2008). Of course, the high elongation of the stellar component in some of the dSphs can also be caused by other effects, including the triaxiality of the surrounding DM halos (Kazantzidis et al. 2010) or tidal deformation in the gravitational field of the MW. Regarding the latter, Martin & Jin (2010) have recently proposed that Hercules dSph is in fact a stellar stream in formation, thus suggesting tidal disruption as the most valid scenario for the extreme shape of this system. Deeper observations to track evidence of such tidal interactions would be able to settle these issues.

The findings of the present study also indicate that the formation of tidally-induced bars is strongly linked with the transformation of rotationally-supported dwarfs to dSphs (for similar conclusions, see Mayer et al. 2001a and Klimentowski et al. 2009a). Indeed, as shown in Table 3, in only one of the 14 simulations that produced dSphs in the end, specifically experiment R16, a bar did not form at some point during the evolution of the progenitor disk dwarf inside the host galaxy. The following sequence of events is typically observed in our simulations. First, the strong tidal forces at the initial pericentric approach trigger a bar instability in the disk of the dwarf. The tidally-induced bar transports angular momentum outwards to the outer regions of the disk and to the DM halo. As tidal stripping removes the outer parts of the dwarf, the entire angular momentum content gradually decreases and the ability of the dwarf galaxy to be supported by

rotation progressively diminishes. Second, subsequent tidal shocks destroy the centrophilic stellar orbits which support the bar and increase the stellar velocity dispersion. As a result, the bar continuously loses its elongation and is tidally heated into a more isotropic, diffuse spheroid. The ultimate outcome of these two physical processes is the formation of pressure-supported stellar systems with values of $V_{\text{rot}}/\sigma_* \lesssim 1$ that are appropriate for dSphs.

We stress that the above discussion describes only one channel for the transformation of a disk dwarf into a dSph via tidal stirring. An alternative mechanism involves the buckling of the bar due to the amplification of vertical $m = 2$ (bending) modes (Mayer et al. 2001a,b). While the loss of angular momentum occurs in exactly the same way as previously described, the buckling of the bar now becomes the main process that leads to the significant vertical heating and the increase of the velocity dispersion of the system (see, e.g., Debattista et al. 2006 for a detailed description of these processes). In this picture, the spheroidal shape of the stellar distribution constitutes the end result of the instability and is not driven by tidal heating as in the simulations of the present study. Because the buckling instability requires a fairly strong bar to develop, this transformation mechanism is relevant to relatively massive systems with high surface densities. Indeed, none of the bars in our low surface density dwarfs showed any signs of buckling.

To summarize, it seems that there are at least two channels for the formation of the spheroidal component in the tidal stirring scenario: prolonged impulsive tidal heating and the bar buckling instability. The former is favored in low mass, low surface density disk dwarfs for which heating is particularly efficient. This mechanism likely applies to the progenitors of the faintest classic dSphs such as Draco, Sculptor or Leo I. On the other hand, bar buckling requires strongly self-gravitating systems with higher surface densities. This channel plausibly operates on the progenitors of the brightest dSphs such as Fornax and Sagittarius, and even more so on those of the bright dwarf elliptical satellites of M31, such as NGC185 and NGC167. This mechanism was also found to be applicable to the transformation of relatively massive and bright spiral galaxies in galaxy clusters (Mastropietro et al. 2005).

Our simulations also suggest that the amount of mass loss that the dwarf galaxies experience can be considerable. Indeed, in the reference experiment R1, the dwarf lost $\sim 90\%$ of its initial mass within r_{max} and still survived as a bound entity (the amount of mass loss for the most heavily stripped dwarfs in simulations R2 and R4 reached $\sim 99\%$). Typically, the maximum circular velocities, V_{max} , decreased by a factor of ~ 2 during the orbital evolution in the cases where dSphs were produced (this factor increased to ~ 3 in experiments R2 and R4). Such substantial evolution in V_{max} occurred despite the presence of the baryons which tend to moderate the effect of tidal shocks by making the potential well deeper, especially after bar formation. These findings are in agreement with those of Klimentowski et al. (2009a) as well as with results of other studies. For example, Kravtsov et al. (2004), using fully cosmological DM-only simulations, reported that the V_{max} of their most evolved subhalos decreased by a factor of $1.5 - 2$ on average during 10 Gyr of tidal evolution. More recently, Diemand et al. (2007) and Madau et al. (2008) found that satellites in the Via Lactea simulation lost between ~ 30 and $\sim 99\%$ of their pre-infall mass, and that V_{max} typically decreased by a factor of $\sim 2 - 3$.

The previous discussion suggests that for subhalos which

¹⁰ We note that there are a number of reasons as to why bars in dwarf galaxies may escape detection in the LG. First, bars are oriented randomly with respect to the observer, so some bar-like structures may appear as only slightly flattened. Second, the smoothing procedures usually applied when measuring the surface density distributions of stars in dwarf galaxies can decrease the detectability of bars in these systems (for a thorough discussion pertaining to the difficulties in identifying bars in dSphs, see Klimentowski et al. 2009a).

have been accreted by their hosts at early cosmic epochs and have completed several orbits with fairly small pericenters, V_{\max} is expected to have evolved significantly. Therefore, the DM halos of present-day dSphs may have had considerably larger masses and circular velocities when they entered the halo of the MW (see, e.g., Kravtsov et al. 2004 and Madau et al. 2008). This has important implications for galaxy formation models. Indeed, the substantial observational work during the past few years suggests that the present-day classic dSphs of the MW and M31 have central stellar velocity dispersions in the range $\sigma_* \sim 7 - 13 \text{ km s}^{-1}$ (see, e.g., Walker et al. 2009 and references therein). Assuming that $V_{\max} \sim \sqrt{3}\sigma_*$, in accordance with the results of § 5.1, implies current values of V_{\max} in the range $V_{\max} \sim 12 - 22 \text{ km s}^{-1}$ and initial V_{\max} values, namely before infall and tidal mass loss, in the range $V_{\max} \sim 24 - 44 \text{ km s}^{-1}$. These numbers are quite important. Indeed, with such relatively high values of initial halo V_{\max} , photoevaporation of the gas by the cosmic ultraviolet background after reionization as well as supernovae feedback could not be the factors that shaped the baryonic content and nature of these dSphs. In fact, according to the radiative transfer simulations of Susa & Umemura (2004), photoevaporation would be effective and remove most of the gas only for $V_{\max} \lesssim 20 \text{ km s}^{-1}$. This is consistent with the lack of a clear signature of the reionization epoch in the star formation histories of dSphs (Grebel & Gallagher 2004; Orban et al. 2008).

In this paper, we have also demonstrated how the orbital parameters and initial structures of the progenitor late-type disk dwarfs determine the final properties of the dSphs. Therefore, the fact that Fornax and Draco have roughly similar masses at present, as inferred from the V_{\max} of their halos (e.g., Kazantzidis et al. 2004b), but differ by about an order of magnitude in luminosity and M/L ratio, can be explained in two ways. One possibility is that the progenitors of these two dwarfs began with very different relative amounts of DM and baryons, for reasons related to their formation history and not to the environment. Alternatively, Fornax and Draco originated from systems that had comparable DM and baryonic masses, but experienced dissimilar tidal evolutions because they entered the primary galaxy at different epochs and/or on different orbits.

Regarding the latter, according to the hydrodynamical simulations of Mayer et al. (2007), gas-rich disk satellites that were accreted by their hosts when the intensity of the cosmic ultraviolet background was much higher than today ($z \sim 2$), can be completely stripped of their gas by ram pressure in one or two pericentric passages. In this case, the final systems would correspond to dSphs with truncated star formation histories such as Draco (e.g., Orban et al. 2008). While the baryonic content of the progenitor dwarfs decreased significantly as a result of gas stripping, the initial DM mass in the central regions around the surviving baryonic core is largely preserved. This is because DM is affected only by tides and not by ram pressure. As a result, exceptional M/L values, of the order of 100, similar to those inferred for Draco and Ursa Minor, can arise. On the other hand, disk dwarfs that were accreted by their hosts at $z \lesssim 1$, when the intensity of the cosmic ultraviolet radiation dropped by more than an order of magnitude compared to $z \sim 2$, were able to retain some gas because tides and ram pressure could not strip it completely. Under these conditions, the infalling dwarf galaxies can undergo tidally-triggered bursts of star formation associated with bar-

driven gas inflows at pericentric approaches. Such a model would be applicable to dSphs with extended star formation histories such as Fornax, Carina, and Leo I. This mechanism can produce dSphs that are brighter for a given halo mass (or central stellar velocity dispersion) compared to the ones that were accreted earlier. While this generic scenario seems to explain the differences in the properties of Fornax and Draco despite their similar masses, it would be important to revisit it in future work with models capable of capturing the multiphase structure of the ISM in dwarf galaxies.

Lastly, it has long been debated whether the inferred high M/L ratios of dSphs indeed signify exceptional DM content or are simply a reflection of strong tidal effects and of the fact that these systems are in reality on the verge of disruption. The findings of the present study have intriguing implications for earlier attempts to model dSph galaxies as unbound systems without DM (e.g., Kroupa 1997; Klessen & Kroupa 1998). Indeed, the tidal stirring model demonstrates how mass loss and the formation of tidal tails can be consistent with the presence of a bound stellar component embedded in a relatively massive CDM halo, even after several Gyr of tidal evolution inside the host. Our results indicate that substantial mass loss and the existence of a gravitationally bound dSph galaxy with a relatively high M/L ratio are not mutually exclusive, confirming earlier claims based on a smaller set of lower resolution simulations (Mayer et al. 2002). The findings of the present study also suggest that the claimed detection of extra-tidal stars in a number of dSphs, including Ursa Minor (Martínez-Delgado et al. 2001), Fornax (Coleman et al. 2005), Carina (Muñoz et al. 2006), and Leo I (Sohn et al. 2007) is consistent with satellite accretion in CDM models. We note in passing that the number of such detections may be low due to the intrinsic difficulties associated with separating the tidal tails from the bound core of the dwarfs (see, e.g., Klimontowski et al. 2009b). Furthermore, in the context of tidal stirring, dSphs embedded in CDM halos exhibit stellar distributions that are adequately fit by exponential or King profiles in agreement with observed dSphs (see review by Mayer 2010). Stellar profiles of this type are difficult to accommodate within models that represent dSphs as systems devoid of DM. Indeed, such models predict nearly flat profiles as expected for objects close to complete disruption (e.g., Kroupa 1997).

5.6. Caveats and Future Directions

Certainly the approach presented in this paper is not without caveats. A first limitation is related to the fact that we have adopted a single primary galaxy with the present-day structural properties of the MW. In general, at the time when the dwarfs are accreted by the primary galaxy at high redshift, the DM and baryonic masses of the host would be different compared to those of the present time. Our methodology thus neglects the cosmological evolution of the host galaxy structure via mergers and smooth accretion during the interactions with the dwarfs. However, this simplification may be justified to a certain degree by recent Λ CDM galaxy formation simulations, which have shown that MW-sized disk galaxies assemble most of the mass in their inner regions between $\sim 8 - 10$ Gyr ago (e.g., Governato et al. 2007, 2009). This is indeed the timescale that we follow in our simulations. Nonetheless, a more complete investigation would have to include the ongoing formation of the host galaxy. In addition, we have assumed a host DM halo that is spherical (except in the very inner regions that are dominated by the potential of

the disk), instead of triaxial as postulated by CDM models (e.g., Frenk et al. 1988). Halo triaxiality and the complexity of halo formation in a realistic cosmological context, with continuous mergers, accretion, and rapidly changing potential wells can have an impact on the orbital evolution of infalling satellites (e.g., Kravtsov et al. 2004), with consequences for the efficiency of their transformation. It will be important to explore these issues in future investigations of tidal stirring.

A second shortcoming of our work is related to the fact that we have focused on experiments where the alignments between the internal angular momenta of the dwarfs, those of the primary disks and the orbital angular momenta were all prograde (45° in most cases; see Table 2). Prograde alignments between the orbital angular momenta of the dwarfs and the spins of the primary disks, or between the angular momenta of the two disks, are expected to be important mainly for orbits with pericentric distances smaller than a characteristic radius containing a non-negligible fraction of the mass of the primary disks. In this case, the tidal effects of the host disks would be enhanced and the orbits of the dwarfs would quickly decay due to the additional dynamical friction provided by the disks of the primary galaxies (e.g., Quinn & Goodman 1986). As our typical pericentric distances are $r_{\text{peri}} \gtrsim 15$ kpc, we expect the efficiency of the transformation reported here to be weakly affected by such effects.

On the other hand, the orientation between the orbital angular momenta of the dwarfs and the internal angular momenta of their disks is particularly relevant for our experiments. For retrograde alignments between these two angular momenta, tidal stripping is considerably reduced (e.g., Read et al. 2006b) and both bar formation and the efficiency of transformation via the tidal stirring mechanism are also suppressed (Mayer et al. 2001a). These facts highlight the importance of coupling between orbital and internal motions. Determining the statistics of alignments between internal and orbital angular momenta would require a series of fully cosmological studies, focusing on the accretion of satellites within halos of disk galaxies, and is therefore beyond the scope of this paper. We stress, however, that the orbital parameters adopted in the present study correspond to only moderate alignments, and therefore our results should not be biased by any strong coupling of angular momenta. Unless there is some yet unknown cosmological bias *against* the mildly prograde alignments that we have adopted here, our findings should be able to illuminate at least some of the details of the typical transformation experienced by infalling disk dwarfs in the LG and similar environments.

Lastly, the most evident limitation of this study is that we have addressed the efficiency of the tidal stirring mechanism only in the collisionless regime. Our results should therefore be viewed as preliminary. A more complete treatment including hydrodynamics is required to illuminate one of the most distinct properties of dSphs, namely their low gas content (see, e.g., Greich & Putman 2009 and references therein) and fully refine the conclusions presented here. The present-day structure of dwarf galaxies originates from a complex interplay of effects and a full explanation requires detailed knowledge of their star formation histories and chemical evolution, amongst others. Adding star formation as a further ingredient will offer the possibility to determine the magnitude of starbursts induced in the dwarfs at pericentric passages, while gaining a deeper understanding of the wide diversity in their star formation histories (e.g., Grebel 2000; Orban et al. 2008). Furthermore, specific predictions for the metallic-

ity of the remnants formed by tidal stirring, let alone comparisons with the luminosity-metallicity relation for nearby dwarf galaxies (Tolstoy et al. 2009), are not currently available. We plan to extend the present investigation in these directions in due course.

Mayer et al. (2007) have also demonstrated how the efficiency of tidal stirring is affected by the presence of a dissipative component, and how it varies depending on the balance between heating and cooling in the gas. This is especially relevant for disk-like progenitors that are able to overcome ram pressure and retain their gas for a longer period of time. Satellites infalling at $z \lesssim 1$ when the intensity of the cosmic ultraviolet background is weaker and the gas can settle in a colder and denser configuration within the potential of the dwarf would fall in this category. In this case, the tidal heating of the bar into a spheroid becomes less efficient. This is because the bar instability causes the gas to flow towards the central region of the dwarf, increasing its central density and causing a more adiabatic response of the system to the external tidal perturbation.

Despite the aforementioned limitations, several facts do suggest that our results for the efficiency of tidal stirring should be regarded as conservative. First, as we discussed above, some of the progenitors of present-day dSphs might have suffered significant tidal perturbations before being accreted by their hosts (e.g., Kravtsov et al. 2004). Therefore, it is plausible that these systems might have entered their primary galaxies already partially transformed. Such a condition would facilitate their complete transformation inside the tidal field of the primary galaxy. Second, if the progenitor disk dwarfs had either very low halo concentration parameters or core-like density profiles, as it is indeed suggested by both the modeling of rotation curves of present-day LSB and dIrr galaxies (e.g., de Blok 2010) and recent cosmological simulations of dwarf galaxy formation (Governato et al. 2010), our conclusions regarding the effectiveness of the transformation would be reinforced. Indeed, in such circumstances the response of the dwarfs to the tidal shocks would be much more impulsive compared to the cases of steep NFW-like profiles like the ones that we used in our experiments. This would give rise to augmented tidal mass loss (e.g., Kazantzidis et al. 2004a) and to a more effective transformation into a dSph. Lastly, none of the disk dwarfs in our experiments passed through the disk of the host galaxy. This is important as it has been recently shown that disk shocking, namely tidal shocks induced by passages through the disk, can affect significantly the evolution of satellites having masses $\lesssim 10^9 M_\odot$ and pericentric distances $\lesssim 30$ kpc, and even cause the disruption of a fraction of them (D’Onghia et al. 2010).

As a final remark, we reiterate that accumulating observational and theoretical evidence suggests that dwarf galaxies are not formed as thin disks, but rather are born as thick, puffy systems (e.g., Dalcanton et al. 2004; Kaufmann et al. 2007). The effect of thermal support, as opposed to rotation, ought to be thoroughly investigated in forthcoming studies of tidal stirring. Indeed, a thicker, more diffuse stellar component suggests a stronger effect of direct tidal heating (Spitzer 1958), but the bar instability, an essential element of tidal stirring, is associated with thin stellar configurations. Moreover, gas stripping by ram pressure should be enhanced in an initially thicker, more diffuse stellar system owing to the reduced gravitational restoring force of the gas. The interplay between all these aspects of the modeling will be assessed with future work where realistic gas-rich

dIrrs will be evolved inside MW-sized hosts with recipes of radiative cooling, star formation, and supernovae feedback (Kazantzidis et al., 2010b, in preparation). These dwarfs have been formed self-consistently in cosmological hydrodynamical simulations (Governato et al. 2010) and are characterized by a turbulent and multi-phase realistic ISM.

6. SUMMARY

Using a suite of collisionless N -body simulations we have investigated the efficiency of the tidal stirring mechanism for the origin of dSphs. Specifically, we have examined the degree to which the sizes, masses, shapes, and kinematics of late-type, rotationally-supported dwarfs are affected by the gravitational field of MW-sized host galaxies for a range of dwarf orbital and structural parameters. Unlike previous work on the subject, we have employed equilibrium numerical models of dwarf galaxies constructed from composite DFs and consisting of exponential stellar disks embedded in cosmologically-motivated DM halos. The self-consistency of the adopted models is crucial for confirming the complex transformation process of a disk dwarf into a dSph. This aspect of the modeling constitutes the major improvement that we introduce in the present study. Furthermore, we have extended earlier contributions on the subject by conducting a simulation campaign which is carefully designed to allow an investigation of a much larger parameter space than before. Lastly, the fairly high numerical resolution of our experiments combined with the growing observational data sets for dSph galaxies provide unique opportunities for systematic and quantitative comparisons between the theoretical models and the data, and we undertake such a task in a companion paper (Łokas et al. 2010, in preparation).

Our main results and conclusions can be summarized as follows.

1. Tidal interactions between rotationally-supported dwarf galaxies and MW-sized hosts can lead to the formation of pressure-supported, spheroidal stellar systems with kinematic and structural properties akin to those of the classic dSphs in the LG and similar environments. Our exploration of a wide variety of initial conditions for the progenitor disk dwarfs suggests that such tidal transformations are fairly efficient and should thus be common occurrences within the currently favored cosmological paradigm. Due to the fact that satellite accretion is a generic feature of hierarchical models of structure formation, the transformation process described in this study should be applicable to at least some of the dSph galaxies in the universe.
2. The transformation mechanism is complex and involves a combination of tidally-induced bar instabilities in stellar disks and impulsive tidal heating of the stellar distribution. Given the self-consistency of our dwarf galaxy models, we can safely conclude that the formation of dSphs can be entirely attributed to tidal perturbations, rather than being a consequence of the initial conditions. In the context of the tidal stirring model, bar formation is intimately linked to the formation of dSphs (see Table 3). Loss of angular momentum caused by the bar instability and simultaneous increase of the stellar velocity dispersion due to tidal heating lead to low values of V_{rot}/σ_* in the simulated remnants comparable

to those of observed dSphs ($V_{\text{rot}}/\sigma_* \lesssim 1$). Heating via tidal shocks at pericentric passages decreases continuously the elongation of the bar and causes the initially disk stellar distributions to transform into spheroids with projected axis ratios of $c/a \gtrsim 0.5$.

3. Bar formation constitutes a sufficient but not necessary condition for the formation of dSphs via the tidal stirring of rotationally-supported dwarfs. In cases where bar instabilities are not triggered by the tidal interactions with the host galaxies, spheroidal stellar systems with negligible amounts of rotation can still be produced solely via the action of impulsive tidal heating (R16; see § 4.2.2).
4. The effectiveness of the transformation into a dSph depends crucially on the orbital parameters of the progenitor disk dwarfs (§ 3). For a fixed eccentricity, $r_{\text{apo}}/r_{\text{peri}}$, tighter orbits which are characterized by shorter orbital times, T_{orb} , and smaller apocentric, r_{apo} , and pericentric distances, r_{peri} , lead to more rapid and complete transformations. For a fixed apocentric distance, orbits with higher eccentricities also induce stronger transformations. Under the right combination of orbital parameters, tidal stirring can yield spherically-symmetric ($b/a \approx c/a \gtrsim 0.95$) and isotropic ($\beta \approx 0$) stellar systems with negligible amounts of rotation ($V_{\text{rot}}/\sigma_* \lesssim 0.1$) (R2 and R4; see Table 3).
5. The degree of the tidal transformation depends on both the number and the strength of the tidal shocks, which are determined by the orbital time, T_{orb} , and the pericentric distance, r_{peri} , respectively. Small pericentric distances and short orbital times, corresponding to orbits associated with a large number of strong tidal shocks, produce the strongest and most complete transformations. However, in order to simply transform a disk dwarf galaxy into a dSph without necessarily inducing the strongest transformation, r_{peri} is the more salient orbital parameter. The last conclusion holds provided that T_{orb} is short enough to allow the dwarfs to complete at least two pericentric passages inside their hosts. Such a condition is likely satisfied for a significant fraction of dwarf galaxies in the LG (see § 5.4).
6. The efficiency of the transformation via tidal stirring is notably affected by the structure of the progenitor disk dwarfs. Specifically, it is enhanced considerably for those with less massive and more extended disks, as well as for dwarfs embedded in halos of lower concentration (see § 4). These properties are akin to those of LSB, gas-rich dIrr galaxies which reside in the outskirts of the LG, a fact that highlights tidal stirring as a plausible causal mechanism for the origin of the morphology-density relation.
7. The robustness of dwarf galaxies to tides and mass loss is increased significantly for those with more massive and more compact disks, as well as for dwarfs embedded in halos of higher concentration (see § 4). This enhanced resilience to tidal effects has important consequences for the missing satellites problem as well as for determining the radial distribution of satellites inside host halos (e.g., Diemand et al. 2004).

8. The products of tidal stirring satisfy the relation $V_{\max} = \sqrt{3}\sigma_*$, where σ_* is the one-dimensional, central stellar velocity dispersion and V_{\max} is the maximum halo circular velocity (see § 5.1). Such a small conversion factor between σ_* and V_{\max} , formally valid for a tracer stellar population with an isotropic velocity dispersion tensor, is in agreement with those originally adopted to formulate the missing satellites problem (Moore et al. 1999; Klypin et al. 1999).
9. The mass-to-light ratios, M/L , of the orbiting disk dwarf galaxies decrease monotonically with time as the extended DM halos are preferentially tidally stripped. In some cases, however, the M/L ratios start to increase later in the evolution when stellar mass loss becomes more effective (see § 5.3). These cases are associated with either enhanced tidal mass loss (R2 and R4) or more extended initial stellar distributions (R13) and demand that the dwarfs are stripped down to the scales where the alignment between the angular momenta of the stars and the orbital angular momenta of the dwarfs has an important effect on stellar stripping. This mechanism causes only a moderate increase of the M/L ratio and it may thus not be able to account for the extreme DM content in some of the classic dSphs (e.g., Draco or Ursa Minor). Producing such systems likely requires hydrodynamical processes.
10. Distant dSphs in the LG, such as Leo I, Tucana, and Cetus, which are likely moving on very wide orbits, should have only been partially stirred by their hosts, assuming

that their properties originate from tidal stirring. As a result, these remote dwarfs should exhibit higher values of V_{rot}/σ_* compared to those of dSphs located closer to the primary galaxies. Future conclusive measurements of rotation in these systems will serve to validate (or falsify) this prediction.

The authors acknowledge useful discussions with James Bullock, Mandeep Gill, Andrey Kravtsov, Andrea Macciò, Chiara Mastropietro, Mario Mateo, Chris Orban, Michael Stamatikos, Justin Read, and David Weinberg. S.K. would like to thank Victor Debattista for valuable conversations on bar instabilities and related issues which significantly informed this work. S.K. also acknowledges the hospitality of the Nicolaus Copernicus Astronomical Center during a visit when the final stages of this work were completed. S.K. is funded by the Center for Cosmology and Astro-Particle Physics (CCAPP) at The Ohio State University. E.L.L. is grateful for the hospitality of CCAPP during her visit. This research was partially supported by the Polish Ministry of Science and Higher Education under grant NN203025333. The work of L.A.M. was carried out at the Jet Propulsion Laboratory (JPL), California Institute of Technology, under a contract with NASA. L.A.M. acknowledges support from the NASA ATFP program. The numerical simulations were performed on the Cosmos cluster at JPL. Cosmos was provided by funding from the JPL Office of the Chief Information Officer. This work was also supported by an allocation of computing time from the Ohio Supercomputer Center (<http://www.osc.edu>).

REFERENCES

- Armandroff, T. E., Olszewski, E. W., & Pryor, C. 1995, *AJ*, 110, 2131
 Battaglia, G., Helmi, A., Tolstoy, E., Irwin, M., Hill, V., & Jablonka, P. 2008, *ApJ*, 681, L13
 Belokurov, V. et al. 2006, *ApJ*, 642, L137
 Bernard, E. J. et al. 2009, *ApJ*, 699, 1742
 Besla, G., Kallivayalil, N., Hernquist, L., Robertson, B., Cox, T. J., van der Marel, R. P., & Alcock, C. 2007, *ApJ*, 668, 949
 Bett, P., Eke, V., Frenk, C. S., Jenkins, A., Helly, J., & Navarro, J. 2007, *MNRAS*, 376, 215
 Binney, J. & Tremaine, S. 2008, *Galactic Dynamics: Second Edition* (Princeton University Press)
 Blumenthal, G. R., Faber, S. M., Flores, R., & Primack, J. R. 1986, *ApJ*, 301, 27
 Blumenthal, G. R., Faber, S. M., Primack, J. R., & Rees, M. J. 1984, *Nature*, 311, 517
 Bruzual, A. G. & Charlot, S. 1993, *ApJ*, 405, 538
 Bullock, J. S., Dekel, A., Kolatt, T. S., Kravtsov, A. V., Klypin, A. A., Porciani, C., & Primack, J. R. 2001a, *ApJ*, 555, 240
 Bullock, J. S., Kravtsov, A. V., & Weinberg, D. H. 2000, *ApJ*, 539, 517
 Bullock, J. S. et al. 2001b, *MNRAS*, 321, 559
 Caputo, F., Cassisi, S., Castellani, M., Marconi, G., & Santolamazza, P. 1999, *AJ*, 117, 2199
 Chiboucas, K., Karachentsev, I. D., & Tully, R. B. 2009, *AJ*, 137, 3009
 Cole, S. & Lacey, C. 1996, *MNRAS*, 281, 716
 Coleman, M. G., Da Costa, G. S., Bland-Hawthorn, J., & Freeman, K. C. 2005, *AJ*, 129, 1443
 Coleman, M. G. et al. 2007, *ApJ*, 668, L43
 Colpi, M., Mayer, L., & Governato, F. 1999, *ApJ*, 525, 720
 Dalcanton, J. J., Yoachim, P., & Bernstein, R. A. 2004, *ApJ*, 608, 189
 de Blok, W. J. G. 2010, *Advances in Astronomy*, vol. 2010, Article ID 789293 (astro-ph/0910.3538), 1
 Debattista, V. P., Mayer, L., Carollo, C. M., Moore, B., Wadsley, J., & Quinn, T. 2006, *ApJ*, 645, 209
 Dekel, A. & Silk, J. 1986, *ApJ*, 303, 39
 Diemand, J., Kuhlen, M., & Madau, P. 2007, *ApJ*, 667, 859
 Diemand, J., Moore, B., & Stadel, J. 2004, *MNRAS*, 352, 535
 D’Onghia, E., Besla, G., Cox, T. J., & Hernquist, L. 2009, *Nature*, 460, 605
 D’Onghia, E. & Lake, G. 2008, *ApJ*, 686, L61
 D’Onghia, E., Springel, V., Hernquist, L., & Keres, D. 2010, *ApJ*, 709, 1138
 Dubinski, J., Berentzen, I., & Shlosman, I. 2009, *ApJ*, 697, 293
 Dubinski, J. & Chakrabarty, D. 2009, *ApJ*, 703, 2068
 Einasto, J., Saar, E., Kaasik, A., & Chernin, A. D. 1974, *Nature*, 252, 111
 Faber, S. M. & Lin, D. N. C. 1983, *ApJ*, 266, L17
 Ferguson, A. M. N., Irwin, M. J., Ibata, R. A., Lewis, G. F., & Tanvir, N. R. 2002, *AJ*, 124, 1452
 Ferguson, A. M. N. et al. 2005, *ApJ*, 622, L109
 Forbes, D. A., Beasley, M. A., Bekki, K., Brodie, J. P., & Strader, J. 2003, *Science*, 301, 1217
 Franx, M., Illingworth, G., & de Zeeuw, T. 1991, *ApJ*, 383, 112
 Fraternali, F., Tolstoy, E., Irwin, M. J., & Cole, A. A. 2009, *A&A*, 499, 121
 Frenk, C. S., White, S. D. M., Davis, M., & Efstathiou, G. 1988, *ApJ*, 327, 507
 Gauthier, J.-R., Dubinski, J., & Widrow, L. M. 2006, *ApJ*, 653, 1180
 Geha, M., Blanton, M. R., Masjedi, M., & West, A. A. 2006, *ApJ*, 653, 240
 Ghigna, S., Moore, B., Governato, F., Lake, G., Quinn, T., & Stadel, J. 1998, *MNRAS*, 300, 146
 Gilmore, G., Wilkinson, M. I., Wyse, R. F. G., Kleyna, J. T., Koch, A., Evans, N. W., & Grebel, E. K. 2007, *ApJ*, 663, 948
 Gnedin, O. Y., Hernquist, L., & Ostriker, J. P. 1999, *ApJ*, 514, 109
 Governato, F. et al. 2007, *MNRAS*, 374, 1479
 —. 2009, *MNRAS*, 398, 312
 —. 2010, *Nature*, 463, 203
 Greich, J. & Putman, M. E. 2009, *ApJ*, 696, 385
 Grebel, E. K. 1999, in *IAU Symposium*, Vol. 192, *The Stellar Content of Local Group Galaxies*, ed. P. Whitelock & R. Cannon, 17
 Grebel, E. K. 2000, in *ESA Special Publication*, Vol. 445, *Star Formation from the Small to the Large Scale*, ed. F. Favata, A. Kaas, & A. Wilson, 87
 Grebel, E. K. & Gallagher, III, J. S. 2004, *ApJ*, 610, L89
 Grillmair, C. J. & Dionatos, O. 2006, *ApJ*, 643, L17
 Hargreaves, J. C., Gilmore, G., Irwin, M. J., & Carter, D. 1994, *MNRAS*, 271, 693
 Hayashi, E., Navarro, J. F., Taylor, J. E., Stadel, J., & Quinn, T. 2003, *ApJ*, 584, 541
 Hernquist, L. 1990, *ApJ*, 356, 359
 —. 1993, *ApJS*, 86, 389

- Ibata, R., Irwin, M., Lewis, G., Ferguson, A. M. N., & Tanvir, N. 2001a, *Nature*, 412, 49
- Ibata, R., Lewis, G. F., Irwin, M., Totten, E., & Quinn, T. 2001b, *ApJ*, 551, 294
- Ibata, R., Martin, N. F., Irwin, M., Chapman, S., Ferguson, A. M. N., Lewis, G. F., & McConnachie, A. W. 2007, *ApJ*, 671, 1591
- Ibata, R. A., Gilmore, G., & Irwin, M. J. 1994, *Nature*, 370, 194
- Irwin, M. & Hatzidimitriou, D. 1995, *MNRAS*, 277, 1354
- Jimenez, R., Verde, L., & Oh, S. P. 2003, *MNRAS*, 339, 243
- Kalirai, J. S., Guhathakurta, P., Gilbert, K. M., Reitzel, D. B., Majewski, S. R., Rich, R. M., & Cooper, M. C. 2006, *ApJ*, 641, 268
- Kallivayalil, N., van der Marel, R. P., Alcock, C., Axelrod, T., Cook, K. H., Drake, A. J., & Geha, M. 2006, *ApJ*, 638, 772
- Kaufmann, T., Wheeler, C., & Bullock, J. S. 2007, *MNRAS*, 382, 1187
- Kazantzidis, S., Abadi, M. G., & Navarro, J. F. 2010, *ApJ*, 720, L62
- Kazantzidis, S., Bullock, J. S., Zentner, A. R., Kravtsov, A. V., & Moustakas, L. A. 2008, *ApJ*, 688, 254
- Kazantzidis, S., Magorrian, J., & Moore, B. 2004a, *ApJ*, 601, 37
- Kazantzidis, S., Mayer, L., Mastropietro, C., Diemand, J., Stadel, J., & Moore, B. 2004b, *ApJ*, 608, 663
- Kazantzidis, S., Zentner, A. R., Kravtsov, A. V., Bullock, J. S., & Debattista, V. P. 2009, *ApJ*, 700, 1896
- Klessen, R. S. & Kroupa, P. 1998, *ApJ*, 498, 143
- Klimontowski, J., Łokas, E. L., Kazantzidis, S., Mayer, L., & Mamon, G. A. 2009a, *MNRAS*, 397, 2015
- Klimontowski, J., Łokas, E. L., Kazantzidis, S., Mayer, L., Mamon, G. A., & Prada, F. 2009b, *MNRAS*, 400, 2162
- Klimontowski, J., Łokas, E. L., Kazantzidis, S., Prada, F., Mayer, L., & Mamon, G. A. 2007, *MNRAS*, 378, 353
- Klimontowski, J., Łokas, E. L., Knebe, A., Gottlöber, S., Martínez-Vaquero, L. A., Yepes, G., & Hoffman, Y. 2010, *MNRAS*, 402, 1899
- Klypin, A., Kravtsov, A. V., Valenzuela, O., & Prada, F. 1999, *ApJ*, 522, 82
- Klypin, A., Zhao, H., & Somerville, R. S. 2002, *ApJ*, 573, 597
- Knebe, A., Gill, S. P. D., & Gibson, B. K. 2004, *PASA*, 21, 216
- Knebe, A., Power, C., Gill, S. P. D., & Gibson, B. K. 2006, *MNRAS*, 368, 741
- Kravtsov, A. 2010, *Advances in Astronomy*, vol. 2010, Article ID 281913 (astro-ph/0906.3295), 1
- Kravtsov, A. V., Gnedin, O. Y., & Klypin, A. A. 2004, *ApJ*, 609, 482
- Kregel, M., van der Kruit, P. C., & de Grijs, R. 2002, *MNRAS*, 334, 646
- Kroupa, P. 1997, *New Astronomy*, 2, 139
- Kuhn, J. R. & Miller, R. H. 1989, *ApJ*, 341, L41
- Law, D. R., Johnston, K. V., & Majewski, S. R. 2005, *ApJ*, 619, 807
- Lewis, G. F., Ibata, R. A., Chapman, S. C., McConnachie, A., Irwin, M. J., Tolstoy, E., & Tanvir, N. R. 2007, *MNRAS*, 375, 1364
- Lisker, T., Grebel, E. K., Binggeli, B., & Glatt, K. 2007, *ApJ*, 660, 1186
- Łokas, E. L. 2001, *MNRAS*, 327, L21
- , 2002, *MNRAS*, 333, 697
- Łokas, E. L., Kazantzidis, S., Klimontowski, J., Mayer, L., & Callegari, S. 2010a, *ApJ*, 708, 1032
- Łokas, E. L., Kazantzidis, S., Majewski, S. R., Law, D. R., Mayer, L., & Frinchaboy, P. M. 2010b, *ApJ* submitted (astro-ph/1008.3464)
- Łokas, E. L., Klimontowski, J., Kazantzidis, S., & Mayer, L. 2008, *MNRAS*, 390, 625
- Łokas, E. L., Mamon, G. A., & Prada, F. 2005, *MNRAS*, 363, 918
- Ludlow, A. D., Navarro, J. F., Springel, V., Jenkins, A., Frenk, C. S., & Helmi, A. 2009, *ApJ*, 692, 931
- Macciò, A. V., Dutton, A. A., & van den Bosch, F. C. 2008, *MNRAS*, 391, 1940
- Macciò, A. V., Dutton, A. A., van den Bosch, F. C., Moore, B., Potter, D., & Stadel, J. 2007, *MNRAS*, 378, 55
- Macciò, A. V., Kang, X., Fontanot, F., Somerville, R. S., Koposov, S., & Monaco, P. 2010, *MNRAS*, 402, 1995
- Madau, P., Diemand, J., & Kuhlen, M. 2008, *ApJ*, 679, 1260
- Majewski, S. R., Skrutskie, M. F., Weinberg, M. D., & Ostriker, J. C. 2003, *ApJ*, 599, 1082
- Malin, D. & Hadley, B. 1997, *Publications of the Astronomical Society of Australia*, 14, 52
- Martin, N. F., de Jong, J. T. A., & Rix, H. 2008, *ApJ*, 684, 1075
- Martin, N. F., Ibata, R. A., Bellazzini, M., Irwin, M. J., Lewis, G. F., & Dehnen, W. 2004, *MNRAS*, 348, 12
- Martin, N. F. & Jin, S. 2010, *ApJ* accepted (astro-ph/1008.0014)
- Martínez-Delgado, D., Alonso-García, J., Aparicio, A., & Gómez-Flechoso, M. A. 2001, *ApJ*, 549, L63
- Martínez-Delgado, D., Butler, D. J., Rix, H.-W., Franco, V. I., Peñarrubia, J., Alfaro, E. J., & Dinescu, D. I. 2005, *ApJ*, 633, 205
- Mastropietro, C., Moore, B., Mayer, L., Debattista, V. P., Piffaretti, R., & Stadel, J. 2005, *MNRAS*, 364, 607
- Mateo, M., Olszewski, E. W., & Walker, M. G. 2008, *ApJ*, 675, 201
- Mateo, M. L. 1998, *ARA&A*, 36, 435
- Mayer, L. 2010, *Advances in Astronomy*, vol. 2010, Article ID 278434 (astro-ph/0909.4075), 1
- Mayer, L., Governato, F., Colpi, M., Moore, B., Quinn, T., Wadsley, J., Stadel, J., & Lake, G. 2001a, *ApJ*, 559, 754
- , 2001b, *ApJ*, 547, L123
- Mayer, L., Kazantzidis, S., Mastropietro, C., & Wadsley, J. 2007, *Nature*, 445, 738
- Mayer, L., Mastropietro, C., Wadsley, J., Stadel, J., & Moore, B. 2006, *MNRAS*, 369, 1021
- Mayer, L., Moore, B., Quinn, T., Governato, F., & Stadel, J. 2002, *MNRAS*, 336, 119
- Mayer, L. & Wadsley, J. 2004, *MNRAS*, 347, 277
- McGaugh, S. S. & Wolf, J. 2010, *ApJ* submitted (astro-ph/1003.3448)
- Milgrom, M. 1995, *ApJ*, 455, 439
- Mo, H. J., Mao, S., & White, S. D. M. 1998, *MNRAS*, 295, 319
- Monelli, M., Cassisi, S., Bernard, E. J., Hidalgo, S. L., Aparicio, A., Gallart, C., & Skillman, E. D. 2010a, *ApJ*, 718, 707
- Monelli, M. et al. 2010b, *ApJ*, 720, 1225
- Moore, B., Ghigna, S., Governato, F., Lake, G., Quinn, T., Stadel, J., & Tozzi, P. 1999, *ApJ*, 524, L19
- Muñoz, R. R., Majewski, S. R., & Johnston, K. V. 2008, *ApJ*, 679, 346
- Muñoz, R. R. et al. 2006, *ApJ*, 649, 201
- Navarro, J. F., Frenk, C. S., & White, S. D. M. 1996, *ApJ*, 462, 563
- Newberg, H. J. et al. 2002, *ApJ*, 569, 245
- Oh, S., de Blok, W. J. G., Walter, F., Brinks, E., & Kennicutt, R. C. 2008, *AJ*, 136, 2761
- Orban, C., Gnedin, O. Y., Weisz, D. R., Skillman, E. D., Dolphin, A. E., & Holtzman, J. A. 2008, *ApJ*, 686, 1030
- Peñarrubia, J., Navarro, J. F., & McConnachie, A. W. 2008, *ApJ*, 673, 226
- Peebles, P. J. E. 1969, *ApJ*, 155, 393
- Peng, E. W., Ford, H. C., Freeman, K. C., & White, R. L. 2002, *AJ*, 124, 3144
- Penny, S. J., Conselice, C. J., de Rijcke, S., & Held, E. V. 2009, *MNRAS*, 393, 1054
- Pohlen, M., Martínez-Delgado, D., Majewski, S., Palma, C., Prada, F., & Balcells, M. 2004, in *Astronomical Society of the Pacific Conference Series*, Vol. 327, *Satellites and Tidal Streams*, ed. F. Prada, D. Martínez Delgado, & T. J. Mahoney, 288
- Purcell, C. W., Kazantzidis, S., & Bullock, J. S. 2009, *ApJ*, 694, L98
- Quinn, P. J. & Goodman, J. 1986, *ApJ*, 309, 472
- Read, J. I., Pontzen, A. P., & Viel, M. 2006a, *MNRAS*, 371, 885
- Read, J. I., Wilkinson, M. I., Evans, N. W., Gilmore, G., & Kleyna, J. T. 2006b, *MNRAS*, 366, 429
- Ricotti, M. & Gnedin, N. Y. 2005, *ApJ*, 629, 259
- Sales, L. V., Navarro, J. F., Abadi, M. G., & Steinmetz, M. 2007, *MNRAS*, 379, 1475
- Sawala, T., Scannapieco, C., Maio, U., & White, S. 2010, *MNRAS*, 402, 1599
- Schulz, J., Fritze-v. Alvensleben, U., Möller, C. S., & Fricke, K. J. 2002, *A&A*, 392, 1
- Sellwood, J. A. & Debattista, V. P. 2009, *MNRAS*, 398, 1279
- Shang, E. et al. 1998, *ApJ*, 504, L23
- Shaw, L. D., Weller, J., Ostriker, J. P., & Bode, P. 2006, *ApJ*, 646, 815
- Simon, J. D. & Geha, M. 2007, *ApJ*, 670, 313
- Skillman, E. D. 2005, *New Astronomy Review*, 49, 453
- Sohn, S. T. et al. 2007, *ApJ*, 663, 960
- Spitzer, Jr., L. 1958, *ApJ*, 127, 17
- Spitzer, L. J. 1942, *ApJ*, 95, 329
- Stadel, J. G. 2001, Ph.D. Thesis, Univ. of Washington
- Stoehr, F., White, S. D. M., Tormen, G., & Springel, V. 2002, *MNRAS*, 335, L84
- Susa, H. & Umemura, M. 2004, *ApJ*, 610, L5
- Tassis, K., Abel, T., Bryan, G. L., & Norman, M. L. 2003, *ApJ*, 587, 13
- Tassis, K., Kravtsov, A. V., & Gnedin, N. Y. 2008, *ApJ*, 672, 888
- Tolstoy, E., Hill, V., & Tosi, M. 2009, *ARA&A*, 47, 371
- Walker, M. G., Mateo, M., & Olszewski, E. W. 2008, *ApJ*, 688, L75
- Walker, M. G., Mateo, M., Olszewski, E. W., Peñarrubia, J., Wyn Evans, N., & Gilmore, G. 2009, *ApJ*, 704, 1274
- Wechsler, R. H., Bullock, J. S., Primack, J. R., Kravtsov, A. V., & Dekel, A. 2002, *ApJ*, 568, 52
- Weinberg, M. D. & Blitz, L. 2006, *ApJ*, 641, L33
- White, S. D. M. & Rees, M. J. 1978, *MNRAS*, 183, 341
- Widrow, L. M. & Dubinski, J. 2005, *ApJ*, 631, 838
- Yanny, B. et al. 2000, *ApJ*, 540, 825
- Zentner, A. R. & Bullock, J. S. 2003, *ApJ*, 598, 49